Alma Mater Studiorum – Università di Bologna

DOTTORATO DI RICERCA IN BIOLOGIA CELLULARE E MOLECOLARE

Ciclo XXXI

Settore Concorsuale: 05/D1 - FISIOLOGIA

Settore Scientifico disciplinare: BIO/09 – FISIOLOGIA

BRAIN GLIAL INTERFACE: ADVANCE MATERIALS AND DEVICES TARGETING MOLECULAR AND FUNCTIONAL STUDY OF ASTROCYTES

Presentata da: Ana Isabel Borrachero Conejo

Coordinatore Dottorato

Prof. Giovanni Capranico

Supervisore e co-supervisori

Prof. Barbara Monti

Dr. Valentina Benfenati

Dr. Marco Caprini

Esame finale anno 2019

Abstract

Astrocytes are fundamental for the physiology of the central nervous system (CNS). Indeed, astrocytes dysfunction has been observed in many brain pathologies making them an attractive target for innovative therapeutical approaches. Proteins mediating calcium signaling are critically implicated in astrocytic function and dysfunction. However, state-of-the-art tools to study and modulate astroglial functions faced limited spatio-temporal sensitivity, cell selectivity and low throughput. While the use of materials and devices enabling photo- and electrical stimulation, have been shown to successfully modulate neuronal activity, their potential to selectively alter astroglial behaviour have largely been neglected. To address this challenging issue, we use materials and devices based on organic semiconductors and graphene as well as Infrared photostimulation to modulate and to study astrocytes physiology in vitro.

We present a device based on N, N'-ditridecylperylene-3,4,9,10-tetracarboxylic diimide (P13) that enables electrical stimulation of astrocytes by evoking increases in intracellular calcium concentrations ($[Ca^{2+}]_i$) in primary astrocytes. Pharmacological evidences show that the channels TRPV4 and TRPA1 are critically implicated in the observed effect. Moreover, we show that electrical stimulation promotes also cell swelling.

We also explore the potential of graphene-based materials as neural interface by using a graphene oxide functionalized with a phospholipid (GO-PL). We demonstrate that GO-PL allows an enhanced adhesion of astrocytes without promoting gliosis, that is not caused by modification of physicochemical properties such as hydrophobicity and roughness.

Finally, we investigate the effect of infrared neural stimulation (INS) on Ca^{2+}-signaling in vitro and in a validated cell culture model of differentiated astrocytes demonstrating that INS represents a new label-free method to modulate astroglial Ca^{2+}-signaling in vitro. Pharmacology and siRNA

experiments, show that INS evoke extracellular Ca^{2+} influx, mediated by TRPV4 and TRPA1 channels, and Ca^{2+} release from intracellular stores. Notably, experiments on astrocytes from AQP4-KO-/- showed a delayed response.

Collectively, we show the impact of novel technologies for understanding the mechanisms behind astrocytes function as well as the use of this technologies to target astrocyte functioning.

Acknowledgment

I would like to thank the people who supported me and helped me during the last years. First of all, I would like to thank my supervisors, Dr. Valentina Benfenati, Dr. Marco Caprini and Prof. Barbara Monti. I will specially thank Dr. Valentina Benfenati for giving me the opportunity to work in such a multi-disciplinary, international and stimulating environment that was essential for this learning experience. I am also very grateful to Dr. Michele Muccini the director of National Research Council-Institute for Nanostructures Materials (CNR-ISMN), the Institution that support the research program of my PhD course, as well as the director of ISOF, Dr. Roberto Zamboni.

I would also like to thank the international research project Olimpia (FP7-PEOPLE-212-ITN, GA 316832) that mainly supported my PhD, as well as the Air Force Office of Scientific Research (AFOSR) project ASTRONIR (FA9550-17-1-0502).

A special thanks to all the people I have worked with at CNR and at the University of Bologna such as Emanuela Saracino, Marianna Barbalinardo, Simone Bonetti, Assunta Pistone, Anna Sagnella, Tamara Posati, Francesco Formaggio and Alessia Minardi for helping me when I needed. I would like to specially thank Emanuela Saracino for her support specially in the last two years, not only in the lab but also outside.

Many thanks to Dr. Stefano Toffanin, Dr. Manuela Melucci, Dr. Vincenzo Palermo and Dr. Francesco Mercuri from CNR and Prof. Grazia Paola Nicchia from the University of Bari for the precious and fruitful collaboration as well as the people from their groups that I had the luck to work with.

I am grateful to Prof. Anita Mahadevan-Jansen for giving me the opportunity to spend some time in her lab in the University of Vanderbilt and to Wilson Adams that was a very supportive colleague in our collaboration between University of Vanderbilt and CNR.

I would also like to thank my family and specially my parents Antonio Borrachero and Isabel Conejo for being there when I need it and my sister Beatriz Borrachero for giving me the motivation to get interested in Neuroscience. I would also like to mention my uncle Francisco Conejo and my grandmother Isabel Reina that left us during my PhD. I really wish I could share this moment also with them. I would like also to thank all my friends with a special mention to Victoria Soler and Moises Alvaro that were there to listen when I needed.

Last but not least, I want to thank Ruben Blanco for being my biggest support during the last years. I want to thank him to be always with me to help in the bad moments and give me the strength to continue but also to be there to celebrate the good ones.

Index

Chapter 1 – Introduction.....9

1. Brain structure.....9

2. History of Neuroscience.....10

2.1 Neuron doctrine.....10

2.2 History of glia.....11

3. Physiological function of astroglia.....14

3.1 Astrocytes and brain homeostasis.....14

3.2 Regulation of synaptic transmission.....20

3.3 The glymphatic system.....22

3.4 Astrocytes and circadian rhythms.....23

4. Astroglial membrane proteins and calcium signaling.....23

4.1 Ion channels.....24

4.2 Receptors.....34

4.3 Calcium signaling and calcium waves in astrocytes.....37

5. Astrocytes pathophysiology.....40

5.1 Edema.....42

5.2 Epilepsy.....43

5.3 Brain tumors.....44

5.4 Alzheimer's disease.....45

5.5 Depressive disorder.....46

7. State of the art techniques to study astroglial cells 47

8. Novel techniques for the study of astrocytes 49

8.1 Biomaterials interface and interaction with astrocytes 49

8.2 Organic bioelectronics 57

8.3 Photostimulation 64

9. Aim of the thesis 68

Chapter 2- Experimental Section 71

1. Astroglial cells preparation 71

2. Biocompatibility assays 72

3. Molecular, functional and morphological characterization of astroglial cells 73

4. Material synthesis fabrication and characterization 75

5. Device fabrication 76

6. Solutions and chemicals 77

7. Statistical Analysis 78

8. Image processing and analysis 78

Chapter 3 – Electrical stimulation of calcium signaling in astrocytes by an organic transistor architecture 79

1. General overview 79

2. P13 is a biocompatible substrate for the growth of primary astrocytes 80

3. Extracellular electrical stimulation by O-CST elicits astrocytic intracellular Ca^{2+} increase 81

4. O-CST operation induces astrocytes swelling and preserves cell viability 88

5. O-CST device architecture enable calcium signalling 90

Chapter 4- Biomimetic graphene for enhanced interaction with the external membrane of astrocytes 93

1. General overview 93

2. GO–PL promotes cell adhesion without inducing gliosis 95

Chapter 5- Astrocyte modulation of intracellular calcium signaling by label-free pulsed infrared irradiation. 99

1. General overview 99

2. INS evoke intracellular Ca^{2+} signaling in primary astrocytes *in vitro* 99

3. TRPV4 and AQP4 expression are essential for the intensity and for the dynamic of the INS evoked response in astrocytes 104

4. INS response in differentiated astrocytes 106

Chapter 6- Conclusion 110

Chapter 7- References 113

Chapter 1 – Introduction

1. **Brain structure**

The human brain is constituted by several cell types. Neurons are electrically excitable cells that can fire action potentials, that is propagated to neuronal network through chemical synapses. On the basis of their ability of generating and propagating action potential, neurons were considered as the functional unit of the brain cells enabling for our cognitive abilities.

Glial cells are non-excitable cells as they do not fire action potentials. Glial cells are broadly classified into macroglial and microglial cells. Microglial cells direct the immune response in the CNS by carrying out phagocytosis of debris and apoptotic cells, remodeling and removal of synapses and response to injury or pathogens[1–5]. They are present in all regions of the CNS and are highly motile. Microglia can extend their processes in any directions[6] due to their small size and round morphology with numerous branches, allowing them to surveil their local environment[7]. Classically, microglia were considered to be quiescent under physiological conditions, nevertheless, it is now known that they can also exhibit localize motility under reactive conditions[8]. Interestingly, recent studies suggested that microglia can play an active role in synaptic plasticity, demonstrating that dynamic interactions occurs between neurons and microglia shape the circuitry of the nervous system in the healthy brain[9].

Oligodendrocytes and astrocytes form the macroglia. Oligodendrocytes possess several short processes that envelope axons in a structure called myelin sheath. Myelin is a membrane rich in saturated lipids and proteins that insulates axons to increase the propagation speed of action potentials, facilitating a process termed saltatory conduction[10,11]. Furthermore, oligodendrocytes secrete neurotrophins such as brain derived neurotrophic factor (BDNF), nerve growth factor (NGF)

and Neurotrophin-3[12] which mediate neural outgrowth. Additionally, oligodendroglial membranes contain monocarboxylate transporter 1 (MCT 1) that can deliver pyruvate, ketone bodies and lactate to the enwrapped axon for metabolic regulation[13].

Astrocytes, or astroglial cells, which are the cells on which this thesis is focused, are the major type of glial cell present in the central nervous system (CNS). Many studies affirm that human brain possess 100 billion neurons and 10 times more glial cells[14–17]. Although these numbers are controversial it is established that glial populations and complexity in the brain increased in the evolutionary ladder. Indeed, a difference in glial has been observed across different species, for instance, human astrocytes are significantly bigger and present more elaborated processes when compared with rodent astroglial cells. The physiological role of astrocytes has been "recently" highlighted in the control and maintenance of ionic balance, of water transport in the extracellular space, as well as regulation and recycling of synaptic neurotransmitters. They are key players in the cerebrovascular regulation of the blood flow [18,19]. Nonetheless they provide metabolic support to neurons. Besides, astroglial cells can release bioactive molecules, such as ATP, glutamate and adenosine, and D-serine that behave as so called gliotransmitters[20]. These data highlight the importance of astrocytes for brain functioning. However, much remains to be known about astroglial functional and molecular characteristics.

2. History of Neuroscience

2.1 Neuron doctrine

The neuron doctrine, that was formally presented in 1891, still widely accepted in modern neuroscience, describes neurons as the single independent unit in the nervous system[21]. Many scientists contributed to this theory during the 19th century. The best known is Santiago Ramon y

Cajal (1852-1934) that described in detail almost every part of the CNS thanks to the Golgi method, although von Waldeyer-Hartz (1836-1921) is generally credited with its formulation. Neuroscience is what it is today largely because of the neuron doctrine and the law of dynamic polarization that describes neurons as a polarized entity where nerve impulses, or action potentials, occurs. [22] [23,24]. The neurocentric view has historically overshadowed the study of glial cells. However, on the basis of unconfutable *in vitro* and *in vivo* evidence, there is a growing attention on the importance of glial cells and their molecular, structural, functional relationship with neurons. Taking into account the function of the multiple cell types comprising the nervous system together may lead to improved understanding of the nervous system, its functions and pathologies.

2.2 History of glia

Rudolf Virchow (1821-1902) was the first one to introduce the term of "neuroglia" that he described as connective tissue that could contain a certain number of individual cells[25,26]. However, the first glial cells were described even before by Robert Remark in 1838 when he observed the covering sheath of the nerve fibers (i.e., Schwann cells)[26]. In 1851, Heinrich Müller first described the radial fiber in the retina that was afterwards known as Müller glial cells[27] but it wasn't till 1858 when Max Schulze obtained detailed images of these cells[26]. In the same year, Karl Bergmann identified radial fibers in the cerebellum that were later identified as glial cells by Camillo Golgi[28]. Around 1865, Otto Deiters described for the first time the presence of stellate cells in the white and gray matter of the human brain[29]. It was not until, Jakob Henle in 1869 published the first image of cellular networks formed by these cells that now we know as astrocytes[29]. Additional discoveries arrived also from the efforts of some of the most prominent histologists at that time, including Camillo Golgi and Santiago Ramon y Cajal. Golgi performed the first histological staining of neuroglia and he described cells that where afterwards identified with astrocytes and oligodendrocytes. He also noted astrocytic endfeet and their contact with vasculature,

suggesting that astrocytes were involved in metabolic support and nutrient exchange[30]. Meanwhile, Ramon y Cajal invented gold-chloride sublimate staining technique, that significantly improved microscopic visualization of glial cells in brain tissue (Figure 1)[31]. Using his technique, Cajal confirmed that radial glia are the origin of astrocytes and also that astroglial cells can divide in the adult brain laying the basis for the current discoveries made on the stem properties of astroglial[26]. In 1893, Michael von Lenhossek proposed the term astrocytes that is used still nowadays while in 1894 Carl Ludwig Schleich (1859-1922) first claimed that the interaction between neurons and glial cells are important for brain functioning [25,29]. The latter thought that glial cells represented the inhibitory mechanisms of the brain, controlling brain functions by changing their cellular volume. According to Schleich, swelling of glial cells inhibits neuronal communications while shrinkage facilitate signal propagation[29]. The first involvement of astrocytes in disease was given by Wilder Penfield and Pío del Río-Hortega in the 1920s when they investigated the role of glial cells in response to injury, studying the changes in cells after a wound[32]. Río-Hortega developed also the ammoniacal silver carbonate method (figure 1), that allowed him to distinguish between the three main glial cell types in the brain being able to separate the "third element" described by Cajal into two different cell types: microglia and oligodendrocytes.[33]. Despite the description of glia appeared almost 50 years before the neural doctrine. During the 20th century, glial cells were largely much ignored by neurobiologists. In the early 1960s was the first demonstration that glial cells present electrophysiological properties different from neurons. Glial cells were also found to have a lower resting membrane potential than neurons[7,8]. First electrophysiological recordings from glial cells were performed by the group of Stefen Kuffler in 1964-1965[35]. The importance of astrocytes in uptake of extracellular potassium released by neurons after synapses was first described in 1965[36]. Similarly, electrical coupling between glial cells was first presented in 1966 leading to the hypothesis of potassium spatial buffering, which was not confirmed until 1969 until the identification of gap junctions in astrocytes[37,38].

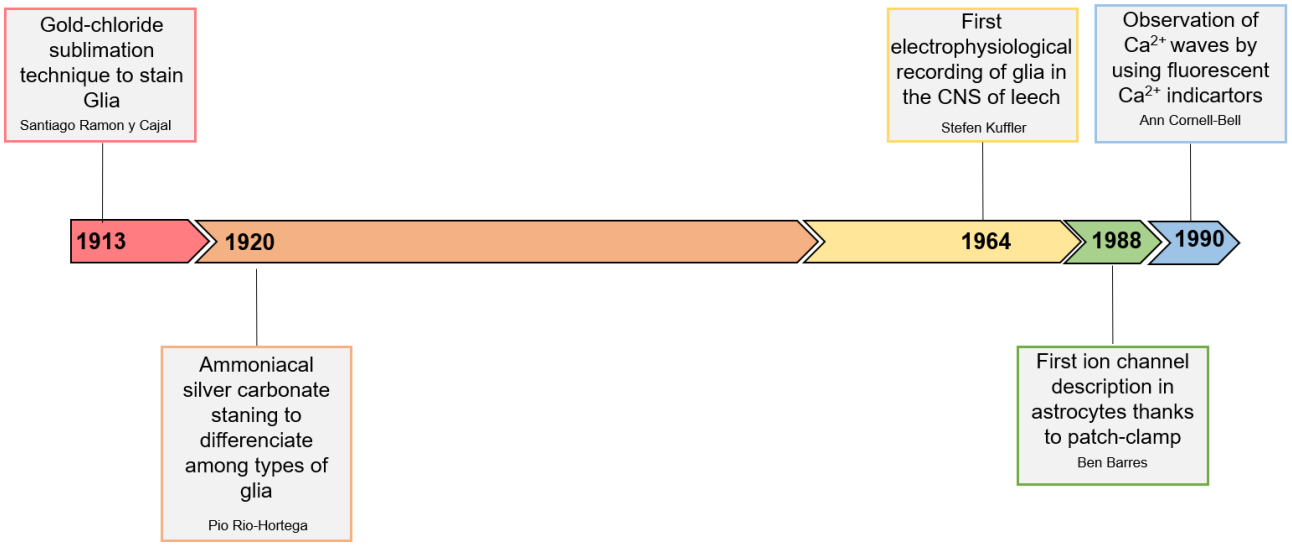

Figure 1. Abbreviated timeline of the main technological advances in the research of astroglial cells.

A new era in the study of glial cells physiology began at the end of the 1970s and early 1980s due ***to several important technological advances***. Specially, the patch-clamp electrophysiology, fluorescent calcium indicators, and the preparation and maintenance of glial cell cultures (Figure 1)[39–43]. It was not until the 1980s were glial cells were started to be seen as an active cell with a supportive role when glutamate and GABA receptors were identified in astrocytes and oligodendrocytes[44–47]. In 1990, it was demonstrated that astrocytes can communicate via calcium (Ca^{2+}) waves. Subsequently, in 1994 astrocytes were shown to stimulate Ca^{2+} elevation in neighboring neurons, establishing thus for the first time a bidirectional communication between astrocytes an neurons (Figure 1)[48,49]. Both discoveries together and the fact that astrocytes can respond to neurotransmitters with propagating intra- and intercellular Ca^{2+} waves suggested that astrocytes were capable of sensing and likely participated in synaptic transmission. Such a suggestion implied that astroglial cells were important for information processing in the brain[50]. In 1994, two independent studies reported that astrocytes-neurons co-cultures can trigger Ca^{2+} increases in neighboring neurons, giving support to the emerging idea that astrocytes were key partners in higher order brain processes through modulating synaptic transmission[49,51]. Currently,

it is known that astrocytes express a wide number of ion and water channels, as well as membrane receptors that make them critical for brain physiology and pathophysiology.

3. **Physiological function of astroglia**

Current data about astrocytes suggest that they are critically involved in many brain functions. The primary function is sustaining CNS homeostasis at all levels of organization, from ionic and molecular up to cellular network and whole organ systemic control. The main function of astrocytes defined over the past decades by *in vitro*, in situ and *in vivo* studies are overviewed in the following sessions, describing molecular and cellular mechanism so far believed to be responsible for the respective physiological astrocytic role.

3.1 Astrocytes and brain homeostasis

Extracellular space (ECS) ECS is the interstitial volume between brain cells that occupy 20% of the brain volume. ECS is composed by ions, essentially Na^+, K^+, Ca^{2+} and Cl^- that are unequally distributed across the plasma membrane (Figure 2). The maintenance of ions, water, organic molecules (such as neurotransmitters) concentrations between the ECS is critical for brain function[52]. Indeed, electrochemical gradient across the plasma-membrane generated by differences in ions concentrations across the plasma-membrane serve as driving force for electrical activity of neurons setting and determining their membrane potential, and in turn, the threshold of action potential initiation. Accordingly, unbalanced changes in the ECS electrolytes concentration, might induce alteration of the neuronal excitability and that, affect neuronal network capability to generate action potential and propagate communication signal through synapse [53,54].

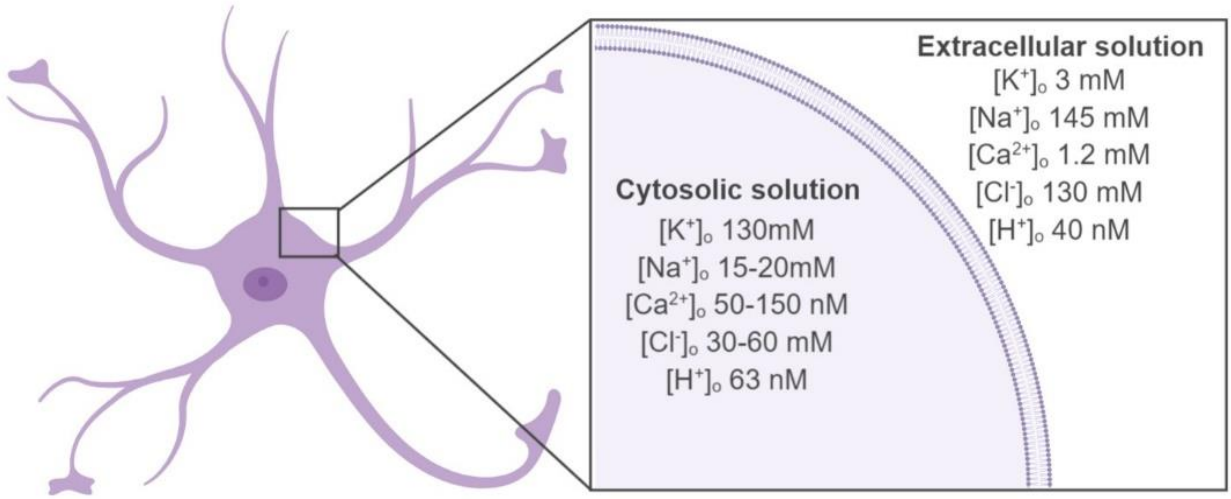

Figure 2. Intracellular and extracellular ion composition in CNS [20].

In this context, astrocytes are the cells responsible for the homeostatic regulation of water and ion concentration regulation as well as the control of neurotransmitter distribution in the ECS [52,55,56].

The exchange between microvessels and ECS are regulated by the physical barriers formed by epithelia separating the blood from the ventricular cerebrospinal fluid and from the subarachnoid cerebrospinal fluid. Endothelial cells forming the blood brain barrier (BBB) that delimit the boundary between the interstitial fluid of the brain and blood[57]. The BBB is a key player in the mediation of bidirectional communication between cerebral tissue microenvironment and blood and in the control of solutes concentration and water in the interstitial space[58]. Astrocytes are indispensable for the maintenance and formation of the BBB[59]. Endothelial cells forming the brain capillaries are in close contact with astrocytic endfeet processes and mesenchymal-like cells called pericytes (Figure 3C). Astrocytes are therefore, in a key position to act as a bridge enabling flow and control of ions, water, metabolites by neuropil to the blood vessel[60].

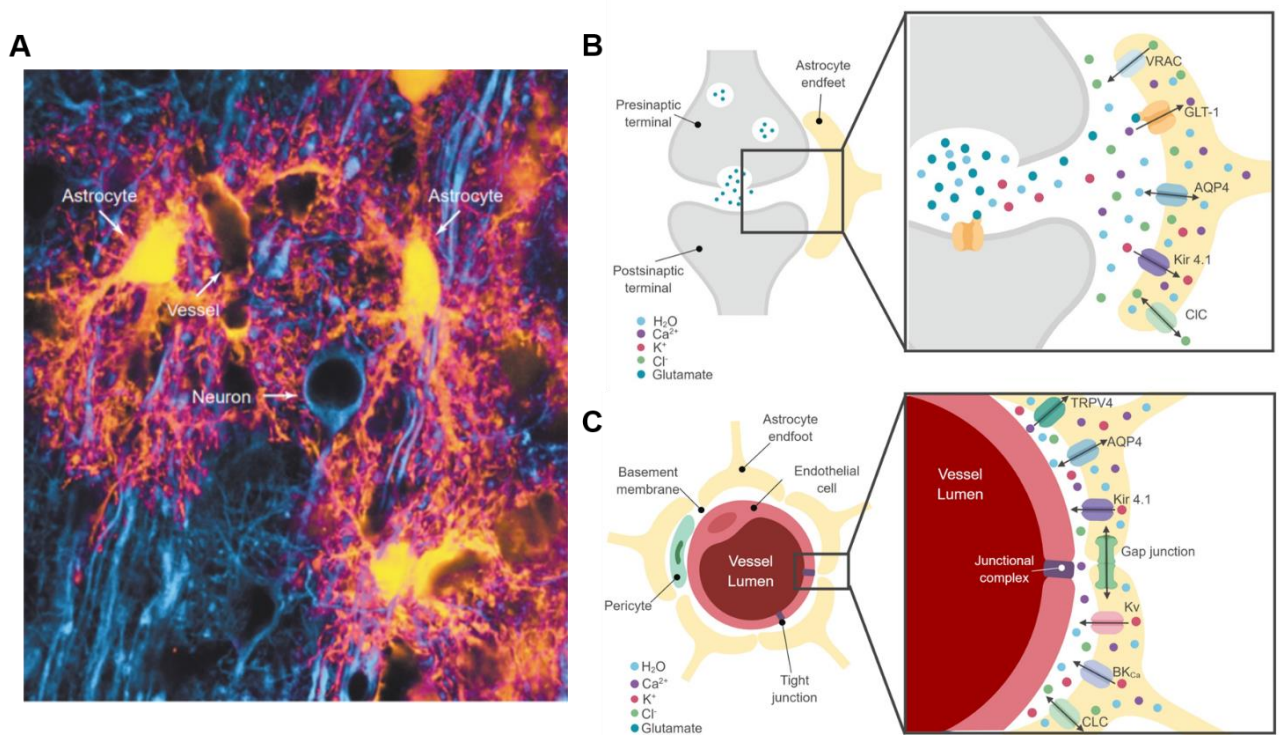

Figure 3. A) Astrocytes and neurons organization in rat cortex. Neurons are marked for microtubule-associated protein 2 (MAP-2) (blue), while astrocytes are marked enhanced green-fluorescent protein (eGFP) (yellow). A vessel is also seen thanks to the enwrap of eGFP-positive astrocytic endfeet. B) Astroglial ion channel expression in contact with synapses. The role of astrocytes to maintain homeostasis is crucial for synapses to occur and as a result of action potential astrocytes are in charge of cleaning the neurotransmitters and ions release in the perineuronal milieu. Astrocytes uptake the extracellularly accumulated K^+ and glutamate to maintain their physiological levels. C) At the glia-vasculature interface K^+ is release. K^+ is spatially buffered through the syncytium of astrocytes connected via gap junctions and is rapidly counteracted by water flux. Intracellular [Cl^-] is important also to set the condition for the passive K^+ uptake. Ca^{2+} channels like TRPV4 has also been shown to be express in astrocyte endfeet. Pumps and transporter in charge to transmembrane movement of ions were not included. Figure A reproduced from ref [61] with permission from Elsevier.

Astrocytes elongations endfeet enwrap neurons and blood vessels form neuron-astrocyte interface and so-called gliovascular interface. Notably at each interface astrocytes expressed a polarized distribution of ion, water channels and transporters in so-called microdomains that are devoted to specific functional homeostatic processes such as ***regulation of extracellular potassium homeostasis, brain and cell volume homeostasis, pH and neurotransmitters homeostasis*** [52,57,62,63] (Figure 3). Besides, astrocytes are highly connected between them by gap junctions allowing astrocytes to act as a functional syncytium enabling a rapid communication and coordinated functionality through larger areas of brain surface[64].

3.1.1 Astrocyte regulation ion homeostasis

One of the main homeostatic functions of astrocytes is the ***maintenance of the extracellular concentration of potassium ($[K^+]_{out}$).*** After a series of action potentials, the basal $[K^+]_{out}$ rises to ceiling levels that, if remains unbalanced, depolarize neuronal resting membrane potential and force inadvertent action potentials. The overexcitation of neuronal network ultimately lead to uncontrolled synaptic release of neurotransmitters, that compromise CNS functionality and over a longer term results in loss of neuronal integrity and viability [65–67].

The mechanisms underlining K^+ balancing by astrocytes are called K^+ uptake and spatial K^+ buffering[68]. Potassium uptake, astrocytes take the excess of K^+ ions by Na+/K^+ ATPase. Electroneutrality is maintained by the efflux of cations like Na^+ and by the influx of Cl^-. K^+ uptake might also be accompanied by osmotically driven water influx and swelling[57].

K^+ ions accumulated in astrocytes are released back into the ECS restoring the distribution of K^+ in the cell[69–71]. Astrocytes are highly permeable to K^+ because of the variety of K^+ channels expressed in their plasma membrane. Among them inward rectifying K^+ channels (Kir) mainly supports and underpin the astroglial K^+ conductance involved in potassium buffering.

Indeed, so called K^+ buffering relies on local K^+ uptake and dissipation through astroglial network connected by gap junctions[57,69]. When K^+ accumulates at the perisynaptic space, the resting membrane potential of astrocytes is negative with respect to the Nernst equilibrium potential for K^+, causing a driving force that leads to an influx of K^+ into astrocytes. Potassium influx in turn propagates through electrically coupled astrocytes to move the K^+ ions to regions with a lower concentration[72].

Chloride homeostasis is also essential for neuronal communication. Indeed Cl^- is an important counter ion for maintenance of electrical equilibrium. Astrocytes can respond to GABA by Cl^- efflux to balance neuronal Cl^- entry and maintaining basal $[Cl^-]$ to preserve the driving force for Cl^-

driving inhibitory neurotransmission[73]. Recent studies have also demonstrated the role of astrocytes in maintaining GABAergic neurotransmission and revealed the role of astroglial syncytium for Cl- homeostasis as connexons, the proteins forming gap junctions, inhibition during GABAergic transmission resulted in the breakdown of Cl^- gradient in neurons[74].

Homeostatic control of pH is pivotal for brain functioning as small changes in pH significantly affects neuronal excitability and synaptic transmission[20]. Astrocytes can regulate extracellular pH by glutamate-mediated uptake of H^+ and by supplying the extracellular environment with HCO^{3-} [75,76]. Astrocytes have also been shown to release H^+ by active protons pump and experiments in situ show that they possess pH buffering capability[77].

The ability of ***astrocytes to regulate their cellular volume*** in response to physiological stimuli is crucial for ***brain volume homeostasis.*** After increases in cell volume induced by aniso-osmotic gradients, a feedback mechanism called regulatory volume decrease (RVD) is activated to recover initial cell volume values by promoting osmolyte efflux and consequent osmotically driven water outflow (Figure 4)[57].

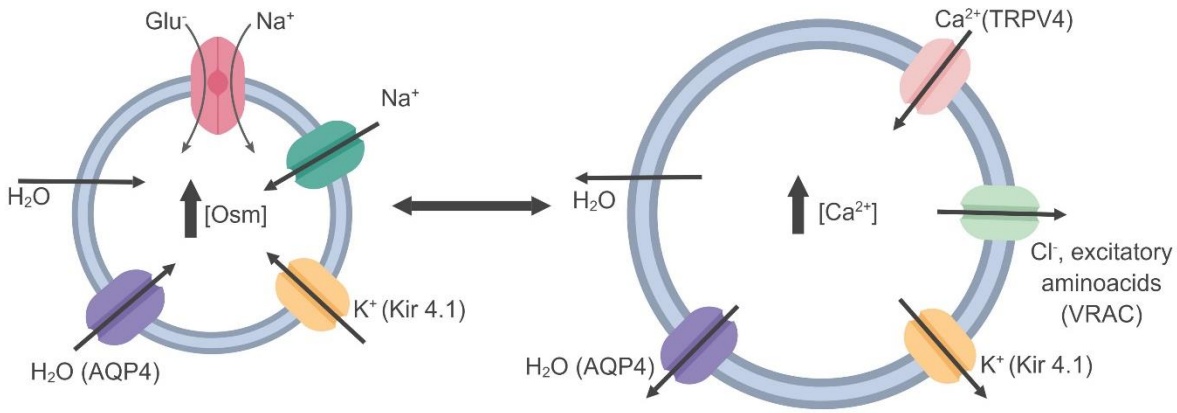

Figure 4. Scheme representing proposed mechanism for astrocyte swelling and cell volume recovery. Astrocytes can modify their volume in response to neuronal action potential when K^+, Na^+ and glutamate uptake occur causing an increase in osmolytes that produce water influx. This leads to a series of events to recover cell volume that is called regulatory volume decrease (RVD). Studies *in vitro* showed that Ca^{2+} elevation might be involved in osmotransduction. RVD is based on the efflux of intracellular solutes that generate osmotic gradient accompanied by water. For simplification ion pumps and transporters contributing to the transmembrane movement of ions are not included in the representation, for a complete review see[62].

Astrocytes control water movement via several pathways. The most notable one is aquaporins and membrane transporters. In astroglial endfeet, the colocalization of AQP4, the main water channel in astrocytes, and Kir 4.1 has prompted the hypotheses possible link between water and K^+ movement. To fully understand RVD, it is important to consider the role of $[Ca^{2+}]_i$ elevations that occurs in response to cells swelling. RVD on astrocytes caused by hypotonic stress *in vitro* has been shown to be dependent on $[Ca^{2+}]_i$ increases and abolished after decrease of extracellular $[Ca^{2+}]$[78]. Moreover, astrocytes respond to hypotonic challenge by increasing Cl^- conductance by the activation of volume-regulated anion channels (VRACs)[79,80]. Altogether, water influx following intracellular osmolyte concentration (K^+ and Na^+) in astrocytes cause an increase in cell volume that activates RVD that is accompanied by an influx of Ca^{2+} and an efflux of Cl^- and K^+ that cause water efflux and volume decrease.

3.1.2 Neurotransmitters homeostasis

To prune synaptic transmission, neurotransmitters must be quickly removed from the synaptic cleft following their release. Metabolic intermediates must also be restored to the presynaptic terminal to regenerate neurotransmitters and maintain synaptic function[81]. Glutamate act as a major excitatory neurotransmitter in the CNS; concentrations of glutamate can reach millimolar levels in the synaptic space[82]. Astrocytes uptake about the 80% of extracellular glutamate in the CNS and provide the renewal of glutamate in synaptic terminals. Astrocytes express glutamine synthetase, an enzyme fundamental for glutamate conversion into glutamine[83]. Glutamine is also a precursor for glutamate when metabolized in neurons by the phosphate-activated glutaminase[20]. A recent study showed that there is a feedback mechanism that links glutamate uptake in astrocytes with the release and movement of glutamine to neurons, suggesting astrocytic modulation of neuronal

function[84]. Glutamine in neuronal presynaptic terminals can be converted into glutamate in excitatory neurons while in inhibitory neurons, glutamate is then converted into γ-aminobutyric acid (GABA)[85].

GABA is the main inhibitory neurotransmitter in the CNS. Both neurons and glial cells are known to express GABA transporters[86]. Astrocytic GABA transporters surrounding GABAergic synapses are tactically positioned to contribute terminating or modulating GABAergic neuronal transmission by locally GABA uptake[87].

3.2 Regulation of synaptic transmission

Astroglial endfeet cover at least half of the synaptic contract in the CNS, though the degree of coverage differs between diverse brain regions. Perysinaptic astroglial membrane present a great variety of ion channels are ligand receptors. Ion fluxes in this area are of particular importance for the generation of Ca^{2+} and Na^{+} signals in astrocytes, leading to coupling of homeostatic processes of astrocytes with neuronal activity[20]. This intimate contact between astroglial membrane and synaptic areas led to the concept of tripartite synapses (Figure 5) [81].

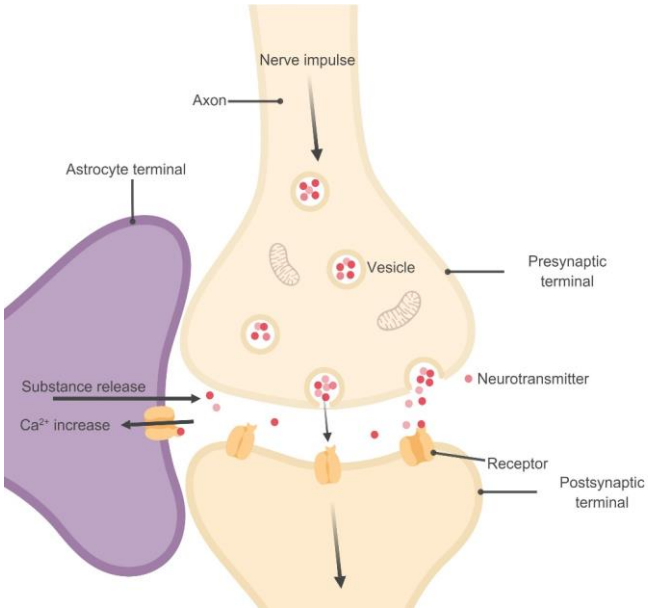

Figure 5. The **tripartite synapse.** Astrocytic receptors can interact with the neurotransmitters released from the presynaptic terminal of neurons activating rises in Ca^{2+} ions in astrocytes. Astrocytes can respond releasing diverse

neurotransmitters and neuromodulators, such as, ATP, glutamate, etc. They can act back on neurons to modulate synaptic activity.

In the tripartite synapse model astrocytes contribute to the regulation of synaptic transmission. Astroglial processes are a structural part of the synapse together with the pre and postsynaptic neuronal terminals. The model focuses on a bidirectional, fast glial-neuronal communication where neurotransmitters induce glial Ca^{2+} signaling causing the release of neurotransmitter from the astrocyte to the synaptic cleft. Astrocytes can control the initiation and shape of synaptic networks, by controlling ion and neurotransmitter homeostasis in the synaptic volume and contributing to synaptic pruning[88].

Experiments performed in the past three decades showed that astroglial cells can release neurotransmitters and neuromodulators, usually known as gliotransmitters because of their glial origin. Among these molecules are ATP, GABA, glutamate, Glycine, L- and D-serine, kynurenic acid and lactate[89–93]. The issue related to astrocytes release of gliotransmitters is still controversial, particularly the extent of its physiological relevance. ATP has been observed to be release from astrocytes, *in vitro*, in situ and *in vivo*, frequently occurring by exocytosis and diffusion through membrane channels[20]. GABA synthetizing enzymes has been documented in astrocyte from the cerebellum, hippocampus and neonatal optic nerve[94–96]. The release can be mediated by GABA transporter or by diffusion via anion channels[20]. Glutamate release from astrocytes has been hypothesize to modulate neuron activity[97]. Glutamate release can occur by diffusion through membrane channels, Ca^{2+} exocytosis or exchange via the cystine-glutamate antiporter[97]. The release of glycine from astroglial cells is crucial for tonic inhibition of motor neurons[98]. As it occurs with GABA, glycine is release by diffusion through anion channels or by specific transporters[20].

Astrocytic release of the neuromodulator D-serine seems to occur after the conversion of L-serine by serine racemase substrate, an enzyme that isomerizes D-serine from L-serine. L-serine is

exclusively synthesized in astrocytes, making astrocytes critical for D-serine neuromodulation[20]. Additionally, kynurenic acid (KYNA) is an endogenous antagonist of NMDA receptor and α7 nicotinic receptors. The release of KYNA from astrocytes is important for the regulation of glutamatergic, GABAergic, cholinergic and dopaminergic synapses[99–103]. Astrocytes can also release the lactate they produce that act is not only an energy substrate but also a signaling molecule capable of mediate astrocyte-neuronal communication[104].

The tripartite model has further developed into a multipartite synapse where apart from the pre- and postsynaptic terminal and the perisynaptic process from astrocytes, and the process of neighboring microglial cells are all in contact with the synaptic structure. The extracellular matrix (ECM) also plays an important role and extends also extrasynaptically[20,105].

3.3 The glymphatic system

For a proper control of tissue homeostasis, it is important to remove the excess of fluid and interstitial solutes. In peripheral tissues, interstitial fluids return to the general circulation via the lymphatic system[106]. The CNS has an extremely high metabolic rate; thus, it is very sensitive to its homeostatic environment. However, the brain lacks lymphatic vessel system. Recent studies has noted lymphatic vessel in the dural and meningeal membranes, though not directly part of the brain[107,108].

Astrocytes endfeet covers the 99% of the vasculature of the CNS creating an unique perivascular space[109]. Recent work identified a coordinated pathway that use the perivascular space for interstitial solute clearance and rapid fluid transport, called the “glymphatic system”. The system works in a similar way with the peripheral lymphatic system but relies on astrocytes AQP4 water channels[110]. This pathway serves as a discarding system for fluid, larger solutes and proteins from the CNS. For instance, 65% of β-amyloid is cleared by the glymphatic system[110]. Studies showed that glymphatic transport rates decrease with age, and increase in rodent models of stroke, diabetes

and Alzheimer's disease[111–114]. They glymphatic system can also deliver lipids and glucose to maintain brain metabolism, and can play an important role in removal of lactate[115–117]. Altogether, the glymphatic system may therefore act as a crucial pathway for the elimination of toxic substances and the delivery of metabolic substrates for the brain.

3.4 Astrocytes and circadian rhythms

Astrocytes possess circadian genes that go through rhythmic expression[118]. Human circadian clock is localized in the suprachiasmatic nuclei (SCN) in the anterior hypothalamus. Isolated astrocytes from SCN present also circadian activity, that consist on circadian ATP release following inositol triphosphate ($InsP_3$)-induce Ca^{2+} signaling and controlled by mitochondria[119,120]. Moreover, astrocytes in the SCN present rhythmic morphological changes from stellate at day to more protoplasmic shape at night. These changes are accompanied by modifications in glial fibrillary acidic protein (GFAP) and glutamate transporter expression. This circadian cycle is also associated with a different glial coverage of synapses being higher at night[121].

4. Astroglial membrane proteins and calcium signaling

All the functions mentioned in the previous section depend on membrane proteins, such as ion channels and receptors, that helps maintaining proper ion distribution – an indispensable function for normal brain physiology (Figure 2). Moreover, membrane proteins are also involved in the release of neurotransmitters. Another important mechanism that enable astrocytic function is the **oscillations in the intracellular calcium concentration ($[Ca^{2+}]_i$).** The latter is the main intracellular communication signaling pathways that mediates and it is implicated in almost all astrocytic functionality.

4.1 Ion channels

4.1.1 Potassium channels

Inward rectifying K^+ channels (Kir) are potassium channels that allow K^+ ions pass easier into the cell than outward from the cell at membrane voltages more negative to the equilibrium potential of potassium ($E_{rev}K^+$). Structurally, Kir channels have 2 transmembrane domain and are presented in 16 subtypes classified into 7 families[122]. Kir 4.1 is the most common inward rectifying K^+ channel expressed in astrocytes[123]. They present voltage dependence and gating properties dependent by $E_{rev}K^+$. Kir currents are inhibited by Cs^+ and Ba^{2+}[124]. Kir 4.1 is usually concentrated in astrocytes endfeet that contact synapses and blood vessels[125]. It contributes significantly to the resting membrane conductance of astrocytes and elevations in $[K^+]_i$ increases inward K^+ currents, making Kir 4.1 a key channel for K^+ uptake and buffering in the brain and therefore for the control of brain homeostasis[124].

Voltage-gated K^+ channels (K_v) structurally present six transmembrane segments and are inactive at resting membrane potential. K_v channels open upon cell depolarization. There are 12 subfamilies of K_v channels, including delayed rectifying (K_D) and transient (K_A) channels, which are expressed in astrocytes[126–128]. Among K_D channels, K_v 1.5 and K_v 1.4 are dominantly expressed in astrocytes[129,130]. Transient currents recorded in astrocytes have been identified mainly with K_v 4, K_v 3 an K_v1 channels, with K_v 4 the channel that contributes to the 70% of this currents[131].

Calcium-dependent potassium channels (K_{Ca}), have been reported in astrocytes. Gating properties of these channels depends on cytosolic $[Ca^{2+}]$ and membrane depolarization[132]. Big conductance (BK), channels in astrocytes are expressed in endfoot processes and in contact with blood vessels they play a key role in rapid dilation of arterioles following neuronal activity[18]. Intermediate conductance (IK) channels have been identified also in endfeet in contact with vasculature contributing to neurovascular coupling and vascular tone[133].

***Two Pore-domain potassium channels* (K_{2P}),** are open at resting membrane potential. Single-cell PCR and immunocytochemistry studies revealed that several channels from this family are expressed in hippocampal astrocytes[20]. However, evidences for their contribution to astrocyte resting conductance is still controversial[20].

4.1.2 Sodium channels

Voltage-gated Na^+ channels (Na_v) are represented in thirteen isoforms that have been observed in astrocytes *in vitro* and in situ. Na^+ channels have been identified in different regions of the brain, but their exact localization and the physiological activation is not known yet. Experiments shown that Na^+ channels, in particular Na_v 1.5, play an important role in gliosis *in vitro*, but results *in vivo* are still lacking[134]. Furthermore, a constant Na^+ influx is also necessary to maintain internal [Na^+] needed for the proper functioning of Na^+/K^+-ATPase that in turn, is needed for K^+ homeostasis in the CNS[135].

4.1.3 Calcium channels

Voltage-gated calcium channels (VGCCs) mediate Ca^{2+} influx following membrane depolarization. They are complex proteins made of four or five different subunits encoded by several different genes[136]. Ca^{2+} current mediated by voltage-gated Ca^{2+} channels present diverse physiological and pharmacological properties, giving rise to classifying them in different types. L-type Ca^{2+} currents need a strong depolarization to be activated, and are blocked by phenylalkylamines, dihydropyridines and benzothiazepines. N-type, P/Q-type, and R-type channels also require a strong depolarization, but they are blocked by specific polypeptide toxins from snail and spider venoms. Instead, T-type Ca^{2+} currents are transient and activated by weak depolarization

and they are not sensitive to any of conventional antagonists[136,137]. L-type current have been recorded in cultured astrocytes, among them at molecular level Ca_v 1.2 and Ca_v 1.3 channels were found in cortical astrocytes[138,139]. In neonatal cortical astrocytes in culture expression of N-type, L-type, R-type and T-type has been detected at transcriptional and translational levels[140]. There are less evidence for their expression in situ. Activation of gliotic reaction in astrocytes induce an increase in L-type Ca^{2+} channels suggesting a role of L-type Ca^{2+} channels in astrogliosis. Astrocytes treated with LPS showed an upregulation of Ca_v 1.2 channels while deletion of these channels avoided gliotic response[141].

The superfamily of Transient receptor potential (TRP) channels is made of 27 known members in humans classified into 6 subfamilies[142]. TRP channels contribute to many different physiological functions being especially important for thermosensation, nociception, chemoception and taste[143,144]. They are permeable to Na^+, Ca^{2+} and K^+[145]. Several types of TRP channels are found in the CNS with particularly high expression of vanilloid (TRPV), ankyrin (TRPA), mellastain (TRPM) and canonical (TRPC) family receptors[146]. The structure of TRP channels is based on six transmembrane domains (Figure 6).

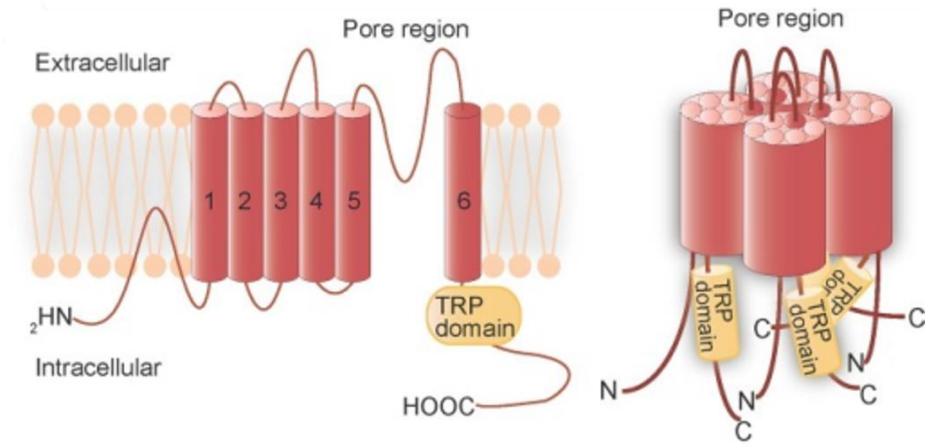

Figure 6. Transmembrane topology of TRP channels. The TRP proteins have six transmembrane domains and a TRP domain in the C-terminal region. The pore region is formed between the fifth and sixth transmembrane domains. Reproduced from [147] published in frontiers in physiology.

Several types of TRP are express in astrocytes. Among them a member of the TRPV family have been detected in astroglial cells. TRPV4 (Figure 7A and B) has been detected in cortical and hippocampal *in vitro* and in situ and with dominant expression observed in endfeet[148–150]. TRPV4 in primary cortical astrocytes can be activated by cell swelling and cause an increase in $[Ca^{2+}]_i$ that is blocked by TRPV inhibitor ruthenium red. Meanwhile, specific agonist 4α-phorbol 12,13-didecanoate (4αPDD) induce cationic currents[149]. Likewise, increases in $[Ca^{2+}]_i$ mediated by TRPV4 were recorded in hippocampal slices[148]. Furthermore, TRPV4 can act together with AQP4 in the development of RVD following hypoosmotic shock (Figure 3)[151].

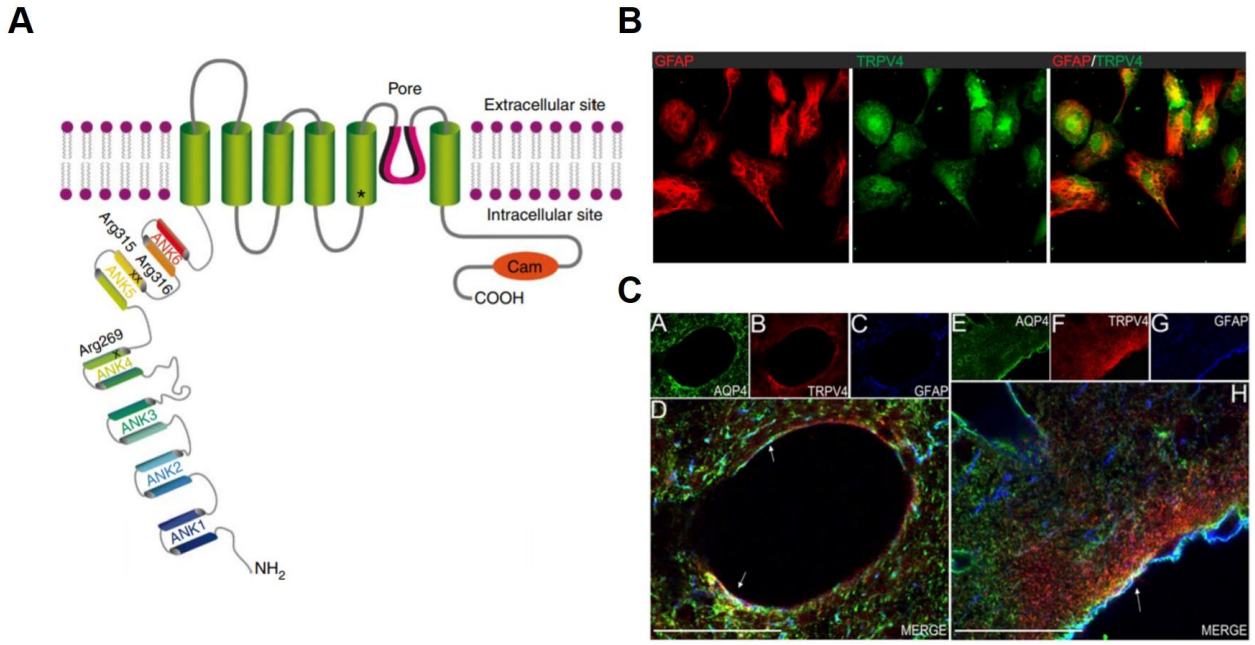

Figure 7. **TRPV4 structure and expression on astrocytes.** A) The TRPV4 protein is composed of six transmembrane domains (green) that includes the pore region (pink), a cytosolic N-terminal and an intracellular C-terminal tail. Reproduced from [152] with permission from Springer Nature. B) GFAP (Red) and TRPV4 (Green) immunostaining of Astrocytes isolated from sham-operated rats cultured from 4-5 days. Reproduced from [148] published by plosONE. C) (a-c) Single-plane confocal immunofluorescence images of large-caliber blood vessel of rat occipital cortex showing triple labeling for AQP4 (Green), TRPV4 (Red) and GFAP (blue). Merge is shown in d. (e-g) Single plane confocal immunofluorescence images of sagittal section of rat occipital cortex showing triple labeling for AQP4 (Green), TRPV4 (Red) and GFAP (blue). Merge is shown in h (Scale bar 50 µm). Reproduced from [151] published by PNAS.

TRPA1 channels are also expressed in astroglial cells. They are activated by noxious cold stimulus and diverse pungent substances and proinflammatory agents[142,144]. TRPA1 is implicated in the control of basal levels of $[Ca^{2+}]_i$ by frequent and "spotty" Ca^{2+} fluxes localized near the membrane

(Figure 8). Decrease in resting [Ca^{2+}] concentration mediated by TRPA1 reduced GABA uptake via GAT-3 elevation, thus modulating extracellular GABA concentration to regulate inhibitory synapses[153]. They also can mediate also D-serine release into the extracellular space contributing to NMDA receptor-dependent long-term potentiation (LTP)[154].

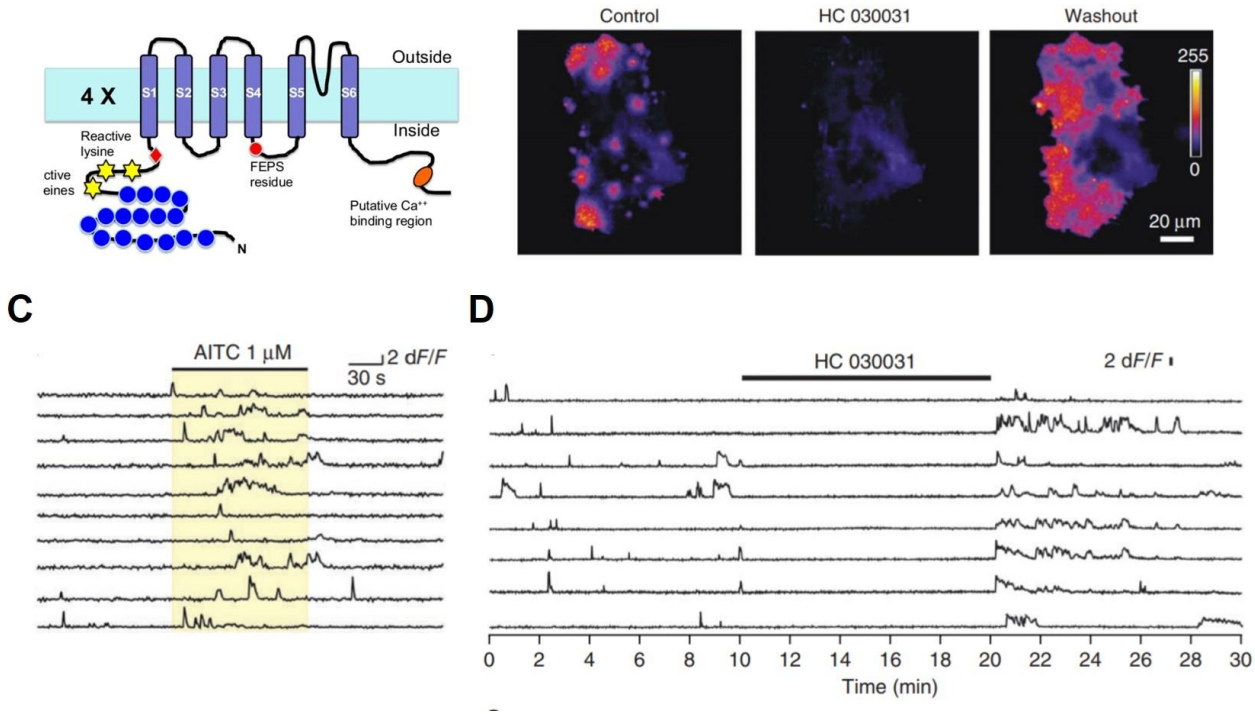

Figure 8. **Structure of TRPA1 and evidences of mediation of spotty Ca^{2+} signals in astrocytes.** A) The TRPA1 protein is composed of six transmembrane domains (purple), a cytosolic N-terminal and an intracellular C-terminal tail. Reproduced from [155] published by Springer. B) Calcium imaging frames obtained by 300-frame video before (control), during and after (washout) of HC 030031 (40 µM) showing that HC030031 almost completely block spotty Ca^{2+} signals. C) Intensity versus time of ten regions of interest (ROIs) of calcium imaging experiments performed in astrocytes *in vitro*, showing the spotty Ca^{2+} signals observed when adding AITC (1µM). D) Intensity versus time of eight ROIs of calcium imaging experiments showing the blocking of spotty Ca^{2+} signals using HC 030031 (40 µM). B,C and D are reproduced from [156] with permission from Springer Nature.

TRPC channels have also been detected at protein and mRNA level in freshly isolated and primary culture astrocytes. Seven members (TRPC1-7) exist under the TRPC subfamily. They are activated by phospholipase C (PLC), diacylglycerol (DAG) and mechanical stimulation[146]. In astrocytes, activation of TRPC channels contributes to Ca^{2+} signals mediated by purinergic, glutamatergic and mechanical stimulation[157]. Data also suggest that TRPC1 in astrocytes and most likely assembles as a heterotetramer with TRPC3, 4 and 5, which are responsible for store operated calcium entry

(SOCE), a central mechanism in astrocyte Ca^{2+} signaling and control of Ca^{2+} balance that connect endoplasmic reticulum with plasmalemmal entry of Ca^{2+}[146].

Calcium release activated calcium channels (CRAC) are plasma membrane Ca^{2+} channel that activate to slowly refill endoplasmic reticulum following depletion[158]. CRAC currents are the main component of SOCE in most of the non-excitable cells. Orai proteins are the molecular substrate of CRAC currents and STIM proteins control their gating acting as endoplasmic reticulum (ER) Ca^{2+} sensors[159]. Orai proteins have been detected in primary culture of astrocytes, while STIM1 and STIM2 are expressed in cultured astroglial cells with STIM1 being the dominant isoform[160]. siRNA silencing of Orai1 reduces SOCE in primary cortical astroglial cells. On the other hand, hippocampal rat astrocytes express Orai3 as the main isoform at levels six time higher than Orai2, while Orai1 is not detected[161].

Orai proteins have been detected in primary culture of astrocytes, while STIM1 and STIM2 are expressed in cultured astroglial cells with STIM1 being the dominant isoform[160]. siRNA silencing of Orai1 reduces SOCE in primary cortical astroglial cells. On the other hand, hippocampal rat astrocytes express Orai3 as the main isoform at levels six time higher than Orai2, while Orai1 is not detected[161].

Intracellular calcium channels and pumps are expressed in endomembrane of the ER and they are divided in two families that are inositol trisphosphate receptors ($InsP_3Rs$) and Ca^{2+}-gated Ca^{2+} release channels or ryanodine receptors (RyRs). The $InsP_3Rs$ are formed by three members: $InsP_3R1$, $InsP_3R2$ and $InsP_3R3$, which are all of them activated by $InsP_3$. While $InsP_3R1$ presents an open probability that increase at resting Ca^{2+} levels between 50-100 nM and 1μM the activity of $InsP_3R2$ and $InsP_3R3$ increase with $[Ca^{2+}]_i$. Data suggest that $InsP_3R2$ is the main isoform present in astrocytes; the deletion of $InsP_3R2$ strongly reduced or abolish ER Ca^{2+} release in cortical and hippocampal astrocytes[162–165]. There are also three types of RyR channels: RyR1, RyR2 and RyR3.

They are all activated by intracellular Ca^{2+} acting as an amplifier of Ca^{2+} signals[166]. The function of RyRs in astrocytes is still not clear. Ca^{2+} signal mediated by RyRs channels have been described *in vitro* and in situ from thalamic cells, but not from hippocampal cells when agonists were used[167–169].

4.1.4 Chloride channels

The CLC family of channels has nine members that show different tissue distribution and function in multiple tissue types. They are expressed not only in the plasma membrane but also in intracellular organelles. Structurally, they present 10-12 transmembrane domains[170].

ClC-1, ClC -2 and ClC -3 channels expression have been detected in astrocytes at protein levels and ClC-mediated currents have been characterized in cultured astroglial cells and hippocampal slices[79]. ClC-2 channels are localized in astrocyte processes near GABAergic synapses suggesting a role of GABAergic transmission by regulation $[Cl^-]$ in the synaptic cleft[171]. ClC-2 channel has a high open probability at resting potential, which is modulated by changes in cell volume Cl^- release in response to cell swelling[172].

Volume-regulated anion channels (VRACs) are activated upon hypotonic stress. They are made of close paralogues of the leucine-rich repeat-containing protein 8 (LRRC8) that forms hexameric complexes in the extracellular membrane[173]. In astroglial cells, VRACs are crucial for RVD and its currents have been characterized *in vitro*[79,174]. VRAC is involved also in the release of excitatory amino acids like glutamate, taurine and aspartate which can be blocked by the gap junction antagonist carbenoxolone (CBX)[175,176]. A recent study described that VRAC mediated ATP release is involved in Ca^{2+} wave propagation to not neighboring[177]. Therefore, the volume-regulated release of excitatory aminoacids and other molecules from astrocytes could in turn affect transmitter release from the presynaptic terminal[174].

4.1.5 Aquaporins

Three members of the aquaporin family are expressed in astrocytes, AQP1, AQP4 and AQP9, being AQP4 the dominant channel[178,179]. AQP4 is made of eight transmembrane segments and two translation initiation sites called Met1 and Met23 defining therefore two AQP4 isoforms known as M1 and M23[180]. AQP4 is concentrated in astrocyte endfeet where they are assembled into orthogonal arrays of particles, the basis for which is still unclear (Figure 9 B and C)[181].

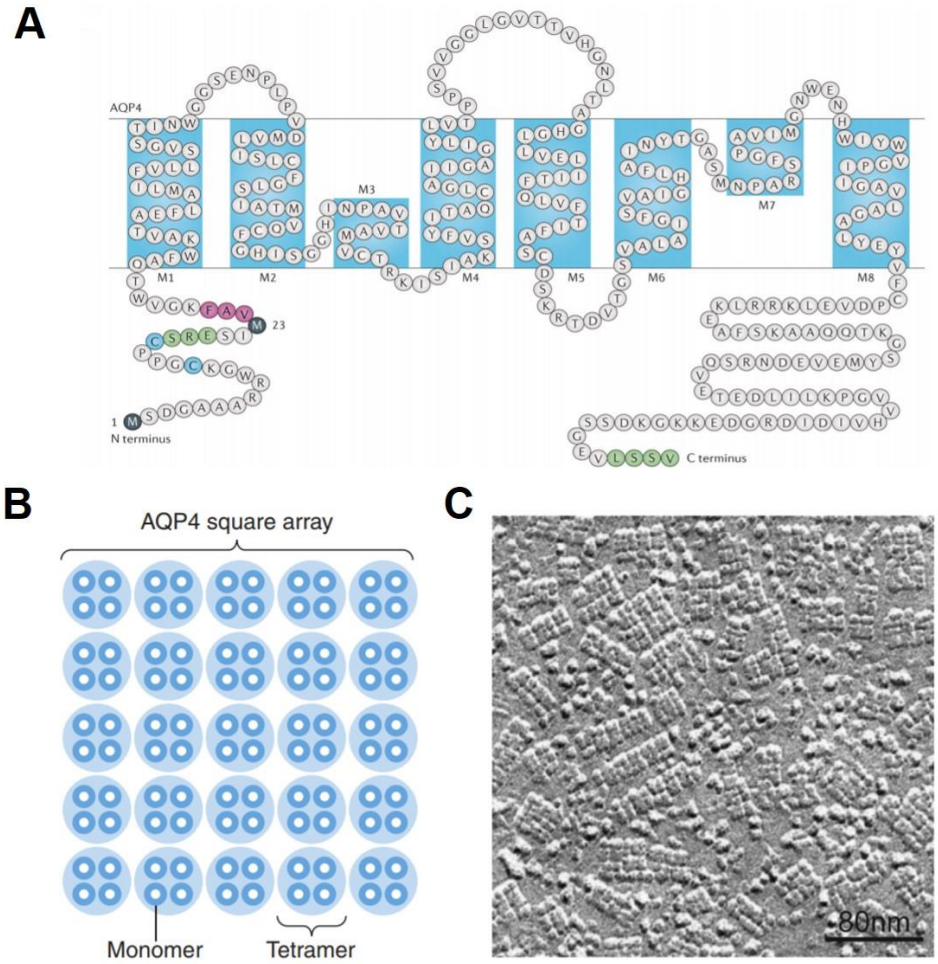

Figure 9. AQP4 structure and plasma membrane organization. A) Schematic representation of the primary aminoacids sequence and membrane topology of AQP4. It presents eight membrane-embedded segments that are labelled as M1-M8 as well as two translation initiation sites named Met1 and Met23, respectively. Reproduced from [180] with permission from springer Nature. B) AQP4 tetramers cluster in the plasma membrane forming orthogonal arrays of particles (OAPs). A and B are reproduced from [182] published by the American physiological society. C) Freeze-fracture electron micrograph of OAPs in the membrane of astroglial cells. Reproduced from [183] with permission from Elsevier.

AQP4 seems to be implicated in a wide variety of CNS functions. It is essential for water permeability, K^+ buffering and regulation of extracellular space[184,185]. Furthermore, it is crucial for cognitive functions like hippocampal LTP/LTD and spatial memory[186,187]. Finally, AQP4 was found to be linked to astrocyte Ca^{2+} signaling following osmotic stress[188].

4.1.6 Connexons

Connexons are gap junction proteins expressed in astrocytes, which are essential for syncytia formation. Connexons between two cells can interact when they become accurately aligned to form a gap junction (Figure 10). Instead when they are not aligned, they can act as pores known as hemichannels. Connexons are formed by six subunits known as connexins (Cx) (Figure 10). There are 21 types of connexins that have molecular masses between 26 and 62 kDa. All of them present four transmembrane domains. Connexons pore diameter range between 6.5 and 15 Å that allows the passage of not only ion but also hydrophilic molecules up to 1kDa[189,190]. In astrocytes, connexons can also connect different parts of the same cell through reflexive gap junctions creating shortcuts in highly arborized astroglial cells[191].

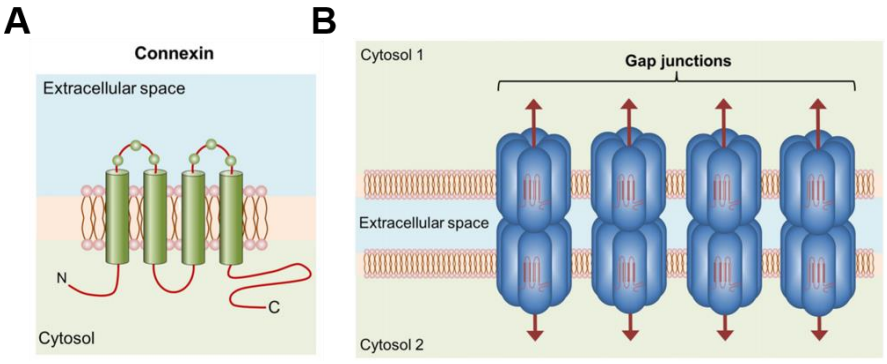

Figure 10. **Structure of connexins and gap junctions.** A) Connexins consist of a four α-helical transmembrane domain connected by 2 extracellular and 1 intracellular loop and having both the C- and N-terminal in the cytosol. Relative positions of cysteines (Green balls) are also shown. Connexons are formed by the combination of 6 connexins. B) Gap junctions are from by the connection of two connexons. It facilitates the intercellular exchange of metabolites, second messengers and ions. A and B are reproduced from [192] published by frontiers of molecular neuroscience.

Astrocyte homocellular gap junctions are formed mainly by Cx26, Cx30 and Cx43 of which the Cx43 is the most abundant. Cx30 and Cx43 can form homo- and heteromers, while Cx26 is implicated just in the formation of homomers[193,194]. Gap junctions' biophysical properties are regulated by many factors, such as, pH, $[Ca^{2+}]_i$ and phosphorylation state[20].

Hemichannels have been identified in astroglial cells *in vitro* and *in vivo*, being formed by all the three types of connexons[195]. Natively, hemichannels are closed in physiological conditions, but can be activated by low extracellular $[Ca^{2+}]$, by depolarization or specific intracellular Ca^{2+} signals or proinflammatory agents. Hemichannels may provide a release pathway for neurotransmitters and neuromodulators[20].

4.1.7 Pannexons

In contrast to connexons, pannexons don't form intercellular channels and then they form single pores (Figure 11) [196]. In the CNS, Pannexin 1 (Panx 1) was reported to be present in neurons and glial cells *in vivo* an *in vitro*. Cultured astrocytes express functional Panx1 forming hemichannels which can mediate ATP release after activation by membrane depolarization or $P2X_7$ stimulation[197]. Panx 1 can also form a complex with $P2X_7$ receptor that has been shown to be implicated in ATP-release mechanism that helps in the propagation of intercellular Ca^{2+} waves and D-serine release [198,199]. Panx1 can also be activated by elevations in extracellular $[K^+]$[200].

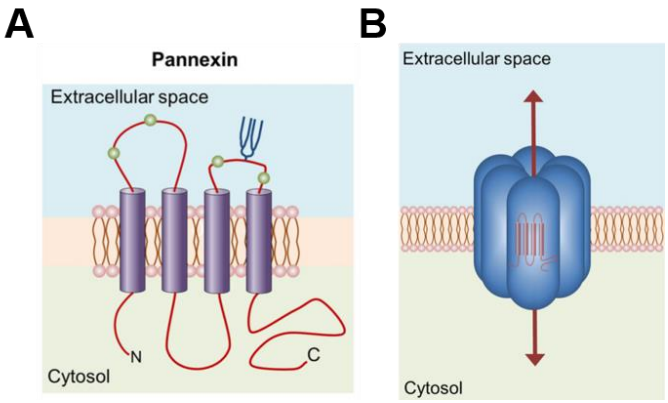

Figure 11. Structure of pannexin and hemmichannels. A) Pannexin consist of a four α-helical transmembrane domain connected by two extracellular and on intracellular loop and having both the C- and N-terminal in the cytosol. Relative positions of cysteines (Green balls) are also shown. Pannexons are single membrane channels composed of six

pannexin subunits. B) Hemichannels are closed under resting conditions but they are activated by diverse physiological and pathophysiological conditions representing a transmembrane route between the intracellular and extracellular environment. A and B are reproduced from [192] published by frontiers of molecular neuroscience.

4.2 Receptors

4.2.1 Purinoceptors

Purinergic signaling, as it is called the extracellular signaling mediated by purine and pyrimidines, represent the most ubiquitous signaling system as it is present in every organ of the human body. In the CNS, purines and pyrimidines have been shown to be released by both neurons and glial cells. $[Ca^{2+}]_i$ increases in astrocytes can be mediated by both ionotropic and metabotropic purinergic receptors[201].

Ionotropic P2X receptors are ligand-gated cationic channels permeable to Na^+, K^+ and Ca^{2+}. They can assemble as homo- or heterodimers from seven different subunits that are classified from $P2X_1$ to $P2X_7$[202]. Homo- and heteromeric assembly of $P2X_1$ to $P2X_6$ subunits are activated by low ATP concentrations, whereas homomeric $P2X_7$ receptor requires millimolar ATP concentration to be activated[203].

Astrocyte $P2X_7$ receptor has been widely studied mainly because of its pathological significance. These receptors present a very low ATP sensitivity, the ability to create large transmembrane pore and almost complete lack of desensitization[202]. Contributions of P2X7 in astrocyte physiology seems to be related with the release of molecules like glutamate, GABA, ATP and other purines by exocytosis[204,205].

P2X7 receptor can also respond to diverse intracellular signaling pathways thanks to the extended COOH terminus that is able to interact with several proteins, such as, serine-threonine kinase (Skt), protein kinases (ERKs), p38 kinase, mitogen-activated protein kinase (MAPK) and c-Jun NH2-

terminal kinases (JNKs)[206]. This $P2X_7$ mediated signaling is activated a lower ATP concentration, showing a possible non-channel mode of receptor function in physiological condition[207].

Metabotropic P2Y receptors are classified into two groups depending on the G protein preference. $P2Y_{1, 2, 4, 6, 11}$ couple to PLC via G_q/G_{11} pathways leading to Ca^{2+} release through $InsP_3$ receptors. $P2Y_{12, 13, 14}$ receptors can modulate ion channels and inhibit adenylyl cyclase through $G_{i/o}$ pathways[208]. P2Y receptors are widely expressed in astroglial cells[209].

Stimulation of P2Y receptors in astrocytes *in vitro* lead normally to production of $InsP_3$ and Ca^{2+} release from the ER[210,211]. Pharmacological study of intracellular Ca^{2+} dynamics in astrocytes *in vitro* and in situ shows the leading role of $P2Y_1$ and $P2Y_2$ receptors, although other receptors like $P2Y_{14}$ seems to be also implicated in the signal[212,213].

Among the roles of P2Y receptors in astroglia they have been demonstrated to be couple with numerous intracellular signaling pathways, including MAP kinases[214]. P2Y1, P2Y2 and P2Y4 are linked to glycogen synthase kinase (GSK)-3, that is involved in cell survival, proliferation and differentiation[215]. They are also involved in coupling with $\alpha^v\beta^3/\beta^5$ integrin in astrocytes controlling cytoskeletal remodeling and motility[216]. Furthermore, stimulation of P2Y2 receptor induce the activation of epidermal growth factor receptor (EGFR), that regulates astrocyte proliferation[217].

4.2.2 Glutamate receptors

There are several types of **ionotropic glutamate receptors (iGluRs)**. Based on their biophysical properties and pharmacological response, iGluRs are divided into three families: cl-amino-3-hydroxy-5-methyl-4-isoxazolepropinonic acid (AMPA), kainite and NMDA receptors[218].

AMPA receptors are expressed in astrocytes *in vitro* and in situ[219,220]. All four types of AMPA receptors (GluA1-GluA4) have been observed in astrocytes[20]. Functionally, AMPA receptors are expressed by hippocampal astrocytes show changes in their electrophysiological properties during

postnatal development presenting lower currents in the younger stages. Immature astroglial cells also showed a prolonged activation of AMPA receptors, inducing an influx of Na^+ and Ca^{2+} increasing its response as astrocytes mature[221]. Functional expression of kainite receptors have not been identified in astroglial cells yet, although its subunits were identified at transcriptional and translational level[222].

Astrocytes expression of **NMDA receptor** was discovered in astrocytic processes from cortical preparations[223]. Transcripts for all seven NMDA receptor subunits have been described in human astrocytes. Experiments in animal models suggest the involvement of NMDA receptors in astroglial signaling[224]. NMDA receptors in cortical astrocytes produce miniature spontaneous currents but also currents mediated by neuronal synaptic inputs[225]. In primary cortical astrocytes they were found to be activated also by mechanical stimulation caused by fluid shear stress[226].

Metabotropic glutamate receptors are divided in three groups according to the G protein they are coupling to. Group I that includes mGluRs 1 and 5, group II that compromise mGluRs 2 and 3 and group III that includes mGluRs 4, 6, 7 and 8. Generally, group I receptors interact with PCL to form $InsP_3$ and release Ca^{2+} from intracellular stores while receptors from groups II and III are coupled to adenylyl cyclase modulation. They all structurally present as seven-transmembrane domains[227].

The mGluR3 subtype is the most abundant in astrocytes[228]. The mGluR5 is also expressed in astrocytes and has been correlated to Ca^{2+} signals that accompany hippocampal synaptic transmission providing astrocytes with a mechanism to regulate elementary aspects of synapses[229].

4.2.3 GABA receptors

Ionic currents mediated by ***$GABA_A$ receptors*** have been extensively studied in astrocytes *in vitro* and in situ from various brain regions. According to their pharmacological, electrophysiological and biochemical properties GABA receptors are divided in two groups, $GABA_A$ and $GABA_B$. The

recorded currents are inward currents mediated by Cl^- efflux that occurs at resting membrane potentials[230–232]. They might also have an important role in extracellular [Cl^-] regulation[20].

Metabotropic $GABA_B$ receptors are expressed in astrocytes. Their activation results in ER Ca^{2+} release[233]. Activation of $GABA_B$ receptors induces $[Ca^{2+}]_i$ oscillations in astrocytes that have been observed *in vitro*, in situ and *in vivo*[231,234].

4.3 Calcium signaling and calcium waves in astrocytes

Astrocytes express a variety of ion channels and membrane receptors that allow them to respond to neuronal activity by changing their membrane potential or/and changing their $[Ca^{2+}]_i$ (Figure 12). These findings lead to the hypothesis of Ca^{2+} signaling in astroglial cells provides a crucial role in CNS for not only maintaining homeostasis but for the processing of information[64]. Furthermore, astrocytes are able to respond to external chemical and mechanical stimulus with increases in $[Ca^{2+}]_i$ as well as transmitting these Ca^{2+} signals to neighboring astrocytes, termed intercellular Ca^{2+} wave (ICWs)[235].

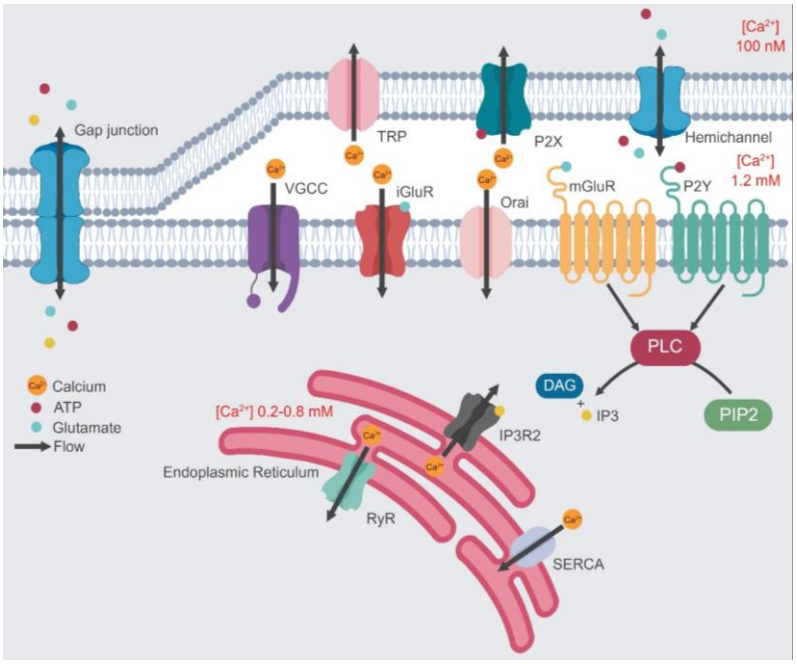

Figure 12. Astroglial Ca^{2+} signaling. Intracellular Ca^{2+} signaling is driven by the influx and efflux of Ca^{2+} from the extracellular space and the intracellular stores. Upon opening of plasmalemmal or intracellular Ca^{2+} channels, Ca^{2+}

fluxes will generate creating $[Ca^{2+}]_i$ dynamical changes. The release of Ca^{2+} from the intracellular stores is mediated by inositol triphosphate (IP3) after activation of metabotropic receptors and can be amplified by ryanodine receptors (RyR). The entry via plasmalemmal Ca^{2+} channels can occur via ionotropic receptors (iGluR and P2X), Voltage gated Ca^{2+} channels (VGCC), Orai and transient receptor potential (TRP) family of ion channels. Sarco (endo) plasmic reticulum Ca^{2+}-ATPase (SERCA) restores intracellular stores Ca^{2+} concentrations. Astrocytes are communicated with each other by gap junctions forming a syncytium where Ca^{2+} waves can spread. Hemichannels can collaborate in the propagation of Ca^{2+} waves by mediating the release of molecules.

In situ and *in vivo* experiments showed that Ca^{2+} signals in astroglial processes can develop independently from somatic Ca^{2+} signals showing also a different kinetic profile. Often, $[Ca^{2+}]_i$ transients are larger and longer in the soma while in the terminal processes' where fluctuations in $[Ca^{2+}]$ tend to be faster and more frequent, although some slow events were also identified[236–238]. Ca^{2+} signals localized in the endfeet have been observed to occur in "microdomains" as a response to neural activity and without any clear link to synaptic activity[236,237,239,240].

The observed anatomical segregation of Ca^{2+} signals suggest different molecular pathways are responsible for Ca^{2+} signals in different parts of the astrocytes. One of the basic mechanisms to induce intracellular Ca^{2+} waves in astrocytes involve activation of G-protein-coupled receptors (GPCRs). These receptors lead the activation of phospholipase C (PLC) and production of $InsP_3$ that can cause Ca^{2+} release from the ER via $InsP_3R$[241]. The intracellular Ca^{2+} currents occurring after activation of these receptors are spatially and temporally complex events. Then, Ca^{2+} signals can propagate throughout the cell by an amplification mechanism that involve four components, including the activation of nearby IP_3Rs by co-agonistic action of Ca^{2+} on these receptors, the generation of IP_3 by Ca^{2+} activation of PLC, the buffering power of mitochondria and the presence of low affinity Ca^{2+} buffers limiting the diffusion of Ca^{2+}[64].

Astrocytes also express ionotropic receptors and ion channels that function at the external membrane and can mediate external Ca^{2+} entry. The role of ionotropic receptors in Ca^{2+} signaling is often neglected despite of the fact that astrocytes are known to express these receptors. Recent data shows that synaptic stimulation induce $[Ca^{2+}]_i$ increases in cortical astrocytes and which are sensitive to inhibitors of NMDA and $P2X_{1/5}$ receptors[242].

Activation of VGCCs can also lead to $[Ca^{2+}]_i$ transients. Nevertheless, expression of VGCC often requires trophic remodeling *in vitro*, such as that obtained with the dibutyryl-cAMP treatment, co-culturing with neurons, or acute oxidative stress.

TRP family of ion channels are also responsible for Ca^{2+} signaling. Activity of TRPA1 channels contributes to set the resting $[Ca^{2+}]_i$ in astrocytes. Inhibition of these channels resulted in a notable reduction of basal $[Ca^{2+}]$. This decrease in basal $[Ca^{2+}]$ reduced in turn functional expression of GAT-3 transporters that results in an elevated extracellular GABA concentration and desensitized of $GABA_A$ receptors in adjacent hippocampal neurons, decreasing inhibitory synaptic transmission[156]. On the other hand, TRPC1 channels contribute to $[Ca^{2+}]_i$ transients following simulation of purinergic and glutamatergic GPCRs, and blocking TRPC1 activity with an anti-TRPC blocking antibody decreased the Ca^{2+} response[157]. TRPC1 channels are also sensitive to mechanical stimulation[243]. The knock-down of antisense RNA of TRPC1 and the inhibition of the channels demonstrated a reduction of SOCE in cortical astrocytes showing the interdependence of TRPC1 in SOCE[157,244]. Finally, TRPV4 channels are widely expressed in astrocytes and known to be activated by hypotonicity, which triggers substantial Ca^{2+} influx and subsequent $[Ca^{2+}]_i$ increases[149]. In cortical astrocytes, TRPV4 is known to complex with AQP4, which has been demonstrated as a critical complex for volume decrease ensuing hypo-osmotic shock[151].

The $[Ca^{2+}]_i$ elevations can pass to adjacent astrocytes forming a syncytium. There are two pathways by which Ca^{2+} signals can be transmitted between cells. The first pathway involves the transfer of Ca^{2+} via second messengers from the cytosol of one cell to the neighboring cell through gap junctions. The second pathway involves the generation of secondary messengers in adjacent cells through the activation of membrane receptors by diffusion of agonists in the extracellular environment. These two pathways are likely to work together in order to provide coordinated activity within group of cells[64,235].

Ca^{2+} signalling are known to be involved in the control of synaptic activity. Observations were made in co-cultures by recording neuronal evoked activity induce by intercellular Ca^{2+} waves in the neighboring carpet of astrocytes[245]. This data was afterwards confirmed on in situ experiments that showed that astrocytes can release neurotransmitters to modulate neuronal activity[246,247]. A new role of Ca^{2+} waves has been recently demonstrated in the generation of Na^{+}-mediated waves in astrocytes. Single cell stimulation in astrocytes *in vitro* generate Na^{+} waves in parallel to Ca^{2+} waves but with different spatial and temporal properties[248]. Lastly, $[Ca^{2+}]_i$ elevations in astrocytes processes have also been reported in producing dilation and constriction of blood vessels[249,250]. Astrocytes in the somatosensory cortex *in vivo* have been shown to be able to control vasodilation, suggesting that the control of microcirculation in response to neural activity and its dysfunction is one of their physiological roles[251].

5. **Astrocytes pathophysiology**

Alterations in astroglial cells physiological roles have been demonstrated to contribute to cerebral pathology. Given the fact that astrocytes are critical for normal brain functioning, it was likely to consider that they could also play a pivotal role in pathological conditions. Analysis of human tissues and animal models of CNS pathologies showed that indeed, astrocytic dysfunction contribute to several neurological and psychiatric disorders[252].

A wide variety of CNS diseases are commonly characterized by reactive astrogliosis, which consists on molecular, cellular and functional astrocytic changes in response to CNS injuries (Figure 13). Weak and moderate astrogliosis is normally associated with mild trauma or located far from the lesion sites and astrocytic proliferation is almost nonexistent. An increase in GFAP expression is commonly observed, as well as cell body and process hypertrophy[253]. Moderate astrogliosis stimulates the expression of inducible nitric oxide synthase, and liberation of trophic factors and cytokines[254]. This type of mild or medium reactive gliosis can disappear if the insult resolve or is

removed and the cells return to similar conditions than healthy cells[255]. On the other hand, near the lesions, neurodegenerative areas and infection severe astrogliosis occur and is characterized by an increased proliferation. This increased proliferation cause overlapping of adjacent astrocytic processes disrupting individual astrocyte domains. In some cases, this reaction can lead the formation of the glial scar which can form around the damage tissue. In this case, the changes are long-lasting and persist after the damage disappears[255]. Nevertheless, the glial scar can also act as a barrier to protect the surrounding healthy tissue from the areas of intense inflammation. Reactive astrocytes can also protect brain cells by uptaking excess of glutamate, degrading amyloid β peptides, regulating extracellular space volume and ion balance, regulating CNS inflammation and helping in the repair of blood brain barrier[256].

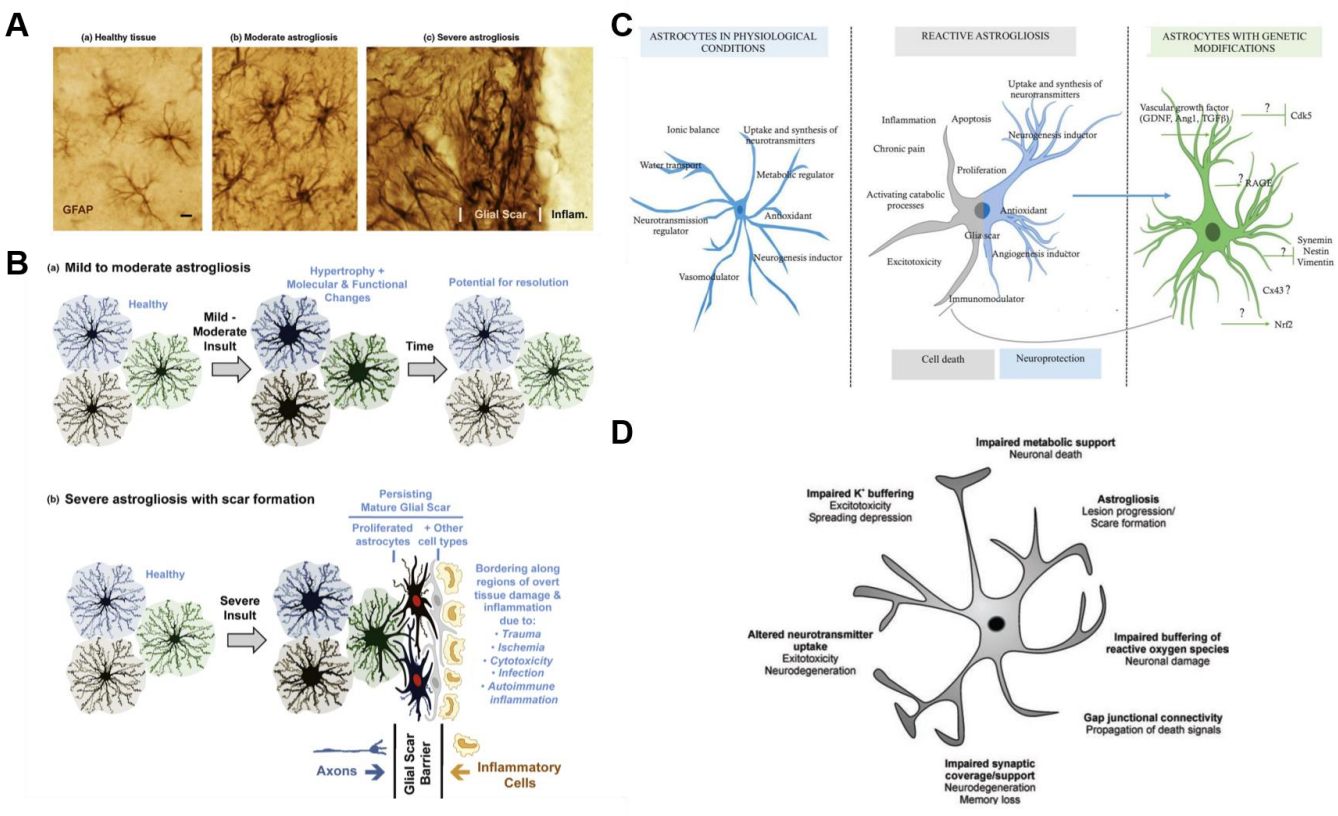

Figure 13. Immunohistochemical and schematic representation of several grades of astrogliosis. A) Immunohistochemical staining of GFAP in wild type mice of (a) astrocytes in healthy cerebral cortex, (b) moderately reactive astrogliosis produced by intracerebral injection of the bacterial antigen lipopolysaccharide (LPS) and (c) severely reactive astrogliosis and glial scar formed after a traumatic injury and inflammation. (Scale bar=8mm). B) Schematic representation of reactive astrogliosis in different states of severity. (a) Mild to moderate astrogliosis are characterized by variable changes in molecular expression, functional activity and cellular hypertrophy. These changes

depend on insult severity. (b) Severe astrogliosis and the formation of glial scar along the borders of tissue damage and inflammation. A and B reproduced from [257] with permission from Elsevier. C) Role of astroglial cells in physiological conditions, during reactive astrocytosis where they present a double function of cell death and pro-neuroprotection and during reactive astrogliosis showing genetic modifications. Reproduced from [258]. D) Scheme of the pathological potential of astroglial cells. Reproduced from [259].

5.1 Edema

Brain edema is characterized by disruption of BBB integrity after injury in the CNS. As brain is surrounded by a rigid skull, increases in brain volume following edema, translate into brain herniation and impaired blood supply in the brain. Astrocytes are key participants in brain edema due to their close contact with vasculature and their role in water and ion homeostasis. The formation of cytotoxic edema is a critical event following ischemia/hypoxia. During ***cytotoxic edema***, astroglial cells uptake Na^+ forming an electrochemical gradient that drives edema formation[260]. To counteract this effect, anions and water enter the cell causing cell swelling. Cytotoxic edema by itself does not trigger brain swelling. However, it cause the depletion of extracellular Na^+ causing a Na^+ gradient that induce the movement of Na^+ from vascular to parenchymal compartments that is again compensated by water flow[261]. This transport of substances across endothelium cause vasogenic edema that increase brain volume[260].

The principal water channel in astrocytes is AQP4 and its role in water flux in brain edema has been intensely studied. Nevertheless, AQP4 role is still contradictory in different types of edema. Several studies showed that AQP4 gene deletion was protective against the formation of edema[262–264]. On the other hand, AQP4 gene deletion was also shown to increase edema load[265]. Additionally, the physiological localization of AQP4 in astrocytes processes is altered after injury, where AQP4 distributes uniformly on astrocyte membrane[266]. After injury, astrocytes undergo a series of activities that depend on AQP4 such as morphological change, migration, hypertrophy, cytokine release and cell division, suggesting that AQP4 dysregulation might not happen in the earlier stages of edema formation[260].

A recent study also showed that the polymodal TRPV4 channel was upregulated after cerebral hypoxia/ischemia in adult rat hippocampal CA1 region. TRPV4 upregulation coincides with the development of astrogliosis. Moreover, TRPV4 mediated Ca^{2+} entry was observed[148].

Extracellular K^+ and glutamate has been shown to accumulate after injury, triggering astrocyte pathological swelling during the clearing of this excess[267,268].

5.2 Epilepsy

Epilepsy is one of the most commons neurological diseases that is characterized by repetitively recurrent seizures, that affect normal brain functioning. It is commonly thought that epileptic activity is generated solely by neurons but research showed an astrocytic basis for epilepsy[269].

Reactive astrogliosis is present in almost all types of epilepsy[270]. Astroglial cells are key players in the regulation of extracellular K^+, and since increased levels of extracellular [K^+] have been related with the pathophysiology of epilepsy, Kir channels have been investigated to understand their role in epilepsy. Studies in slices showed impaired K^+ buffering. Moreover, patch-clamp recordings and single cell RT-PCR carried out in human sclerotic hippocampus slices showed a significant diminution or complete loss of Kir 4.1 currents[271,272]. This data was supported by western blot and immunohistochemistry analysis showing a decrease of Kir 4.1 expression in epileptic tissue compared with normal patients[273].

Water transport is also altered in epileptic patients. RT-PCR, immunohistochemistry and gene chip analysis showed an elevated expression of AQP4 accompanied by a reduction on the levels of dystrophin, that is involved in AQP4 anchoring to the endfeet membrane[274]. This altered flow of water can affect extracellular K^+ buffering and in turn contribute to epileptogenicity.

Furthermore, astrocytes have a critical role in removal of glutamate and GABA from the synaptic cleft. Extracellular glutamate and GABA are uptake by astroglial cells through GLAST and GLT-1 for glutamate and GAT3 for GABA. *In vivo* microdialysis showed that epileptic patients presented

five-fold higher levels of glutamate in the extracellular environment in the hippocampus when compared with healthy patients[275]. Besides, immunocytochemical analysis showed a decrease in GLT-1 and GLAST expression in epileptic patients[276]. On the other hand, an increased expression of GAT3 was observed reducing GABA extracellular levels[277]. Indeed, *in vivo* microdialysis demonstrated that epileptogenic hippocampus of epileptic patients showed lower extracellular GABA concentration and higher glutamate levels right before seizures onset[277].

Finally, an increased expression of voltage-gated channel, expressed in astrocytes at a low level in healthy brain, has been observed in epileptic brain specimens[278].

5.3 Brain tumors

Gliomas represent the majority of brain tumors and they are one of the most aggressive. Specially, tumors derived from astrocytes are the most common type of glioma. Tissue of glioma patients presents an overexpression of GFAP correlated with tumor size but not degree of malignancy[279].

Extracellular glutamate levels are increased in tumoral and peritumoral regions. This altered glutamate homeostasis explains why 60-80% of glioma patients suffer from seizures during the development of the disease[280,281]. Brain tissue from glioblastoma patients presents a very low expression of GLT-1 while GLAST is normally expressed but mislocalized in cell nuclei. Decrease in GLT-1 levels seems also to be related with high-grade astrocytoma[256].

Moreover, impairment of gap junction mediated intercellular communication might result in anomalous growth and tumor development. Low-grade gliomas present a strong Cx43 immunoreactivity being particularly present in reactive astrocytes, on the other side, surgical removed tissue from high-grade astrocytoma patients present low levels of Cx43 and only non-phosphorylated forms of Cx43 were found[256]. Interestingly, the reduction in Cx43 expression is proportional to the tumor proliferation capacity and tumor grade[282].

Glioma present also changes in the expression of Na^+ and K^+ channels. Indeed, astrocytoma cells presented delayed rectifying K^+ currents but no transient A-type and Kir channels have been detected. Besides, they also present an increase TTX-sensitive Na^+ currents, allowing them to generate spike-like events after current injections[283].

5.4 Alzheimer's disease

Alzheimer's disease is the most common neurodegenerative disease affecting the 60-80% of the dementia patients[284]. It its characterized by a loss of memory and a deficit in recalling the near past because of the loss of long-term memories. The pathological hallmarks of Alzheimer's disease are the extracellular deposits of amyloid-beta (Aβ) protein and abnormally phosphorylated tau protein[285]. Effective treatment is still lacking, and the origin of the disease is still unknown. Reactive astrocytes have been observed in Alzheimer's, although the role is not totally understood yet. Astrocytes present an increased expression of GFAP and hypertrophic morphology near amyloid plaques[286]. Reactive astrogliosis and GFAP overexpression are accompanied by dysregulation of other cytoskeleton proteins such as, β-actin, dynein and integrins[287].

The stimulus inducing astrogliosis in Alzheimer's disease is still elusive. Studies showed that Aβ plaques can induce astrocyte activation *in vitro*, causing GFAP up-regulation and changes in the morphology[288]. Moreover, Aβ42 is accumulated in the cytoplasm of astrocytes and this accumulation is directly linked with Alzheimer's disease pathology. Nevertheless, Aβ42 has a neuronal origin and it derives from the internalization of dendrites phagocytosis and degenerating synapse. Besides, Aβ42 accumulated in astroglial cells can undergo lysis forming small $GFAP^+$ amyloid plaques[289].

Glutamate function seems to be also impaired in Alzheimer's disease. GLT-1 immunoreactivity is decreased in the frontal cortex of Alzheimer's while no change in GLAST expression was observed[290]. Moreover, the control GABA homeostasis is also altered in astrocytes in Alzheimer's

disease. Accumulation of GABA and increase in GAD67 and GAT3 have been observed in $GFAP^+$ astrocytes[291].

Gap junction communication and K^+ buffering are also altered in Alzheimer's disease. Increased expression of Cx43 has been found in human tissue near the areas containing amyloid plaques[292]. Furthermore, An alteration in the expression of Kir 4.1 and AQP4 has also been observed[293].

Alterations in Ca^{2+} levels seem to be implicated in initial steps to Alzheimer's disease. Basal Ca^{2+} levels are elevated and Ca^{2+} transients are more frequent and coordinated along big distances as well as independent of neuronal activity[294]. Besides, mGluR5 has been observed to be overexpress in proximity of Aβ plaques in hippocampal astroglial cells of Alzheimer's disease patients[295].

5.5 Depressive disorder

Major depressive disorder is a chronic mental illness that is characterized by depressed mood, sleep alterations, difficulties of concentration and thought of death and suicide among other symptoms. Astrocytes have been observed to be altered in this disease, affecting their morphology, density, membrane channel function and protein expression. Indeed, decrease in astrocyte number and packing density has been observed[256]. Moreover, increases in the size of the nuclei seems also to be present on these patients[296]. Major depressive disorder patients present lower concentrations of glutamate, glutamine and the complex formed by glutamate/glutamine (Glx) in several brain regions as well as reduce expression of GLAST and GLT-1. Reduce GABA levels have also been observed and $GABA_A$ receptor subunits are up-regulated[256]. Lastly, astrocytes in major depressive disorder present altered K^+ and water homeostasis. Kir 4.1 channels and AQP4 were found to be down-regulated and a poor coverage of blood vessels by astroglial endfeet was observed[297,298].

7. State of the art techniques to study astroglial cells

Currently, the available methodologies to study astroglial cells rely mainly on the development of molecular and optical tools. Although astrocytes are electrically silent cells as they cannot fire action potentials. However, Ca^{2+} signaling in astrocytes could be consider a kind of excitability. Nowadays, many questions related with the role of Ca^{2+} signaling in astrocytes remains unsolved, mainly because a lack of methodologies to properly address these questions. Research of Ca^{2+} signaling is mostly based on bulk-loaded Ca^{2+} indicators capable of passing through the membrane. There are many commercially available organic Ca^{2+} indicators that present different spectral properties. These indicators can be used both to measure florescence changes and for radiometric probes that allows the calculation of absolute Ca^{2+} concentrations[299]. This allows the imaging of somatic regions and the bigger processes but does not allow to properly observe Ca^{2+} changes in astrocytes microdomains[300]. Moreover, the lack of specificity of these membrane-permeable Ca^{2+} indicators makes necessary the use of secondary markers to allow the differentiation of neurons and astrocytes[301]. However, the use of these secondary markers can alter functional studies. To address this issue, transgenic animals expressing fluorescent proteins that allows astrocyte identification can be used as an alternative[302]. Moreover, genetically encoded Ca^{2+} (GECI) represents also an alternative for non-invasive imaging of Ca^{2+} signaling in brain slice and *in vivo*[303].

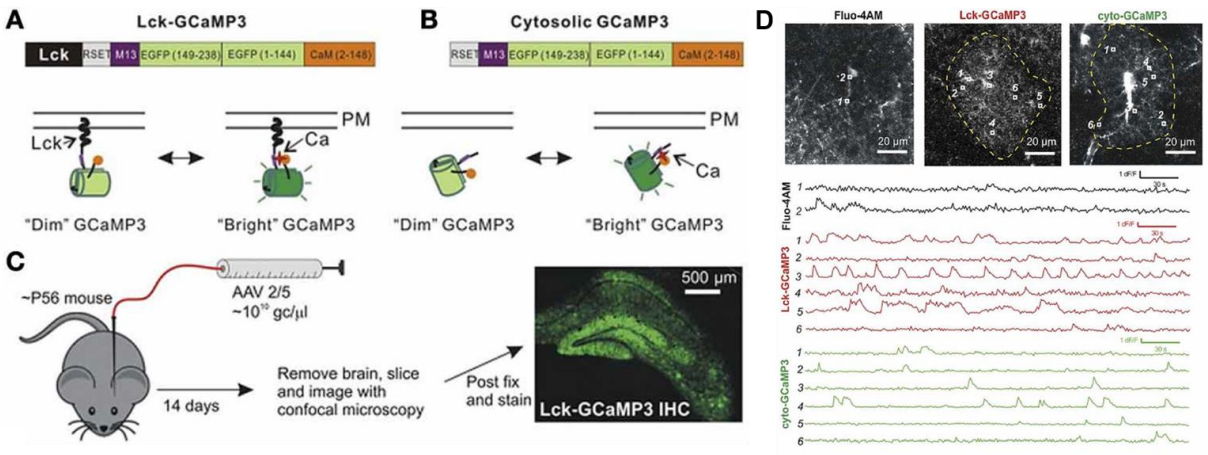

Figure 14. Methods to study Ca^{2+} signaling in astrocytes. Expression of GCaMP3 in astroglial cells and comparison with Fluo-4, cyto-GCaMP3 and Lck-GCaMP3. A-B) Representation of membrane-targeted LcK-GCaMO3 and

cytosolic non-targeted Cyto-GCaMP3. C) Scheme of the protocol of AAV2/5 injection into the hippocampus of a mouse. D) Fluorescent micrographs (top) and representative traces (down) of Ca^{2+} signals imaged with Fluo-4AM (black traces), cyto-GCaMP3 (green traces), and Lck-GCaMP3 (red traces). Adapted from [304].

Optical limitations need also to be overcome. Two-photon microscopy presents a great potential for monitoring Ca^{2+} in astroglial cells. Nevertheless, the limited spatial resolution is still an issue to detect small morphological and $[Ca^{2+}]_i$ changes[305]. On the other hand, two-photon microscopy combined with two-photon stimulated emission depletion (STED) presents an increased lateral resolution[306]. Recently, super-resolution images of dendrites were reported in brain mouse *in vivo*[307]. This increase resolution makes two-photon STED microscopy an attractive and promising optical tool for observing the finest parts of astrocytes.

Specific tools capable or modulating astrocyte activity are also necessary in order to properly understand their physiology and the interaction between neurons and astrocytes. Recently, optogenetics emerged thanks to the interaction of channelrhodopsin 2 (ChRs2), a blue sensitive cation channel found in cyanobacteria, with light[308]. Optogenetics is based in genetically encoded light-sensitive ion channels driven by rhodopsin isomerization to cause the opening of ion channels to allow the flow of certain cations or anions to alter the bioelectrical properties of the targeted cell. It has been used as a neuromodulation technique that allows a reduced radiant exposure to decrease phototoxicity. Optogenetics have been widely used in neuroscience, in fact, the first experiments were performed by introducing ChRs in hippocampal neurons, where they demonstrated millisecond precision control of neuronal response[309]. Additional studies followed both in cell lines and primary neurons by inserting light-activated signaling proteins as well as retinal neurons to convert them into photosensitive cells in order to restore the ability of retina to encode and transmit light signals[310–313]. Experiments performed in astroglial cells showed that photoactivation of ChR2-expressing astrocytes can induce gliotransmitter release[314]. Moreover, *in vitro* experiments performed on mouse cortical astrocytes showed that activation of ChR2 triggered weak and variable Ca^{2+} elevations[315].

8. Novel techniques for the study of astrocytes

Despite the advances in methodologies to study astroglial cells, the technology to allows us to understand their communication with neurons and their role in many important roles such as cognition is still lacking. Recently, the design and development of novel biomaterials and devices such as bioelectronic and photonic devices capable of read-out and stimulate electrical and chemical signals in the nervous system have created a unique opportunity to understand normal brain functioning as well as to treat dysfunctions caused by disease or injury. Most of these technologies have been validated with neurons, *in vitro* and *in vivo* but not enough attention has been paid to the potential of this tools in the study of glia cells, specially astrocytes.

8.1 Biomaterials interface and interaction with astrocytes

Biomaterials are the materials targeted to the interaction with biological systems. They can be implanted in the body as scaffold or as part of electronic devices, such as electrodes, diodes and transistors. The malfunction of chronic neural implants is often related with the interface biocompatibility, which cause a foreign body response of the neural tissue to the implanted device. Studies performed in animal models with neural implants intended to make recordings, often showed progressive losses in signal read-out a few weeks after implantation[316]. In most of the cases this phenomenon occurs because of brain physiological response and astrocytes have a key role in this response. The foreign-body response to brain implants is caused by glial encapsulation of the device by forming a layered structure that can reach hundreds of micrometers of thickness (Figure 15). The role of reactive astrocytes in this process is important for their effect in connectivity of neural networks and function[317].

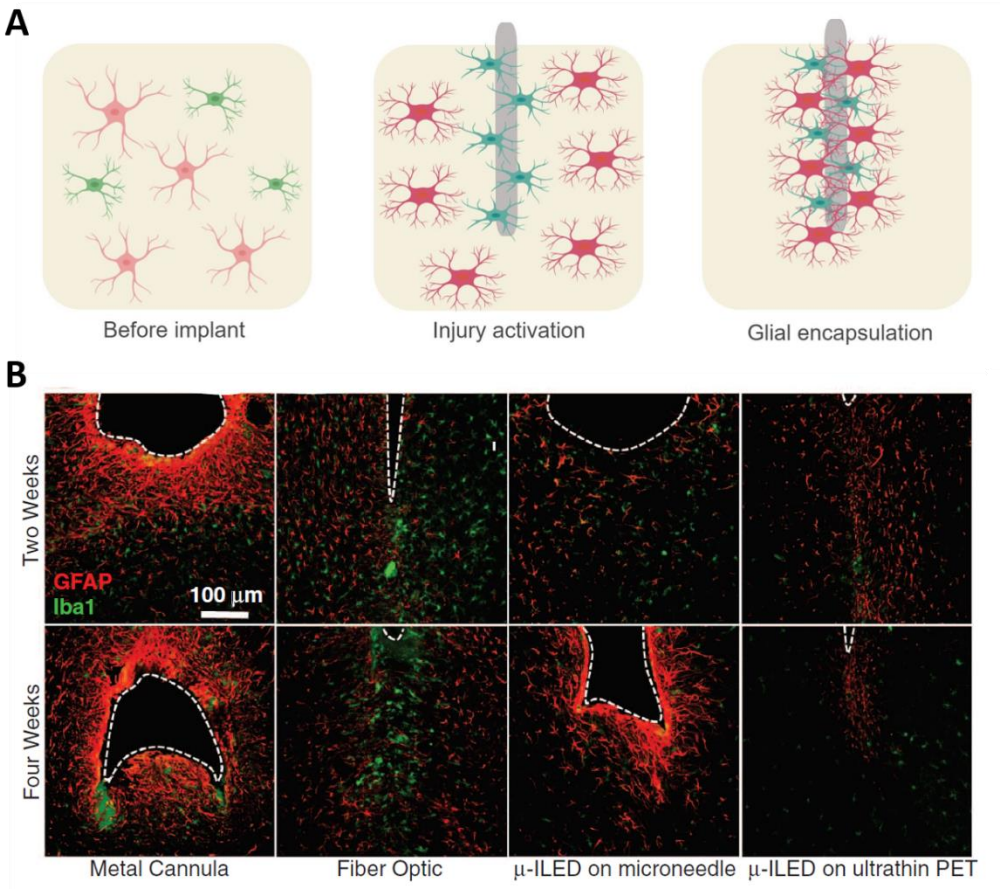

Figure 15. **Astrocytes response to implants**. A) Scheme of foreign body response to brain implants. Before implant (left) the tissue is undisrupted. Right after implant (grey) the acute inflammation phase starts (center), and astrocyte (red) and microglia (green) activation occurs. In the chronic phase (right) takes place the encapsulation of the implant impairing its performance. B) Confocal fluorescence images of 30-µm striatal slices showing GFAP stained astrocytes (red) and Iba1 stained activated microglia (green) at the ventral tip of diverse implanted devices (dashed outline) at 2 and 4 weeks. Figure B reproduce from [318], with permission from the American Association for the Advancement of Science.

Studies performed in this field suggest that chemical, physical and mechanical properties of biomaterials are crucial factors for suppressing chronic tissue encapsulation[319]. A common approach to modulate the inflammatory response and get a better integration of the implant on the brain is the chemical modification of the material with adhesion proteins, bioactive molecules and anti-inflammatory molecules[320–323]. Moreover, a recent study proved that rigid materials enhance the activation of astrocytes and microglia when compared with softer materials[324]. In this context, mechanical modifications of this property can significantly reduce glial scar formation and inflammation response[325–327]. Furthermore, reduced device dimensions may diminish gliosis by

being too small to allow cellular attachment[328]. Nevertheless, diminished stiffness can make softer and subcellular devices hard to be implanted without an insertion tool or soluble shuttle[317]. In addition, electrode surface coating can also be a suitable option for reducing foreign-body response in brain implants. In this view, hydrogel, bioactive anti-inflammatory surface molecules and biodegradable polymers can be used in material coating to increase biocompatibility. Coatings can be design to reduce inflammation through drug release, mask the surface of the implant from being recognized as a foreign body, reduce impedance by increasing the fractal dimension and/or diminished the concentration of cytokines in the site of implantation[317].

Among inorganic materials metals have been commonly used in neural devices. Silicon remains the most frequently used material in primate studies and human clinical trials[329–332]. However, there are limitations for their use in biomedical applications, such as their poor stability in biological systems, the high electrical noise and stiffness that can damage the surrounding tissue inducing foreign body reaction[319].

8.1.1 Graphene

Graphene is a carbon-based two-dimensional layer of sp^2-hybrid carbon atoms that form hexagons (Figure 16A). Among its exceptional properties, graphene present remarkable thermal conductivity, high elastic modulus, outstanding electrical conductivity and low resistivity[319]. Furthermore, its structure allow easy functionalization making graphene a good candidate for biomedical applications[333–335]. Due to its remarkable electrical and mechanical properties, interfacing graphene with brain cells could be extremely advantageous for neural engineering purposes. However, the mechanisms of interaction of graphene and graphene-based materials with brain cells need to be further investigated. Studies performed in neuronal-like cell lines like PC12 showed that graphene induced a toxic response[336]. Besides, graphene oxide (GO) (Figure 16B and C) nanosheets did not cause cytotoxicity at low concentration, but it was observed dose- and time-dependent cell death in

SH-SY5Y cell line of human neuroblastoma[337]. Nevertheless, in primary cultures, viability of neurons and glial cells does not present any changes after graphene exposure, both *in vivo* and *in vitro* (Figure 16D) but neuronal primary cultures exposed to GO nanosheets showed alterations in physiological pathways, synaptic connectivity and plasticity[338,339]. On the other hand, *in vivo* studies showed that GO nanosheets accumulate in small amounts in the CNS of rodents after intravenous injection[340]. The entry of graphene in the body and the dose was shown to affect the biological effects[341].

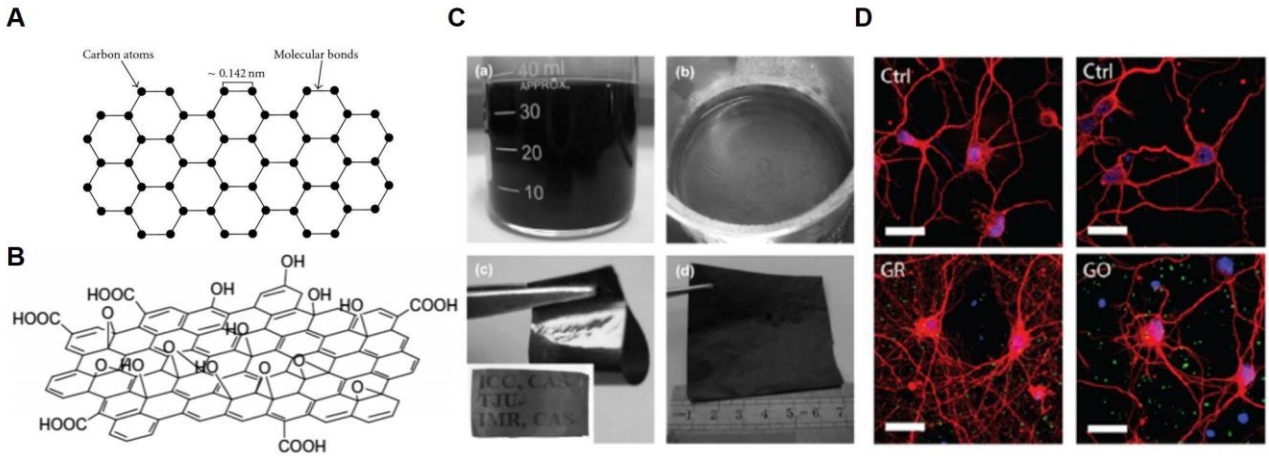

Figure 16. Structure of graphene (GR) and graphene oxide (GO) and interaction with neurons. A) Structure of graphene. Reproduced from [342] B) Structure of graphene oxide (GO). Reproduced from [343] published by the royal society of chemistry. C) (a) Photo illustrating the self-assembly process of GO films. (b) GO film at the liquid-air interface. (c) Photo of a flexible and semi-transparent GO film. (d) Photo showing a large-area GO film. Reproduced from [344] D) Primary rat cortical neurons exposed to GR and GO flakes and immunostained for anti- βIII tubulin (Red) and Hoechst 33342 (Blue). Reproduced from [339] published by ACS nano.

Functionalization of graphene surface could also be a promising strategy to alleviate the observed drawbacks by tuning graphene properties to obtain a higher biocompatibility. Functionalization, might allow graphene to act as a platform for delivery of biomolecules that are usually not passing the BBB[345]. Moreover, it is also possible to modify graphene chemical structure by adding functional groups[346]. This approach could then satisfy the increasing demand of medical platforms able to carry out diverse functions.

Data on the effect of graphene and graphene-based materials on astroglial cells is still limited. GO nanosheets were proven to not affect astrocyte viability *in vitro*, but alter neuron-astrocyte communication by affecting the release of microvessels[338]. Besides, astrocytes treated with graphene and GO flakes *in vitro* showed that they internalized in the cell causing variations in intracellular processes. Moreover, astrocytes exposed to graphene presented cytoskeletal rearrangements while internalization of GO caused upregulation of K^+ channels and Na^+ glutamate uptake[347]. Graphene-based materials resulting from interaction of polymers and graphene have also been under study. PEGylated rGO was shown to cause changes in astroglial cells morphology and production of ROS, affecting astrocyte viability *in vitro* and *in vivo*. Furthermore, electrospun PCL microfiber scaffolds coated with self-assembled colloidal graphene, showed a suppression of microglia and astrocyte activation when implanted into striatum and subventricular zone of adult rat, compared with non-functionalized graphene. Moreover, these implants prevented the formation of glial scar in the brain, even after 7 weeks after implantation[348].

8.1.2 Organic semiconductors and polymers

During the last few years the design and synthesis of new organic materials has grown to implant them in electronic tools such as, transistors and light-emitting devices. Therefore, the research of their structure and properties have been a matter of intense investigation. Among their interesting properties, organic platforms include transparent thin-film materials that allow optical investigation of cells and tissues in direct contact with them, polymers and small molecules that can be easily tuned to achieve the desired properties for different applications, organic semiconductors that can be self-assembled to mimic biological structures, organic substrates easy to functionalize to promote cell viability and natural, cheap, bio-degradable and bioresorbable materials such as SF[320,321,349–351]. In the last decade organic electronics have been used in the field of bioelectronics and the development of neural interfaces, specially based on organic semiconductors and

conductive polymers. Nevertheless, organic neural interfaces present some disadvantages such as, poor electrochemical stability in water environments and organic devices often present lower performances than their inorganic counterparts[352].

Perylene-derivates can be found in form of polymer and small molecules and they are one of the best performing n-type materials for the building of filed-effect transistors[353]. Among them, N-N'-ditridecylperylene-3,4,9,10-tetracarboxylic diimide (P13) has been shown to be a permissive material to grow primary rat DRG neurons, where they can adhere, grow and differentiate maintaining their electrophysiological properties even at long term[349]. Perylene derivates can also be functionalized to offer more advantageous properties. In this context, lysine substitution of perylene diimide (PDI-Lys) enhancing the hydrophilicity of the material allowing an elevated biocompatibility *in vitro* as well as differentiation of DRG neurons[321]. Lysine functionalization of other organic material was reported. Lysine substitution of quaterthiophene (T4-Lys) increased notably the number of DRG neurons adhered to the substrate. Furthermore, longer neurites were found when compared with regular T4 and poly-L-Lysine control samples[320]. However, studies on glial cells and specially on astrocytes to understand the impact of these materials in brain implants are needed as well as to understand the influence of this material on astrocyte physiology.

Polymers provide several advantages over other kind of materials for their wide range of chemical structures and the possibility of tunability of their properties[319]. Synthetic polymers can be commercially obtained and besides they are often cost-effective for fabrication. Among synthetic polymers, conductive polymers (CPs) have receive much attention, in specially in the fabrication of organic electronics. They present alternate single and double bonds that allows electron movement providing the material with electronic conductivity after suitable doping (Figure 17A-D). Besides in response of redox reactions they can change their properties, such as, wettability, color, and conductivity[319]. They present a great amount of advantages for their use in biomedical applications, that includes their ability to work as a drug release platform, capability of be

functionalized with bioactive molecules and the possibility of alter the chemical and physical properties of the surface to induce a cellular response[354–356]. Some of the better-known CPs are poly(pyrrole) (Ppy), poly(aniline) (Figure 17E) (PANI) (Figure 17E), poly(thiophene) (PT) and poly(3,4-ethylenedioxythiophene) (PEDOT) (Figure 17 E). For their great electrical conductivity and their biocompatibility, they are excellent materials for neural interface[319,357].

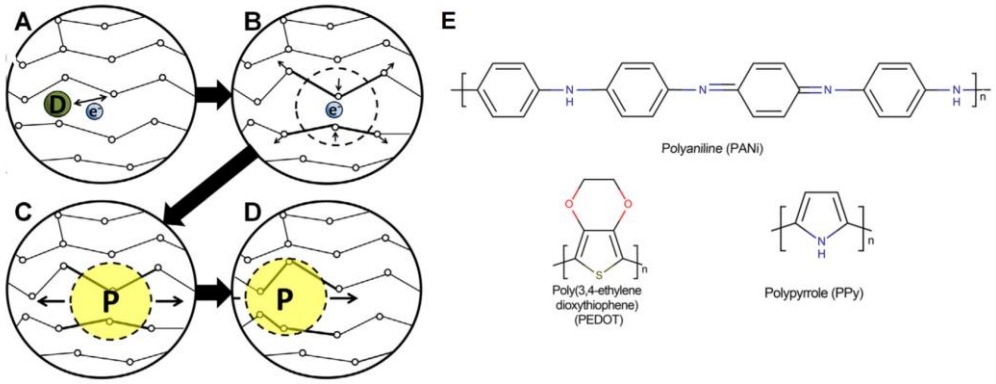

Figure 17. **Conductive polymers.** A) The dopant removes or adds one electron from/to the polymer chain. B) The charge delocalizes with a local distortion of the crystal lattice. C) The charge surrounded by the distortion is a polaron. D) The polaron travels along the polymer chain conducting electricity. Reproduced from [358] published by Elsevier E) Structures of PANI, PEDOT and PPy, three of the most commonly used conductive polymers. Modified from [359] published by ACS publications.

Novel substrates based on CPs, like poly(ethylene terephthalate) (PET) nano-fibers coated with PEDOT doped with toxylate showed that SH-SY5Y neuroblastoma cell line can attach well and show a healthy morphology. Besides, electrical stimulation induced Ca^{2+} signaling[360]. Furthermore, PEDOT doped with PSS was also show as a biocompatible substrate promoting neural growth and synapses formation with reduce glial response *in vitro*[361]. Moreover, PPy fibers doped with p-toluene sulfonate has been use to control growth direction of DRG neurons[362].

To what concern tissue engineering applications, biodegradable polymers that can decompose into non-harmful biological molecules that can be remove from the body through natural pathways are needed. Apart from the synthetic polymers discussed above, natural polymers such as proteins, amides and polysaccharides can be used for this purpose. This kind of macromolecules are

completely recognized by the biological environment. Among natural polymers, several studies have showed the great potential of SF in neural tissue engineering[351]. SF can be process in divers form, being SF films and hydrogels very promising for the results they showed *in vitro* and *in vivo*. SF films show optical transparency and tunable mechanical properties thanks to surface modification. On the contrary, hydrogels present diverse formulation for gelation and it can also be easily delivered by injection[363,364].

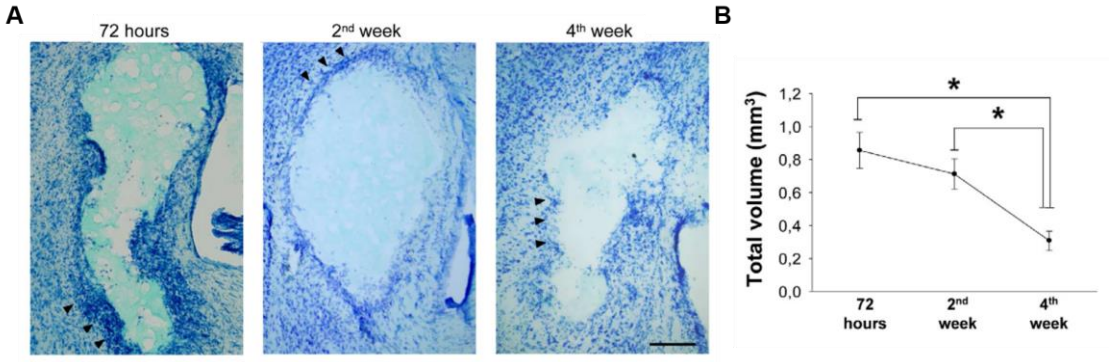

Figure 18. Histological study of silk fibroin deposits over time after intracerebral injection. A) High magnification images of SF deposits 72h, 2 weeks and 4 weeks after injection. Arrowheads show cellular hyperdensity (scale bar: 200 lm). B) Time-course of SF degradation after implantation. The data are shown as the means ± the SEM of four independent experiments with 24 mice in total; 8 mice per temporal point. The asterisks denote significant differences between temporal points (one-way ANOVA; *p < 0.05). Reproduced from [365] with permission from Elsevier.

In vitro and *in vivo* studies confirmed the use of SF substrates for peripheral nerve repair by using this material as nerve guides. *In vitro* experiments performed on PC12 cells showed that SF guides nerve conduits while increasing the differentiation and proliferation by delivering NGF[366]. Besides SF promoted DRG neurite growth while preserving their electrophysiological properties *in vitro*[350,367,368]. *In vivo* studies using SF scaffolds show promising results by filling the tissue gap and delivering NSCs and neurotrophic factors like neurotrophin-3 (NT-3) while improving NSCs differentiation to repair the lesion on rat spinal cord transection model[369].

Regarding astrocytes interaction with SF *in vitro* studies showed that SF is a beneficial platform to grow primary rat neocortical astrocytes without promoting glial fibrillary acidic protein **(**GFAP)[370].

Besides, SF film matrix can target and drive ion channels by selected trophic and neuroprotective factors[370]. These results open a path to study astrocyte interaction with SF-based materials. Research focused on SF-astrocyte interface could certanly improve the efficientcy of NSCs therapies that is currently the gold standard of of SF-brain interactio studies. Furthermore, studies confirm SF hydrogels as a favorable substrate for *in vivo* experiments in adult male mice showing low gliosis and inflammatory response that were often transitory[365].

8.2 Organic bioelectronics

Bioelectronics involve the development and study of electronic devices capable of operating as translators between biological signals and electronic systems. They can be used to selectively convert relevant parameters into electronic readouts as well as to regulate physiological processes.
The methodologies that are available nowadays to record neural activity includes intracellular recording and stimulation by patch electrodes, extracellular stimulation and recording by microelectrode arrays (MEAs) and optical imaging with fluorescent indicators or genetically encoded molecular probes. Intracellular recording exhibits a great electrical coupling with the cell and provide accurate information of the changes in voltages in the cell. Nevertheless, the use of sharp microelectrodes is limited to individual cells and cause damage in cell membrane. On the other hand, *in vitro* cell-non-invasive extracellular recordings with MEAs and *in vivo* recordings performed with polytrodes shows an attenuated electrical signal, but it enables the simultaneous recording of a big population of cells without causing mechanical damage to the plasma membrane[371–373]. Great attention is paid in the improvement of MEAs to get better extracellular recordings mainly by increasing the density and number of electrodes and by developing nano- and micro- electrophysiological technologies. Research efforts are also made to use these technologies to enable also simultaneous intracellular recording and stimulation of many cells *in vitro* and *in vivo*[374].

A recent study reports an intracellular electrode platform based on vertical metal-coated silicon nanowires that allows the interface with several rat cortical neurons simultaneously and intracellular recordings of their activity[375]. Promising results were obtained with an array of non-invasive gold-mushroom-shaped microelectrode that maintain extracellular position but can provide intracellular stimulation and recording of several neurons without damaging cell membrane. It allows the recording of action potentials obtaining an improved signal-to-noise ration when compared with intracellular sharp electrodes[376].

One of the main disadvantages of conventional inorganic based devices is its high cost. Nonetheless, inorganic materials have mechanical properties and biocompatibility issues that limit the possibility of using them in devices for prolonged recording. Notably one of the main challenge is the interaction of inorganic device with glial cells[317].

Organic materials-based bioelectronics offer promising tools for the study and modulation of the physiology of astroglial cells. Organic materials present an improved biocompatibility with brain cells when compared with inorganic substrates, allowing them to preserve their functionality[349,350,370]. Furthermore, they present advantageous iono-electronic transport properties combined with optical transparency[377]. Moreover, organic bioelectronic devices capable of recording and modulating neurons *in vitro* and *in vivo* were reported[378,379]. Collectively, these results show the potential of organic bioelectronics for fundamental studies in the field of neuroscience as well as for their use in clinical neurology to treat brain pathologies.

Organic devices have also emerged as a low-cost alternative that can also be printed on flexible substrates. Although in general they present lower performances and stability, they present a decisive advantage that consist on the possibility of tailoring the organic material to modify its properties[380].

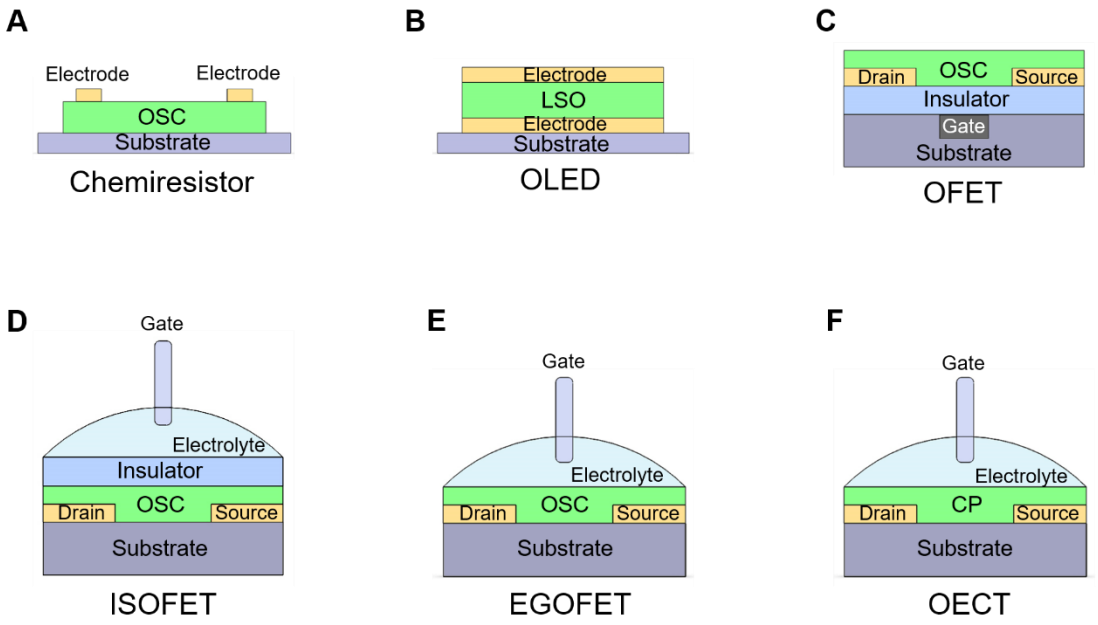

Figure 18. Devices structure of A) Chemiresistor, B) organic light emitting diode (OLED), C) Organic field effect transistor (OFET), D) Ion sensitive organic field effect transistor (ISOFET), E) Electrolyte gated organic field effect transistor (EGOFET), F) Organic electrochemical transistor (OECT). OSC represent organic semiconductor, LSO is light sensitive organic, and CP is conducting polymer.

The simplest organic electronic structure is made by a thin organic layer connected by two electrodes that provide the injection and collection of charges. This is the basic structure used for resistors and chemiresistors (Figure 18A)[381]. On the contrary, when the organic layer is between the two electrodes it is called diode. In this configuration electrons are injected by one of the electrodes and holes by the other[382]. When the organic material is luminescent, this device can produce electroluminescence forming an organic light emitting diode (OLED) (Figure 18B)[383]. Studies showed that blue light between 450-460 nm can activate modified neurons expressing channel rhodopsins (ChRs)[318,384]. A recent study showed an OLED capable of activate ChRs, operating at 5V *in vivo* in drosophila melanogaster expressing ChR2 in motor neurons. Pulsed blue and green illumination triggered contraction in the animal that was coupled to the timing of illumination, giving blue OLEDs a better response[385].

When we combine the vertical electrode configuration of the diode with an extra lateral electrode, to have one electrode to act as gate and two electrode to act as drain and source, and we include also

a gate insulator to separate it from the organic semiconductor we have the classical structure of a field effect transistor (OFET) (Figure 18C)[386]. Different dielectric can be used as insulators such as, vacuum, polymers and self-assembled monolaters. When the gate electrode is negatively polarized in a device with a p-type semiconductor, free holes will place in the semiconductor-insulator interface to compensate the negative charged gate-insulator interface. On the other hand, when the device is based on an n-type semiconductor and the gate is positively polarized, free electrons will place in the semiconductor-insulator interface[380]. They have a voltage threshold necessary to turn on the flow of current from source to drain and crate a conductor transistor channel. As cells are in highly polarizable solution, this kind of transistors are ideal as they can also operate in aqueous medium. When a potential difference is applied between the gate and the source, a double electric layer forms in the solution-semiconductor interface[387]. A recent study showed the interface of OFET and primary DRG neurons to provide bidirectional stimulation (Figure 19) and recording. The device called organic cell stimulating and sensing transistor (O-CSTs), enabled not only depolarization but also hyperpolarization of membrane potential. Besides the extracellular recordings achieved by the O-CST device present a maxima amplitude-to-noise ratio 16 times better than regular MEA[378].

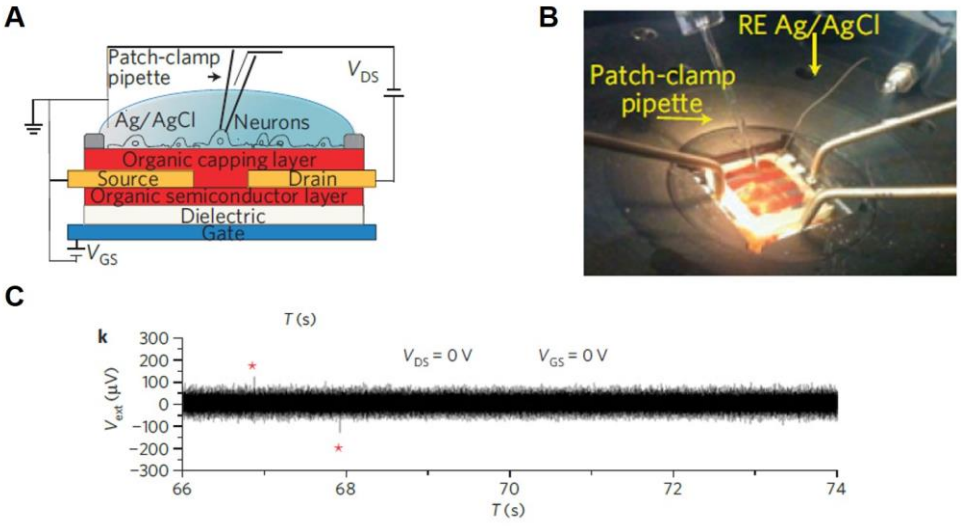

Figure 19. Neuronal stimulation by O-CST and patch-clamp detection. A) Schema of the experiment performed for extracellular/intracellular stimulation and recording. B) Image of the patch-clamp set-up interfaced with the O-CST

device. C) O-CST signal recorded. Red stars represent detected spikes by performing data analysis off-line using custom software. Modified from [378] with permission from Springer Nature.

On the contrary, when a reference electrode act as gate electrode and the electrolyte is in contact with the insulator we obtain the structure of a ion-sensitive organic field effect transistor (ISOFET) (Figure 18D)[388]. In this configuration, by making the insulator sensitive to a given analyte, it is possible to detect a wide variety of biomolecules. A Poly(3-hexylthiophene-2,5-dyl) (P3HT) based ISOFET with a layer of silicon nitride as insulator was shown capable of detecting changes in pH in the range of 2-10 [389]. These transistors can also be used to detect glucose by using a sensitive layer made of an enzymatic layer immobilized in a Ta_2O_5 layer. When the device gets in contact with a solution containing glucose, an enzymatic reaction occurs mediated by glucose oxidase forming gluconic acid allowing the transistor to sense the variations in the pH[390].

Electrolyte-gated organic field effect transistor (EGOFET) structure is similar to the one of ISOFET but in this case the semiconductor is in contact with the electrolyte (Figure 18E). When a voltage is applied in the gate an electrical double layer appears at both the interface gate-electrolyte and electrolyte-semiconductor[380]. As the electrolyte acts as gate dielectric, this produce a drastic lowering of operational potentials[391]. Interaction of murine neural stem cells and pentacene based EGOFET was recently reported allowing *in vitro* recording and stimulation of neural activity. The transistor showed good stability for nine days in cell culture conditions[392]. EGOFETs have also emerge in the field of biosensors thanks to the easy functionalization of gate/electrolyte and semiconductor/electrolyte interface allowing the detection of biomolecules such as DNA and proteins[393].

Organic electrochemical transistor (OECT) structure is very similar to EGOFET structure but OECT but the working principle is different (Figure 18F). While EGOFET semiconducting channel is modulated by changes in the electrolyte, OECT functioning relies on the doping and dedoping of the polymer layer that modifies its conductivity[380]. The most used conducting polymers used are

Ppy and PEDOT. Research performed *in vivo* with a PEDOT:PSS based OECT showed electrophysiological recordings of brain surface of epileptiform models. This device showed a superior signal-to-noise ratio when compared with surface electrodes thanks to local amplification. Besides they were able to record surface low-amplitude brain activities that are often poorly resolved with surface electrodes[379]. The same group demonstrated that OECT can also be used in depth probes to stimulate neurons. Devices tested in situ in mouse hippocampal preparations, were only 4μm thick reducing invasiveness in this way (Figure 20). Besides they showed that the induced $[Ca^{2+}]_i$ increase in pyramidal neurons in contact with the transistor were directly correlated with the delivered stimuli[394] (Figure 20 D). OECT have also shown promising result in their used as biosensors. In this view, a PEDOT:PSS based OECT were used for the selective detection of dopamine in the presence of interfering compounds such as ascorbic acid and uric acid while obtaining sensitivities and limits of detection alike or even higher than the ones obtained by differential pulse voltammetry[395]. Recently, an PEDOT:PSS based OECT was also used for pH sensing applications[396].

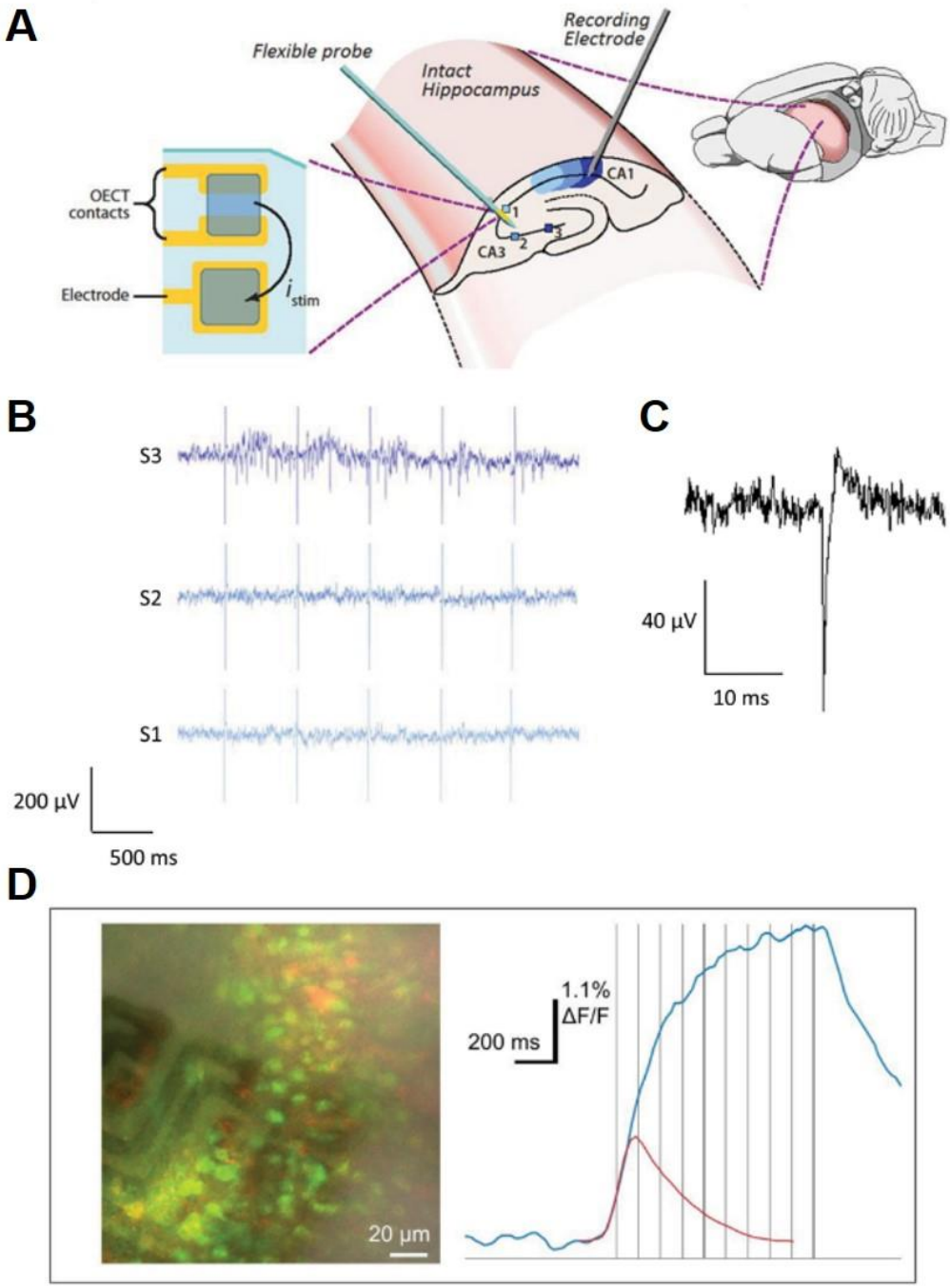

Figure 20. Stimulating pyramidal neurons in hippocampal preparations. A) Pyramidal neurons from the section CA1 (dark blue) were recorded and stimulated using the OECT, as shown, starting from the section CA3 (lightest blue to dark blue). B) Recorded response during stimulation at sites 1, 2 and 3. Physiological activity is evoked only when the stimulation is applied in site 3. The five pulses shown in all three traces are typical stimulation artefacts. C) Selected action potential from stimulation at site 3. D) (Left) Two-photon image of the OECT implanted in the hippocampus preparation. Neurons are seen in green (OGB1-AM) and glial cells in red (SR-101). Cells are located 20 µm above the transistor channel. (Right) Averaged change in fluorescence, corresponding with rises in $[Ca^{2+}]_i$ in neurons after stimulation. The blue trace is the average response at 10 Hz and the red trace is the average response to single pulses. Reproduced from [394] published by WILEY-VCH.

Organic bioelectronics are a promising tool for neuroscience research, nevertheless, available studies till now are mainly focus on neuronal recording and stimulation while no attention is paid to glial cells. In this context, studies of astrocytes interface with organic bioelectronics that can stimulate and/or read out their bioelectrical activity are lacking.

8.3 Photostimulation

The electricity-centered view has been the gold standard in the development of brain-machine interfaces due to the known electrical properties of neurons. However, the 3-dimensional architecture of the brain difficult the implantation of foreign objects targeted to deeper areas of the brain. Often, these implants cause a trauma that activates in turn a glial response that cause device encapsulation compromising device functioning[317]. Moreover, devices are till now unable to target specific cells within the same region, increasing the chance of activating undesired neighboring tissue. In this context, the study of optical methods as alternative to electrical stimulation has been proposed. Light has also been investigated to modulate neural activity. This was first demonstrated by using a 488nm Argon ion continuous wave laser to enhance the firing rate in Aplysia pleura abdominal nerve preparation[397]. On the other hand, studies also reported inhibition of neural signal after long term laser exposure[398–400]. These results paved the way to study the potential of light as a tool for neuromodulation. Later, photochemical uncaging of free-floating neurotransmitter to excite neurons in brain slices was studied showing that caged neurotransmitters can alter neuronal activity[401]. This technique was adapted for several neurotransmitters as well as to multiphoton format[402,403].

Ultrafast femtosecond lasers have also been used for label-free neuronal activation. Experiments performed in mice slices showed two different mechanisms depending on the intensity and exposure time. While prolonged lower-intensity depolarization seemed to be resistant to sodium channel blockers and susceptible to antioxidants suggesting the implication of reactive oxygen

species, the faster high-intensity mechanism of neuronal depolarization appeared to be related with nonoperation[404]. However, this technique suits better for research applications than clinical used due to high cost and the susceptibility to misalignment. In 2005 optogenetics first appeared as a method that allows the elimination of wires and enables the stimulation of specific neuronal subtypes[309]. However, even if optogenetics has been successfully applied in rodents, relevant results in non-human primates are still lacking. Moreover, it is still far from being used in humans given the safety concerns.

An alternative technique using light to stimulate is based in pulsed infrared (IR) stimulation and has been shown to elicit neural activity. It was first demonstrated in rat sciatic nerve using a free electron laser[405,406]. Infrared neural stimulation (INS) present attractive clinical potential due to its contact-free capacity, lack of electrical stimulation artifact, and label-free. The mechanism of INS is based in transient and localized heating caused by the absorption of IR light by water molecules[407].

They observed that the ideal penetration depth was achieved when the used wavelength was close to the first two absorption peaks of water or the valley at higher wavelength. They also showed that the minimal energy necessary for INS to work was around 0.3 J/cm^2[406]. Importantly, INS is a label-free technique that does not require genetic manipulation as it occurs in optogenetics. Additionally, it presents several advantages over electrical stimulation. For instance, it presents a high spatial precision as the cells stimulated are the ones right in the illumination spot (Figure 21). Moreover, the stimulation of upper cortical layers can be performed without penetration of the tissue avoiding brain damage[408]. Furthermore, INS was shown not to interfere with electrical recordings when electrodes are out of the illumination spot and it is also compatible with magnetic resonance imaging (MRI)[406].

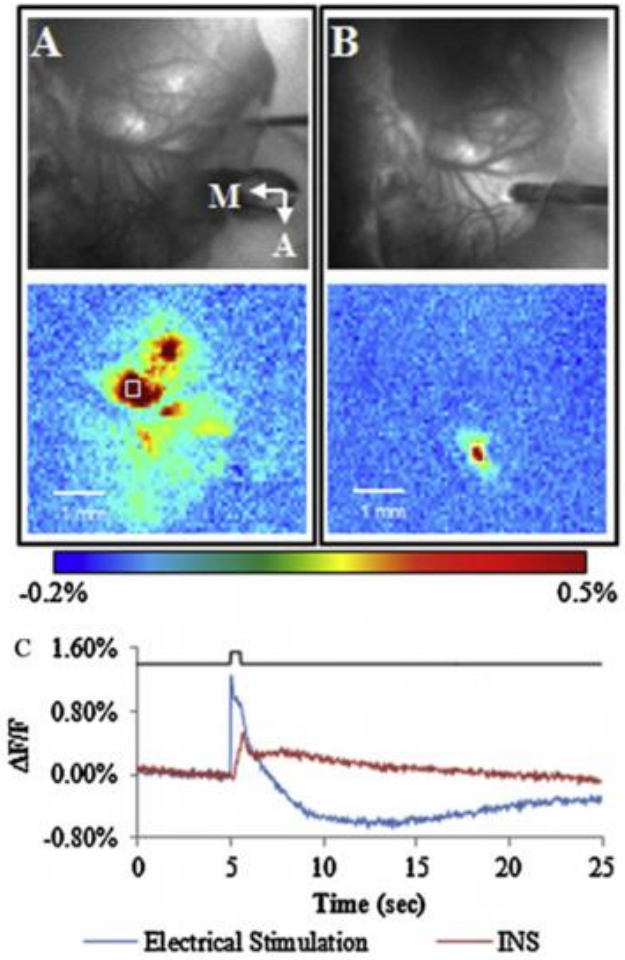

Figure 21. Comparison of electrical and INS-induced Ca^{2+} signals. A) Top panel: Blood vessel map showing the position of the electrode. Bottom panel: Activation map of Ca^{2+} signal induced by electrical stimulation (Image shows from 5 to 6 s and the stimulation protocol consisted of 0.3 mA, repetitionrate:200 Hz, pulse width 250 µs and pulse train length 500 ms). B) Top panel: blood vessel map showing the location of the optic fiber. Bottom panel: Activation map of Ca^{2+} signal induced by INS in the same animal. (Image shows from 6 to 11 s and laser parameters were 1875nm, repetition rate 200 Hz, pulse width 250 µs, pulse length 500 ms and radiant exposure 0,68J/cm^2 C) Timecourse of electrical and INS-evoked Ca^{2+} signals. Reproduced from [409] with permission from Elsevier.

The mechanism of transduction of thermal energy in alteration of membrane potential remains to be elucidated. A recent studied proposed a capacitive mechanism by performing voltage-clamp in *Xenopus* oocytes, human embryonic kidney cells and artificial bilayers to investigate INS mediated membrane potential depolarization.[410]. On the other hand, the involvement of thermosensitive ion channels was also proposed[411]. Members of the TRPV family are well known for being thermosensitive and specially TRPV4 was proposed as the primary source of INS response in retinal and vestibular ganglion neurons[411].

INS has been successfully used to activate sciatic nerve in frogs and rats causing a control contraction of isolated leg muscles [405,406]. INS has also been successfully applied in the CNS. A recent study showed by mean of calcium imaging experiments the viability of INS application in the cortex of rodents[409]. They observed that upon INS a wave-like propagation of Ca^{2+} occurred that consisted on a slow and fast component[409]. These Ca^{2+} transients were observed both in neurons and astrocytes. These results paved the way for the study of the involvement of astroglial cells in response to INS. Moreover, it is long-stablished that astrocytes express TRPV4[151], that was proposed as one of the possible translating mechanism of thermal increases.

Photostimulation mediated by photoactive organic materials has also been reported. In this context, the prototype material for organic photovoltaics, called, regio-regular poly(3-hexylthiophene-2,5-diyl) with phenyl-C61-butyric-acid-methyl ester (rr-P3HT:PCBM) coated with PLL was used to plate primary neurons. This interface can be used to photostimulate neuronal activity by using visible light and without using any externally applied electric field[412]. Interestingly, the same approach can be used to photostimulate primary culture of astrocytes[413].

9. Aim of the thesis

Studies of the past four decades has moved the neurocentric attention of the neuroscientist towards to non-excitable glial cells, called astrocytes. It has been well-established that the astroglial syncytium is a key player in the process of maintenance of homeostatic equilibrium in the brain, which is a condition essential for proper neuronal network function. Astrocytes control the concentration of ions and water, through the selective transmembrane movement of inorganic and organic molecules and the equilibration of osmotic gradients by means of transmembrane proteins forming ion channels and aquaporins (AQPs)[62]. Nonetheless, astrocytes' ion channels and aquaporins play a critical role in several physiological functions of the brain, including neuronal synaptic communication, neurogenesis and differentiation of new-born neurons, brain fluid exchange, regulation of cerebral blood flow[20]. On this regard, physiological activity of astrocytes relies on intracellular Ca^{2+} signals that can occur locally or spread globally through the astrocytic syncytium[64].

Despite important knowledge and discoveries have been provided on the role of astrocytes there is a need to uncover ***cellular and molecular mechanisms*** related to astrocytes function and disfunction. Currently available tools to study and modulate astrocyte functions and studying astrocytes/microglia interaction are facing technical ***issues such as spatio-temporal sensitivity, cell selectivity and low throughput.*** In this context, new technologies capable to selectively alter astrocytic functionality might open the view for selective analyses of the role of their ion channels and Ca^{2+} signalling.

In particular, the use of nanostructured biomaterials interface, based on carbon materials, and the use of electrical stimulation by organic bioelectronics and photostimulation by Infrared Pulsed

Laser have been demonstrated to be successful for the spatially resolved stimulation of neuronal electrical activity [347,378,414].

Interestingly, an emerging literature is demonstrating that astrocytes can responds to electrical and photo-stimulation [317,409,413,415]. However, astrocytes have been for so long considered electrically silent, and the study of the response of astrocytes to physical stimuli such as electrical and photonic ones, have been so far largely neglected [306]. Accordingly, at present, *in vitro* and in vivo studies reporting on these topics are mainly phenomenological and there is a ***lack of a mechanistic explanation of the observed responses, at molecular, biophysical and cellular level***.

On this basis, the general aim of my PhD was to validate materials interface and advanced biomedical device to alter astrocytes physiology and to unravel and understand the molecular and cellular mechanisms beyond the response of astrocytes to electrical, photonic and topographical stimulation.

In this view I developed my PhD research activities at the Laboratory for Bio Organic Interface at the Institute for the study of Nanostructured Materials and at the Institute of Organic Synthesis and at the Lab for Biology Photoreactivity of the National Research Council of Italy (CNR-ISMN and CNR-ISOF), under the supervision of Dr Valentina Benfenati, with the aim to explore firstly the potential of nanostructured carbon based-materials to fabricate device capable to modulate astrocytic function and to uncover the molecular mechanisms underpinning the observed effect. My research training program was supported and developed mainly in the framework of Marie Curie Training Project called Olimpia project FP7-PEOPLE-212-ITN, GA 316832, where the Lab of Cell Physiology of Dr Marco Caprini, FABIT Dept of the University of Bologna, was Associated Partner. In collaboration with Dr Manuela Melucci and Dr Vincenzo Palermo, from CNR-ISOF, I also had the chance to test the ability of Graphene Oxide and its bio-functionalized derivatives to be used as substrates to grow astrocytes *in vitro*.

Moreover, during the last year of my PhD, I was developing the research activities related to an International Grant supported by Air Force Office of Scientific Research (AFOSR) called ASTRONIR (FA9550-17-1-0502), where we explore the use of Infrared Pulsed laser photostimulation to evoke Ca^{2+} signaling in astrocytes and to uncover the molecular and cellular clues involve in the effect. The latter project involves Centre for Biphotonics of the University of Vanderbilt, led by Prof Anita Mahadaven- Jansen, where I spent part of my PhD.

One of the goal of my training was also to develop multidisciplinary skills such as materials and device characterization and devices fabrication that was allowed by the environment and the excellence of the frameworks in which I worked, and by close collaboration with a highly multidisciplinary team of researchers from CNR institutes (ISMN, ISOF, IMM) as well as national and international Universities, Research Centers and Private Companies. Nonetheless soft skills such as Intellectual Properties courses, Ethical Issues in Neuroscience as well as Gender issue in Science were part of my training.

Chapter 2- Experimental Section

1. Astroglial cells preparation

Preparation of primary astroglia culture

Primary cortical astrocytes were prepared from Sprague Dawley pups (P0-P2)[416]. Cerebral cortices were removed and placed in cell culture flask after dissociation. Culture medium consisted in DMEM-Glutamax medium supplemented with 15% of fetal bovine serum (FBS), 100 U/ml penicillin and 100 mg/ml streptomycin. Astroglial cells were maintained in incubation at 37 ºC and 5% of CO2 and proper humidity levels during three-four weeks before using them. Cell medium was changed every three days and flasks were gently shaken if necessary, to detach undesired cells. Cells were then seeded in samples or devices for experiments and maintained in medium with a 10% of FBS. Primary astroglial cultures were prepared at the University of Bologna and performed in concordance with the Italian law of protection of laboratory animals (ethical protocol number no. 360/2017 PR).

Preparation of primary AQP4 (-/-) astrocytes

Mouse AQP4 (-/-) astrocyte primary cultures were kindly provided by Prof. Grazia Paola Nicchia from the University of Bari from newborn pups as previously described [417]. Cells were cultured in DMEM-Glutamax medium supplemented with 10% fetal bovine serum (FBS), 100 U/mL penicillin and 100 mg/mL streptomycin and maintained at 37°C in a 5% CO_2 incubator. All the cell culture products were purchased from Thermoscientific.

siRNA and Transfection.

Stealth RNAi siRNA select RNAi (a set of three oligos: ID RSS330372, designated " number 7"; ID RSS330373, designated "number 9"; and ID RSS330374, designated "number 11") which respectively target nucleotides 1322–1346, 1201–1225, and 1642–1666 of rat TRPV4 (GenBank accession no. NM_023970.1) were purchased from Invitrogen. Transfection was performed on 2- to 4-weeks-old primary astrocytes using Lipofectamine RNAiMAX and Opti-MEM I reduced serum medium according to the manufacturer's instructions (Invitrogen). The final concentrations were 50 nM for the selected RNAi or negative control and 10 μL for Lipofectamine RNAiMAX in a T75 flask and cells were incubated for 6h. After this time cells were gently washed twice and DMEM with 10% of FBS was added for 24h. After 24h the medium was replaced with complete 10% FBS DMEM containing penicillin/streptomycin (100 U/mL and 100 μg/ mL, respectively) medium.

2. Biocompatibility assays

Fluorescein diacetate assay

Fluorescein diacetate (FDA) was used as fluorophore capable to stain viable cells. The FDA stock solution (5 mg/mL) was diluted on phosphate buffered saline (PBS, Invitrogen). Astrocytes seeded on the substrates and devices were incubated for 5 min at room temperature (RT) and washed with PBS. Images were taken with a Nikon eclipse 80i microscope equipped with a 20X objective.

Alamar blue assay

Alamar blue (AB, Life Technologies) viability assay was used according to the manufacturer's protocol. AB assay enable to quantitatively measure the cell number and the proliferation rate of living cells on the substrates at different time points. Moreover, since AB assay rely on the REDOX reaction occurring in the cytoplasm of living cells by enzymatic activity related to aerobic respiration[333], it proves also information on cell metabolism. Cells plated on the different

substrates were incubated at 37 ºC for 6 h with AB that was diluted in an amount equal to 10% of the culture volume. Afterwards, 100 µL were taken and then placed into a 96 well plate for fluorescence measurements in a microplate reader (Thermo Scientifict Varioskan Flash Multimode Reader) at by excitation at 570 nm respectively and emission at wavelength of 585 nm. Proliferation rate was calculated as the increase in fluorescence, which is proportional to the number of cells, between two successive days and it was expressed as a percentage.

3. Molecular, functional and morphological characterization of astroglial cells

Immunofluorescence and confocal microscopy

GFAP immunostaining was performed with Mouse anti-GFAP (Sigma Aldrich, Milan, Italy) as primary antibody and it was diluted to 1:300 in 3%BSA and 0.1% Triton X-100 in Phosphate Buffer Saline. We used Alexa 488-conjugated goat anti-mouse as secondary antibody diluted 1:1000. Cultured astroglial cells, seeded on samples, were fixed in 4% paraformaldehyde and washed in PBS. Unspecific sites were blocked with 3% Bovine Serum Albumine (BSA) in PBS and permeabilized with 0.1% Triton X-100 in PBS. Afterwards, cells were incubated with the primary antibody for 3 h at RT and washed in PBS. The incubation with the secondary antibody was of 1 h at RT. Samples were mounted on slides, using ProLong Diamond Antifade Mounting with DAPI and images were taken with a Nikon TE 2000 inverted confocal microscope equipped with a 40X objective and a 400 nm diode, 488 nm Ar^+ and 543 nm He–Ne lasers as exciting sources.

Calcium microfluorometry

Changes in the intracellular free Ca^{2+} concentration ($[Ca^{2+}]_i$) were monitored by calcium microfluorometry using the single-wavelength fluorescent Ca^{2+} indicator Fluo4-AM (Life Technologies, Milan, Italy). Before measurements, a high number of astrocytes were seeded on O-

CST devices pre-coated with Poly-D-lysine (PDL) were loaded with 10 µM Fluo-4 AM dissolved in standard bath solution for 30 min plus 15 min at room temperature. Samples were next rinsed with standard bath solution (see below). Measurements of $[Ca^{2+}]_i$ were performed by using a fluorescence microscope (Nikon Eclipse Ti-S) equipped with long-distance dry objective (40x) and appropriate filters. The excitation wavelength was 470 nm with a light pulse duration of 200 ms and a sampling rate of 1.5 Hz for electrical stimulation and 0.5 Hz for INS. Data acquisition was controlled by MetaFluor software (Molecular Devices).

Electrical stimulation

Specific voltage protocols were applied to the O-CSTs and diodes by a custom-made 2612A Dual-channel System Source Meter Instrument (Keithley).

Inhibitors were diluted in standard bath solution to their respective final concentration and added after rinsing.[151]

Infrared neural stimulation (INS)

Infrared laser exposure of astrocyte cultures was performed with an electrically-pulsed 1875nm diode laser (Capella; Aculight | Lockheed-Martin, Bothel, WA, USA) coupled to a 400-µm diameter low-OH optical fiber patch cable (Ocean Optics, Largo, FL, USA). To irradiate the cells, one terminal of the fiber optic was cleaved to yield a bare fiber face, which was used to irradiate the cells after a series of cleaning and polishing steps. The fiber optic was mounted into a ferrule and attached to a micromanipulator head at a 45-degree angle for precise positioning over the cells within the microscope's field of view. The edge of the optical fiber was carefully place ~10-µm from the surface of the coverslip for exposures. Applied radiant exposures (calculated ex-fiber) spanned 2.42 to 29.95 J/cm^2, with the primary radiant exposure used for pharmacological experiments of 12.74 ± 1.72 J/cm^2. Based on positioning of the fiber around 240 microns from the

surface of the cells and assuming a ~31cm^{-1} absorption coefficient at 1875nm and a ~500um spot size at the sample, we estimate that the radiant exposure observed by the cells ~5J/cm^2 within the microscopes field of view for pharmacological experiments. Single pulses delivered to the cells were primarily delivered as an electrically-pulsed 8-millisecond exposure.

Calcein self-quenching method

Changes in Cell-volume were monitored by Calcein fluorescence self-quenching method.[184] High-density astrocytes were plated on O-CST devices coated with PDL 48h before experiments. Cells were loaded with 10 µM Calcein-AM (Life Technologies, Milan, Italy) dissolved in standard bath solution and they were incubated for 15 min at RT.[184] Data acquisition was controlled by the MetaFluor software. The excitation wavelength was 470 nm with a light pulse duration of 200 ms and a sampling rate of 1.5 Hz. Specific voltage protocols were applied to the O-CST by a custom-made 2612A Dual-channel System Source Meter Instrument (Keithley).

4. Material synthesis fabrication and characterization

Synthesis of GO-PL and Preparation of GO, rGO and GO-PL membranes

The synthesis of GO-PL was performed at from the group of Manuela Melucci and Vincenzo Palermo CNR-ISO that were responsible for providing the graphene-based material and for all the materials characterizations. **12-(Acryloyloxy)-1-dodecanol (1).** Briefly, under N_2 atmosphere, 1,12-Dodecandiol (3.6 g, 18 mmol) was solubilised in 40 ml of dry THF by stirring at about 35 °C. Pyridine (0.57 ml, 7.15 mmol) was added and the solution was cooled to room temperature (r.t.). Acryloyl chloride (0.4 ml, 5 mmol) dissolved in 3 ml of dry THF was slowly added dropwise and the reaction was left under stirring overnight. The mixture was filtered to remove pyridine hydrochloride. The filtrate was evaporated under reduced pressure and the crude was purified by

flash chromatography on silica gel (CH_2Cl_2 : MeOH = 97 : 3). 700 mg of a clear oil were obtained (Y = 62%).

GO and GP-PL membranes were fabricated at CNR-ISOF by filtration of GO or GO-PL dispersions through an Anodisc™ membrane filter (Whatman, 47mm in diameter, 0.2µm pore size), followed by air drying and peeling from the filter. The rGO membrane was prepared by annealing of a GO membrane at 200 °C for one hour under vacuum. The weight of the GO, rGO and GO-PL membranes is around 15 mg and the diameter is ≈ 3,7 cm.

Roughness measurements of GO, GO-PL and rGO

The average roughness (Ra) measurements of the membranes of GO, GO-PL and rGO were performed with a profilometer (Tencor-Alpha Step 200). The roughness was measured respectively in 12 different areas for GO and GO-PL membranes and in 6 different areas for rGO membrane.

Contact angle measurement of GO, rGO and GO-PL

Contact angles of water drops on GO, rGO and GO-PL were measured by the static sessile drop method using a digidrop GBX Model DS. At least 6 drops were measured for each condition. The droplets used for measurement had a volume of 1 µL.

5. Device fabrication

O-CST fabrication

O-CST devices were fabricated in top-contact and bottom-gate configuration by using P13 as semiconducting and capping layer. An additional layer of organic semiconducting material was deposited on top of the contacts as capping layer. The substrates consisted of glass substrates covered with a 150 nm thick layer of Indium Tin Oxide (ITO). Substrates were cleaned by multiple sonications in acetone 99.5% (Scharlau, Milan, Italy) and 2-propanol 99.5% (Sigma, Milan, Italy). 420 nm of PMMA (ALLRESIST GmbH, Strausberg, Germany) were spin-coated on top of the ITO

layer in air and annealed at 120 °C for 12h in vacuum. The 15 nm thick P13 thin film was deposited by sublimation under high vacuum (10^{-6} mbar) in an Edwards 306 sublimation chamber at a rate of 0.1 Å/s. Gold electrodes with a thickness of 30 nm were evaporated in high vacuum (3-4 x 10^{-6} mbar) at a growth rate of 0.1 nm/s. The channel length between two gold electrodes was set to 70 µm. Lastly, a 50 nm thick P13 capping layer was grown on top of the gold electrodes under the same conditions as described before.

Diode fabrication

Diodes were fabricated on the same glass + ITO substrates used for the O-CST devices, following the same cleaning protocol. 420 nm of PMMA were deposited on top of the glass through spin-coating in air and annealed for 12h at 120°C in vacuum. The 15 nm thick P13 thin film was grown by sublimation under high vacuum at a base (10^{-6} mbar) in an Edwards 306 sublimation chamber at a rate of 0.1 Å/s. 20 nm thick gold electrode was deposited in high vacuum at a pressure of 3-4 x 10^{-6} mbar at a growth rate of 0.1 nm s^{-1}. A 50 nm thick P13 capping layer was vacuum sublimed on top of the gold electrode under the same conditions as described before.

6. Solutions and chemicals

Salts and other chemicals were the highest purity grade and were obtained from Sigma. The standard bath solution was composed of (mM): 140 NaCl, 4 KCl, 2 $MgCl_2$, 2 $CaCl_2$, 10 HEPES, 5 glucose, pH 7.4 with NaOH and osmolarity adjusted to ~318 mOsm with mannitol.

Ca^{2+}-free extracellular solution (0$[Ca^{2+}]_{out}$) contained (mM) 140 NaCl, 4 KCl, 4$MgCl_2$, 10 HEPES, 0.5 EGTA, pH 7.4 with NaOH and osmolarity adjusted to ~318 mOsm with mannitol.

Stock solutions of Gadolinium Chloride (Gd^{3+}, 30 mM) and Ruthenium Red (RR, 10 mM), carbenoxolone (CBX, 50mM) and Brilliant Blue G (BBG, 10 mM) were prepared in water and stored at -20ºC. Aliquots of RN-1734 (14.7 mM) and HC-030031 (40 mM) were prepared by

dissolving in DMSO and stored at -20ºC. Aliquots of TPEN (100 mM) were prepared in ethanol and stored at -20 ºC.

7. Statistical Analysis

Statistical analyses were performed with Origin 8.5. For calcium imaging experiments, the ratio of the fluorescence intensity at each time point (F_t) and the initial fluorescence (F_{t0}), that directly correlate with variation in $[Ca^{2+}]_i$[418], was continuously recorded during the experiment. The percentage (%) of inhibition of fluorescence was calculated as follows $[(F_{tcontrol}/F_{t0control}-F_{tblocker}/F_{t0blocker})/F_{tcontrol}/F_{t0control}]x100$, where $F_{tcontrol}/F_{t0control}$ was the fluorescence ratio F_t/F_{t0} recorded at the end of stimulation and 50 s after the end of the stimulation, when we used standard bath solution containing Ca^{2+}. Data were compared by one-way ANOVA with Bonferroni post-test. A statistically significant difference was reported if $p \leq 0.05$. The data derived from at least 3 independent experiments performed at least in triplicate.

8. Image processing and analysis

Image processing and analysis was performed using the FIJI distribution of ImageJ with a custom processing script. Images from the confocal imaging software (Nikon EZ-C1 2.10) were imported into ImageJ, cropped and converted to greyscale TIFF format images. A binary mask was generated to separate cellular fluorescence from the background. This mask was used to generate a region of interest (ROI) covering all the cells in the image. An inverted version of the previous binary mask was used to identify a ROI for the image background. The mean fluorescence, ROI area, and integrated density values for the cellular fluorescence and background were measured for each image. These values were used to calculate the corrected total cell fluorescence.

Chapter 3 – Electrical stimulation of calcium signaling in astrocytes by an organic transistor architecture

1. General overview

Organic bioelectronics has a huge potential to generate interfaces and devices for the study of brain functions and for the therapy of brain pathologies. In this context, increasing efforts are needed to develop technologies for monitoring and stimulation of non-excitable brain cells, called astrocytes. Astroglial Ca^{2+} signalling play, indeed, a pivotal role in the physiology and pathophysiology of the brain. In this work, we demonstrate the use of transparent Organic Cell Stimulating and Sensing Transistor (O-CST) architecture, fabricated with N, N'-ditridecylperylene-3,4,9,10-tetracarboxylic diimide (P13), to elicit and monitor $[Ca^{2+}]_i$ in primary rat neocortical astrocytes. The transparency of O-CST allowed performing calcium imaging experiments showing that extracellular electrical stimulation of astrocytes induces a drastic increase in $[Ca^{2+}]_i$. Pharmacological studies indicates that Transient Receptor Potential (TRP) superfamily, are critical mediators of the $[Ca^{2+}]_i$ increase. Experimental and computational analyses shows that $[Ca^{2+}]_i$ response is enabled by the O-CST device architecture. Noteworthy, the extracellular field application induces a slight but significant increase in the cell volume. Collectively, we show that the O-CST is capable to selectively evoke astrocytes $[Ca^{2+}]_i$, paving the way to the development of organic bioelectronic devices as glial interfaces to excite and control physiology of non-neuronal brain cells.

2. P13 is a biocompatible substrate for the growth of primary astrocytes

The first step of our study was to test the biocompatibility of the O-CST device with primary cortical astrocytes. We plated astrocytes on P13 coverslips, the material forming the capping layer of the device. After 2, 7 and 15 days *in vitro* (DIV), we performed fluorescein diacetate (FDA) cell viability assay. Single plane confocal images of astrocytes plated on Glass + PDL and P13 + PDL are shown in Figure 22 A and B respectively. Morphological study showed that astrocytes presented the typical polygonal shape observed when they are cultured *in vitro* on different substrates[370,419,420]. Analysis performed in confocal images is represented in the histogram plot in figure 22C showed that, at 2 and 7 DIV, the viability of astrocytes plated on P13 + PDL was significantly higher compared with the one observed in cells grown on Glass + PDL that was used as control. At 15 DIV the number of astrocytes grown on the two substrates was comparable. The result demonstrates the good biocompatibility of P13 for the adhesion and growth of primary cortical astrocytes. Moreover, it supports the previously published data on P13 and DRG neurons, confirming P13 as a suitable material for the culture of neural cells[378].

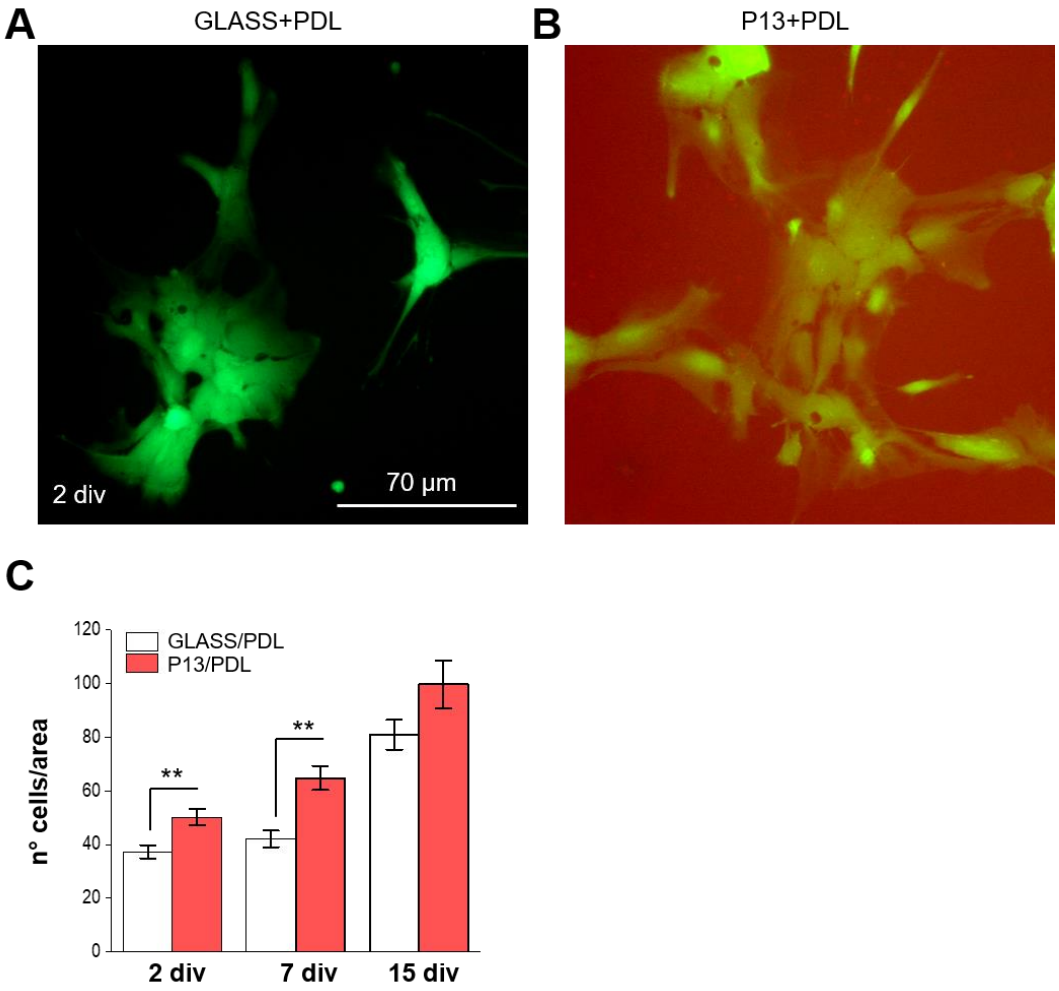

Figure 22. **Biocompatibility study of P13.** Single plane confocal image of astrocytes after 2 DIV stained with fluorescein diacetate (FDA) on (A) Glass + PDL and (B) P13 + PDL; the P13 film is imaged by the red detection channel. (C) Histogram plot shows the average of FDA positive cells/area counted on Glass + PDL and P13 + PDL, after 2, 7 and 15 div. A statistical difference was observed after 2 and 7 div (**p<0.01, ANOVA one-way)[421].

3. Extracellular electrical stimulation by O-CST elicits astrocytic intracellular Ca^{2+} increase

We next explore the effect of electric field application by operation of O-CST on the functionality of primary cortical astrocytes of device. To assess if we could extracellularly stimulate astrocytic $[Ca^{2+}]_i$, we performed calcium imaging experiments, enabled by the transparency of the device. We loaded astrocytes plated on O-CST with Fluo-4-AM (Figure 23B) and we performed calcium imaging experiments in external standard solution containing defined mM concentrations of salts

including Calcium Chloride. The electrical stimulation protocol used is reported in Figure 23C inset. The gate Voltage (V_{GS}) was spanned from 0 to 1V in 85 s, while Drain-Source Voltage (V_{DS}) was kept at 0 V. The applied voltage was chosen to electrically stimulate astrocytes at the top interface of the device avoiding the generation of detrimental Faradaic currents[378]. The total duration of the experiments was 300 s and the O-CST stimulation was applied after 150 s from the beginning of the recording. Figure 23C shows an average trace and SE reflecting the behaviour of the dynamic of F_t/F_{t0}, that is correlated to $[Ca^{2+}]_{i,}$ observed in the majority of the recorded cells (Figure 23 E) (green trace). After electrical stimulation, F_t/F_{t0} rises slowly but constantly. The histogram plot in figure 23D reports the mean and SE of F_t/F_{t0} recorded before (white column), at the end of stimulation (green column) and 50s after the end of O-CST stimulation protocol (blue column). The analyses revealed that, at the end of stimulation, fluorescence intensity increased of the 30% with respect to the baseline recorded before stimulation. Moreover, the value of F_t/F_{t0} 50 s after the end of O-CST operation was 50% with respect to the baseline recorded before stimulation. These data indicated that O-CST operation promoted an increase in astrocytic $[Ca^{2+}]_i$ elevation.

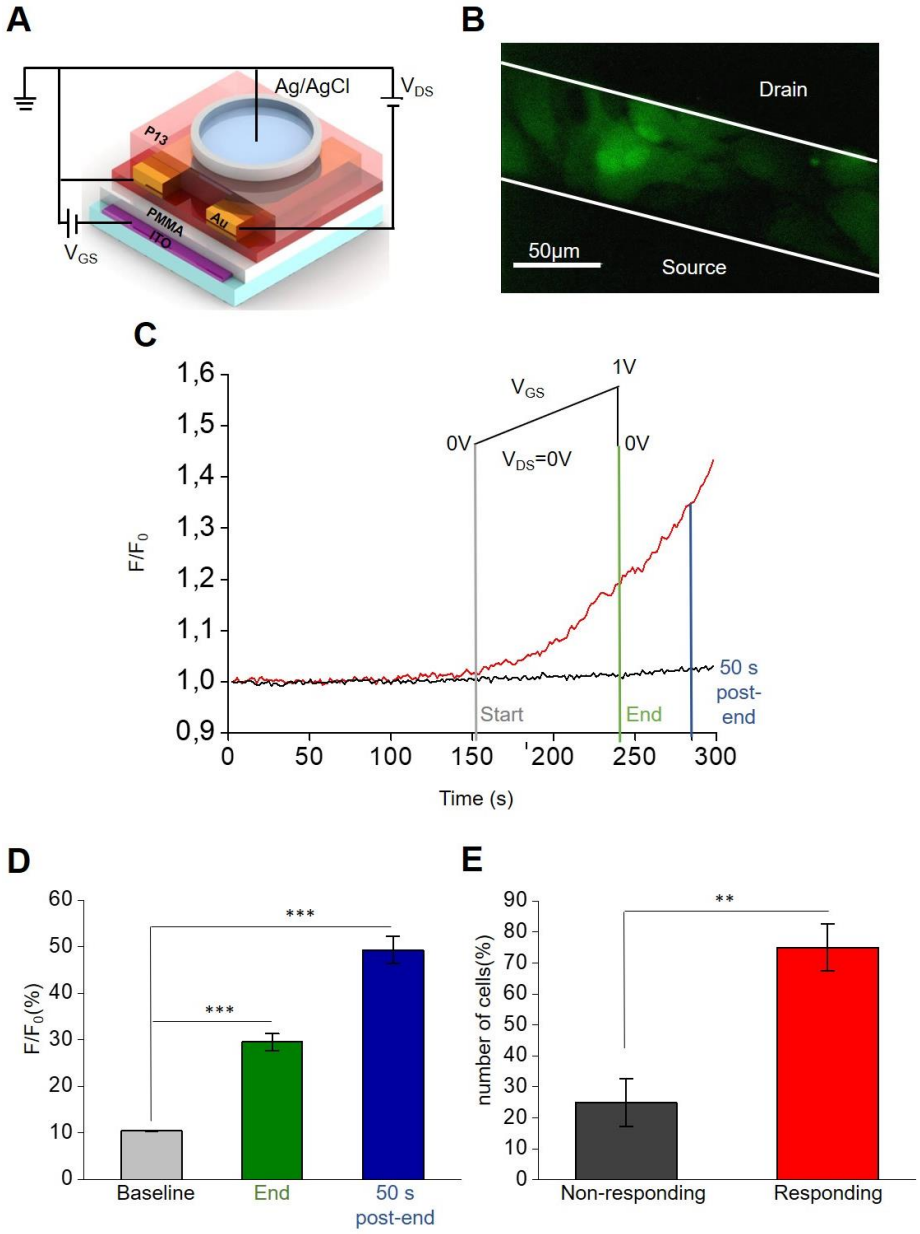

Figure 23. O-CST operation promotes $[Ca^{2+}]_i$ increase in astrocytes. (A) Scheme representing the O-CST device. (B) Fluorescent image of cells on O-CST device, labelled with Fluo4-AM. (C) Representative averaged trace of calcium imaging experiment on O-CST device. The transfer stimulation protocol with V_{GS} = 0-1V and V_{DS} = 0V with a duration of 85s was applied after 150s of the beginning of the experiment. (Ft= fluorescence intensity at selected timepoint; Ft_0= fluorescence intensity at time point = 0s), the grey, green and blue lines represent the timepoint at which the F_t/F_{t0} was considered for statistics calculations. (D) Histogram plot shows the averaged fluorescence intensity F_t/F_{t0} (%) before the stimulation (control, grey column), at the end of the stimulation (green column) and 50s after the stimulation (blue column). The values are presented as mean with standard error (SE). Statistical difference was observed between F_t/F_{t0} (%) recorded before the stimulation (baseline) and at the end of the stimulation as well as 50s after the end of the stimulation. (Control n=135, at the end of the stimulation n=106, 50s after stimulation n=106; *** $p<0.001$, One-way ANOVA). Results represent at least eight independent experiments performed in triplicate. (E) Histogram plot shows the percentage of cells responding (grey bar) and non-responding (red bar) to transfer stimulation. The values are presented as mean with SE. Statistical significance can be observed between the number of responding and not responding cells. (n=135, ** $p<0.01$. One-way ANOVA)[421].

In order to verify the origin of the rise of cytosolic $[Ca^{2+}]_I$ we repeated the experiment using Ca^{2+}-free external solution ($0[Ca^{2+}]_{out}$) (Figure 24). In comparison to the results obtained using standard solution containing Ca^{2+}, when we used a Ca^{2+} free external solution ($0[Ca^{2+}]_{out}$, Figure 24A, trace 8, dark blue) 90.58±3.19% of the $[Ca^{2+}]_i$ induced by O-CST was inhibited at the end of the stimulation (Figure 24B, green column), while the inhibition was of the 94.02±7.335%, 50s after the stimulus (Figure 24B, blue column). These data indicated that the increase in $[Ca^{2+}]_i$ was mediated by an influx of Ca^{2+} from the extracellular environment.

Several studies showed the implication of TRP channels in astrocyte Ca^{2+} influx[151,154]. To investigate the contribution of TRP family in the observed effect, we applied 10 µM Ruthenium Red (RR) (Figure 24A, trace 6, red) and Gadolinium Chloride (10 µM, Ga^{3+}, Figure 24A, trace 7, violet), non-specific inhibitors of TRP channels[151,422]. In both cases, we observed a significant decrease in the fluorescent intensity (83.604±2.91 % at the end of the stimulation (Figure 24B, green column) and 85.50±6.56 % 50 seconds after the end (Figure 24B, blue column) for RR and 72.40±5.13 % (Figure 24B, green column) and 71.69±12.42 % (Figure 24B, blue column for Ga^{3+}) compared to the control condition when the experiment was performed without the blocker (Figure 24B, trace 1, black).

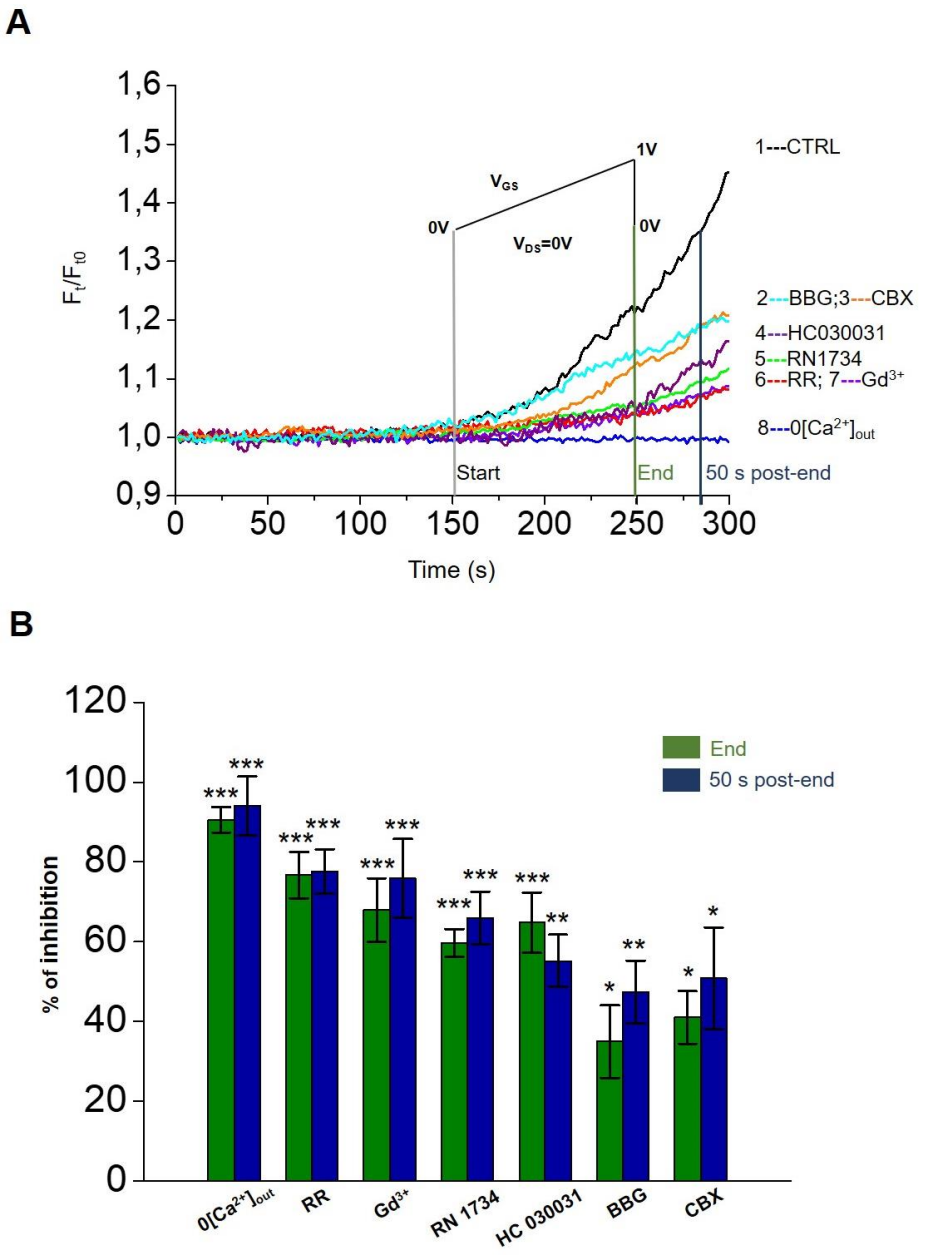

Figure 24. TRPV4 mediates $[Ca^{2+}]_i$ increase in astrocytes elicited by O-CST device. A) Averaged traces representative of calcium imaging experiments performed while stimulating cells on the O-CST channel using as bath: a control extracellular solution (CTRL, trace 1) and Ca^{2+} free external solution (0$[Ca^{2+}]_{out}$, trace 8) or a control extracellular solution added with Ruthenium Red (RR) (10 µM, B, trace 6), Gadolinium Chloride (Gd^{3+}, 10 µM,C, trace 7), RN-1734 (10 µM, D, trace 5), HC-030031 (40 µM, E, trace 4), Brilliant Blue G (BBG, 10 µM, F, trace 2) Carbenoxolone (50 µM , CBX, G, trace 3). H) Histogram plot showing the mean percentage inhibition of fluorescence intensity of the analysed cells at the end of the stimulation (red bars) and 50s after the stimulation (blue bars) normalized to the value recorded when the experiments were performed by using control solution containing Ca^{2+} (CTRL). (Ca^{2+}_free external solution n=69, RR n=39, RN-1734 n=39, Gd^{3+} n=78, HC-030031 n=34, BBG n=76 and CBX n=52). The values are presented as mean with SE. Statistical significance were calculated with respect to the value recorded when the experiments were performed by using control solution (CTRL), considered as 100%. (** $p<0.01$. One-way ANOVA). Results represent at least three independent experiments performed at least in triplicate[421].

To explore the contribution of TRPV4, a member of the TRP family that is widely expressed in astrocytes[151], we applied the selective TRPV4 antagonist RN-1734 (10 µM, Figure 24A, trace 5, green)[423]. We observed that a diminution of the fluorescence intensity of 61.85±4.94% (Figure 24B, green column) at the end of the stimulation and 68.73±8.44 % (Figure 24B, blue column) 50s after the end of the stimulus. Moreover, the application of HC 030031, a selective inhibitor of TRPA1, another member of TRP family expressed in astrocytes, (40 µM, Figure 24A, trace 4, purple)[156], diminished the fluorescence intensity of 64.77±7.60% at the end of stimulation (Figure 24B, green column) and 55.18±6.54 % of inhibition 50 seconds after the end of O-CST operation (Figure 24B, blue column). Collectively, these evidences showed the role of TRPV4 and TRPA1 in the cytosolic $[Ca^{2+}]$ increase evoked by O-CST stimulation.

We next investigated the involvement of $P2X_7$ receptor to the observed response by adding Brilliant Blue G (BBG) to the external control solution [424], (10 µM, Figure 24A, trace 2, light blue). We verified that a significant but smaller inhibition of fluorescence increase occurs (34.97±9.10%) at the end of the stimulation (Figure 24B, green column) as well as 50s after the end of the stimulation (47.35±7.89%, Figure 24B, blue column). Finally we used Carbenoxolone (CBX) [197] (50 µM, Figure 23A, trace 3, orange), a non-selective inhibitor of gap junctional proteins, connexins (Cx) and pannexins (Panx). The inhibition of fluorescence intensity for CBX was significant and it was 40.99±6.57 % at the end of the stimulation (Figure 24B, green column) and 50.82±12.76% 50 s after gate off (Figure 24B, blue column).

The pharmacological analysis performed revealed that extracellular Ca^{2+} majorly contributed to the observed response. Also, we observed that two members of the TRP superfamily, TRPV4 and TRPA1 are involved in the Ca^{2+} increase mediated by O-CST operation. The implication of P2X7 and gap junctional proteins seems to be also to be involved in the stimulation-evoked signal. TRPV4 is a non-selective cation channel that presents a high permeability for Ca^{2+} and other monovalent cations[425]. TRPV4 is activated by different stimuli, such as osmotic changes,

mechanical stimulation, changes in temperature and chemicals like 4α-phorbol 12,13-didecanoate, 4αPDD[425,426]. They were also shown to stimulate Ca^{2+}-induced Ca^{2+} release in astrocytic endfeet[150]. In astroglial cells, TRPV4 plays an important role in cell volume regulation by its interaction with AQP4[151,427–429]. Meanwhile, TRPA1 is also a non-selective cation channel expressed in astrocytes[154]. In hippocampal astrocytes, TRPA1 was recently demonstrated to be implicated in the control of basal levels of $[Ca^{2+}]_i$[156]. It was also showed their implication in the release and uptake of neurotransmitters, such as D-serine and GABA[154]. Altogether, data shows that our finding could be relevant for its application in neurophysiology. TRP channels are known to undergo desentization, a phenomenon that set the basis of the study of drugs capable of interacting with these channels as anti-inflammatory and anti-pain therapies[430]. Nevertheless, the wide distribution of members of the TRP family increase enormously the cost of drugs to interact selectively with specific members of this superfamily of channels. Moreover, TRPV4 is also known to be implicated in other brain pathologies such as ischemia, where TRPV4 was found to be upregulated in the hippocampus of a rat model of ischemia[148]. Furthermore, altered TRPV4 expression was also observed in autoptic samples of patients suffering from Focal cortical dysplasia (FCD), a cause of epilepsy[431]. In this view, O-CST stimulation might be a potential therapeutical tool capable of desensitize TRPV4 to treat this neuropathologies and the bioelectronic approach we present here could be a relevant alternative to the pharmacology.

We also observed that CBX and BBG were capable of reducing $[Ca^{2+}]_i$ response evoked by O-CST stimulation. The effect of these molecules, suggested the involvement of Cx or Panx and $P2X_7$ in the observed increase in $[Ca^{2+}]_i$. Nevertheless, due to the low selectivity [175,197,432] of these compounds the contribution of those protein channels needs further investigations.

Notably, the stimulation protocol used to stimulate astrocytes, failed to evoke action potential in DRG neurons[378]. Therefore, our data indicated that the proposed approach, based on O-CST

stimulation, could be used for selective stimulation of astroglial cells and neurons depending on the need, by simply changing the stimulation protocol.

4. O-CST operation induces astrocytes swelling and preserves cell viability

Several work showed that the application of external electric fields induced cell swelling in several cell types[433–436], that depended by the duration and the intensity of the stimulation[433–436]. Our group previously demonstrated that TRPV4 mediates swelling induce $[Ca^{2+}]_i$ response by extracellular Ca^{2+} influx in astroglial cells[151,437]. Therefore, we hypothesized that the electrical stimulation, mediated by the O-CST operation, might evoke cell swelling and, in turn, activate the observed $[Ca^{2+}]_i$ increase.

To verify this hypothesis, we performed Calcein self-quenching method[184] to assess cell volume changes in astroglial cells exposed to O-CST electrical stimulation. In response to O-CST stimulation (Figure 25A), we observed an increase in Calcein fluorescence that reaches a maximum value few minutes after the cell stimulation. Previous studies showed that the maximal increase in fluorescence we observed (around 2%) corresponds to a significant increase in cell volume[184,438]. Notably we observed cell swelling in the majority of cells analysed (74.40 ± 9.02%, Figure 25B).

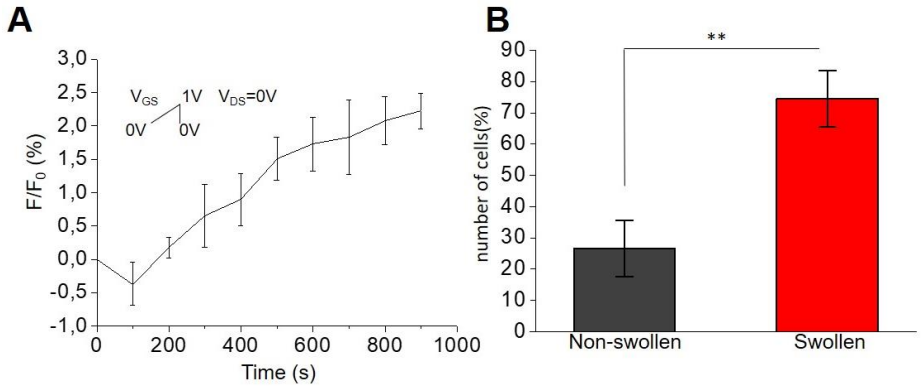

Figure 25. O-CST operation induces astrocytes swelling. (A) Calcein self-quenching method for measurement of volume changes in primary astroglial cells. Time course of the fluorescence intensity of calcein before, during and after

O-CST stimulation (inset reported above the graph). An increase in fluorescence intensity represents cell swelling. Results are representative of at least five independent experiments. (B) Histogram plot shows the percentage of swollen and non-swollen upon stimulation. The values are presented as mean with SE. Statistical significance can be reported between the number of responding and not responding cells. (** $p<0.01$. One-way ANOVA. $n=56$)[421].

A recent computational study showed that the application of external electric field can affect water dipole orientation within the channel pore. They hypostasized that this change in water dipole could in turn modify human AQP4 water permeability[439]. In this context, we can hypothesize that the electric field applied by the operation of the O-CST could induce AQP4 mediated cell swelling, that in turn activate the molecular of functional partner of AQP4, i.e. TRPV4[151]. However, further studies on AQP4 KO models need to be performed to clarify this aspect. Moreover, as TRP channels are polymodal channels, we cannot rule out the possibility that capacitive charging or thermal dispersion at the interface caused the activation of TRPV4 and TRPA1 activation.

Moreover, we performed FDA cell viability assay, 24h after stimulation, to evaluate cytotoxicity of the stimulation. The analysis of confocal images of cells non-stimulated (Figure 26A) and stimulated (Figure 26B) revealed that astrocytes are still viable 24h after device operation. Cell counting showed that there was not significantly difference between stimulated and non-stimulated cells (Figure 26C).

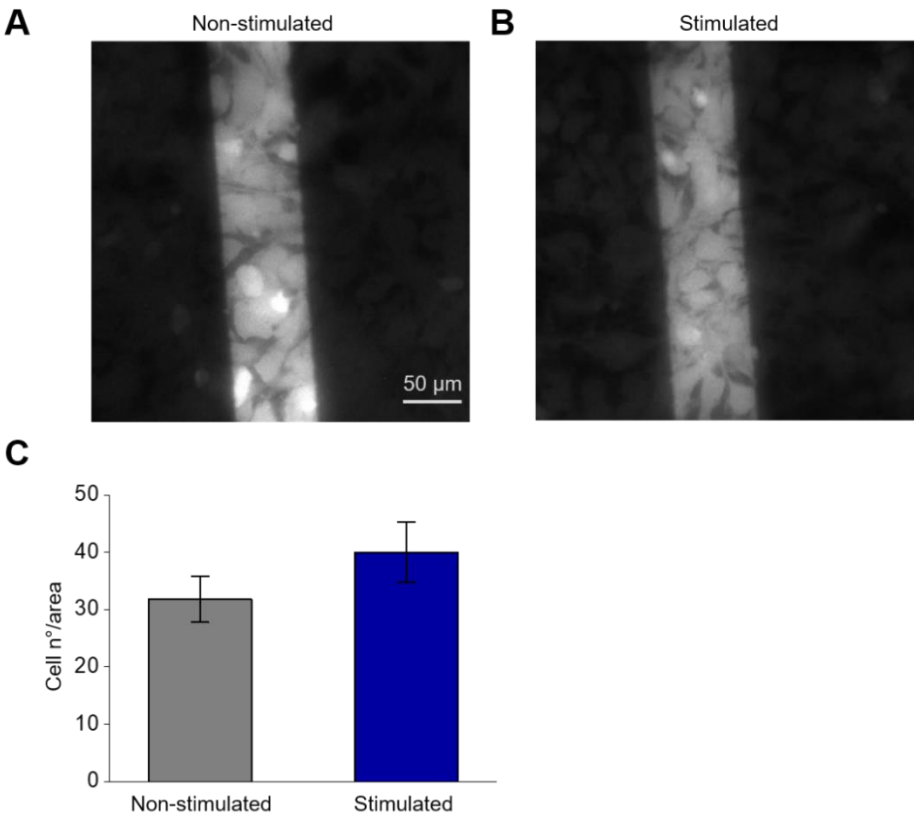

Figure 26. **O-CST operation does not alter cell viability.** (A-B) Fluorescence images showing FDA stained viable cells on O-CST non-stimulated (A) and 24h after device operation (B). C) Histogram plot shows the average FDA positive cells/area. Astrocytes were plated on the device and images were taken 24h after the stimulation (blue). The second group of samples treated under the same condition was not stimulated and used as control (grey). No statistical difference was observed. Results represent mean ± SE collected from three independent experiments (n=30, $p>0.05$, ANOVA one-way)[421].

5. O-CST device architecture enable calcium signalling

We next sought to verify the role of O-CST architecture in the observed increase of $[Ca^{2+}]_i$. We performed calcium imaging experiments using a diode structure with one gold electrode and an Ag/AgCl reference electrode submerged in the bath. The semiconductor and capping layers were also made of P13 (Figure 27A). We observed that by operating the diode with the same linear ramp stimulation we applied in the O-CST (0V to 1V applied to the gold electrode with respect to the reference electrode) we failed to induce any response in the majority of cells (98.57 ± 1.42%, Figure 27B, D). In fact, the fluorescence intensity was the same before, during and 50 s after the stimulation (Figure 27C).

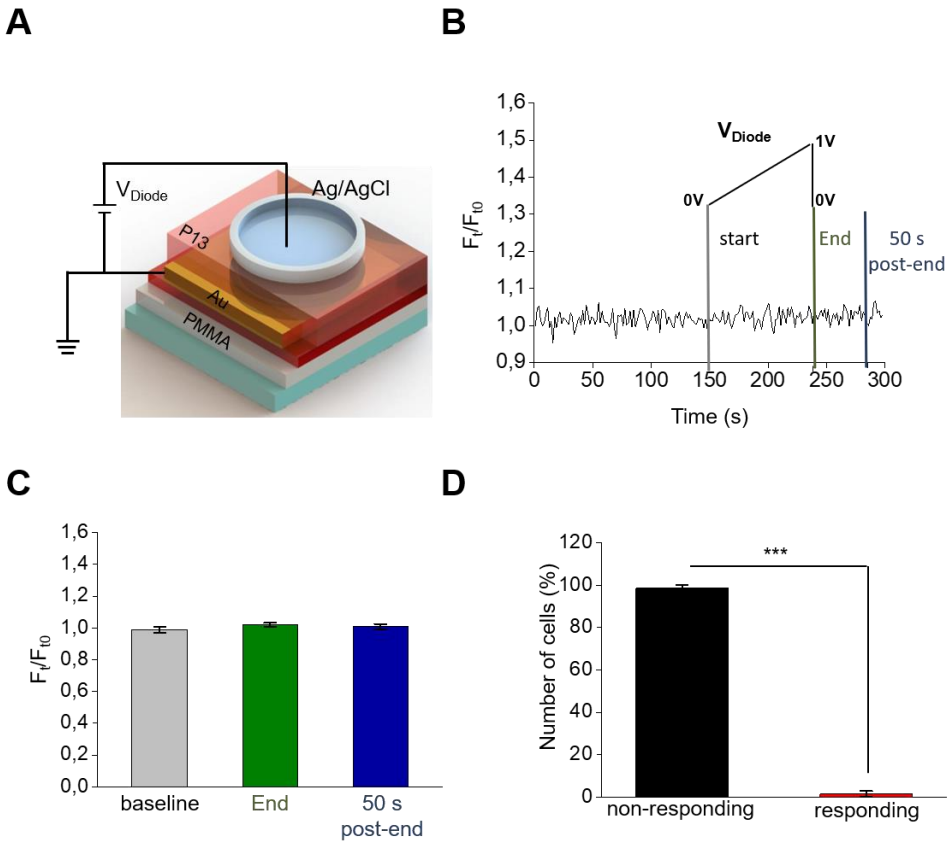

Figure 27. Cellular response in dependence of the device architecture. (A) Representation of the diode device structure and voltage application protocol (V_{Diode} from 0 to 1V). (B) Representative averaged trace of calcium imaging experiment performed on cells plated on a diode. A continuous stimulation protocol with a duration of 85 s was applied at 150 s (red). The voltage between the electrode and the solution (Vdiode) goes from 0 to 1 V as depicted in the inset. (C) Histogram plot depicting the mean fluorescence before stimulation (control, white column), end of the stimulation (red column) and 50s after the end of the stimulation (blue column). Results represent at least ten independent experiments. (D) Histogram plot showing the percentage of cells non-responding and responding to the stimulation. The values are presented as mean with SE. A statistical difference can be reported between the number of responding and non-responding cells (n=115, *** $p<0.001$. One-way ANOVA)[421].

We further investigated the impact of the O-CST structural integrity and device working functionality on the astrocytic response. Figure 28 reports typical gate current of an undamaged O-CST and of an O-CST with a leaking dielectric, recorded upon the stimulation protocol reported above. The undamaged O-CST device has a maximum leakage current of 2 nA (Figure 28A, green circle trace) whereas the device with leaking dielectric shows a thousand-fold higher leakage current of about 2 µA (Figure 28A, blue squares trace). Calcium imaging experiments, applying the protocol reported in Figure 23C, on an O-CST device with a gate leakage-current of 2 µA, revealed that the leaking device failed to evoke $[Ca^{2+}]_i$ signal in astrocytes (Figure 28B, blue trace). These

results show that O-CST architecture and integrity are essential for evoking $[Ca^{2+}]_i$ on astroglial cells and confirm that the cell stimulation is due to a capacitive effect between the ITO electrode and the organic-solution interface. Indeed, only the undamaged O-CST where the leakage current is practically absent, and the field effect is preserved can evoke cell response (Figure 28B, green trace), while the device with defective dielectric and resistive behaviour between the ITO electrode and the organic-solution interface cannot (Figure 28, blue trace).

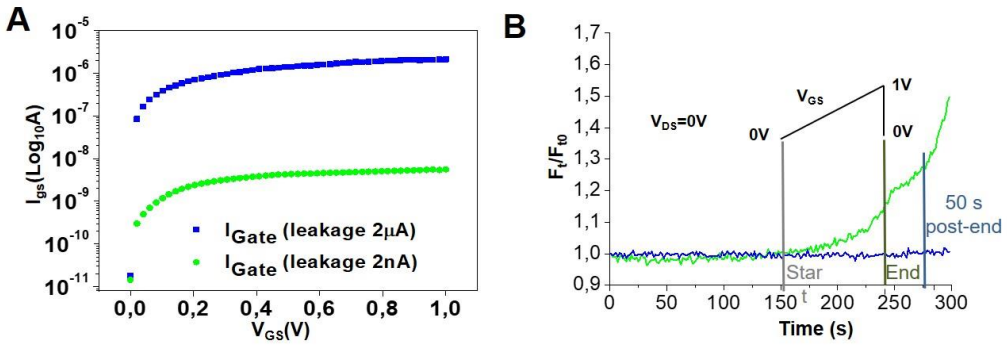

Figure 28. O-CST architecture and structural integrity are essential for cellular response. (A) Gate current plots in an O-CST with minimum leakage current of 2 nA (green circles trace) in comparison to a device with a high leakage of 2 µA (blue squares trace). (B) Representative calcium imaging experiment on O-CST device with a leakage current of 2 µA (blue) and 2nA (green). A continuous stimulation protocol with duration of 85 s was applied at 150 s [421].

Chapter 4- Biomimetic graphene for enhanced interaction with the external membrane of astrocytes

1. General overview

We next sought to investigate the potential of a single sheet of another carbon-based material, i.e. graphene and its derivative graphene oxide (GO) as material interface to interact with the membrane of astrocyte. Indeed, graphene sheet is potentially another carbon-based material suitable to interact with neural cells thanks to its 2-dimensional shape, flexibility, mechanical strength and, even more important, tunable surface chemistry.

The interaction of graphene-based materials such as sheets, films and flakes with neurons was previously studied[339,440,441]. Graphene-based materials were shown to present different purposes such as drug delivery[338], scaffolds for neuroregenerative medicine[442] and transistor and electrodes to read-out and manipulate neurons' functionality[443–445]. A recent study showed that 2-dimensional GO nanosheets do not alter glial viability, nor synaptic communication in primary hippocampal neurons and cortical glial cultures[338]. Nevertheless, another study showed that GO nanosheets disrupted lipid composition and altered Ca^{2+} homeostasis and synaptic transmission in neurons[339]. These latter findings motivated us to explore the use of phospholipids (PL) to functionalize graphene membranes to achieve a better interaction with cell membrane. A new type of GO composites specifically designed and synthesized by the group of Vincenzo Palermo and Manuela Melucci at CNR-ISOF for enhancing GO-neural cells interaction. A synthetic phospholipid (PL) was tailored to bind to graphene oxide, to promote graphene oxide interactions with the cell's membrane (Figure 29). Indeed, PL-functionalized nanomaterials were already proposed for studying the signaling pathways where PL are implicated.

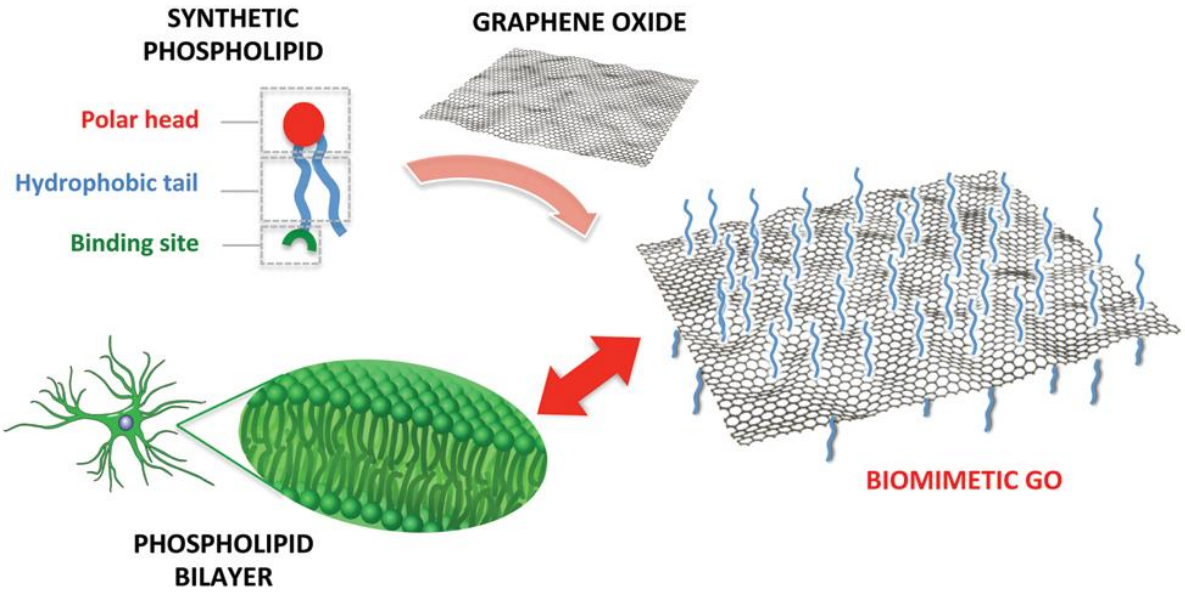

Figure 29. Outline of the rationale of the work. PLs were tailored to bind GO to improve interactions with cell membrane. Reproduced from [333] published by The Royal Society of Chemistry.

Given the key role of astrocytes in brain function, dysfunction and in the response of the brain to implants, we performed experiments where we plated primary rat cortical astrocytes.

GO-PL was processed in flat membranes (Figure 30). GO and reduce rGO membranes were also prepared to verify the effect of chemical properties of the graphene derived materials in the interaction with astroglial cells. Scanning Electron Microscopy (SEM) images of GO-PL showed that the obtained composite presented the typical graphene-like structure. SEM images showed that graphene sheets were tightly packed on each other (figure 30B and C). Membrane surface roughness (Ra) was measured by using a profilometer. We observed a strong difference in surface Ra between GO-PL (Ra= 550 ± 130nm) and GO (Ra= 170 ± 50nm). Contact angle measurements, that indicate the hydrophobicity and hydrophilic properties of the material surface (Figure 30 D-F) showed higher hydrophobicity for GO-PL (78 ± 1) with respect to GO (41 ± 1), but similar to rGO (86 ± 1.68) (Figure 30 D-F). These results suggest that PL moieties are arranged in such a way that they do not expose their polar heads to the outer surface of the membrane.

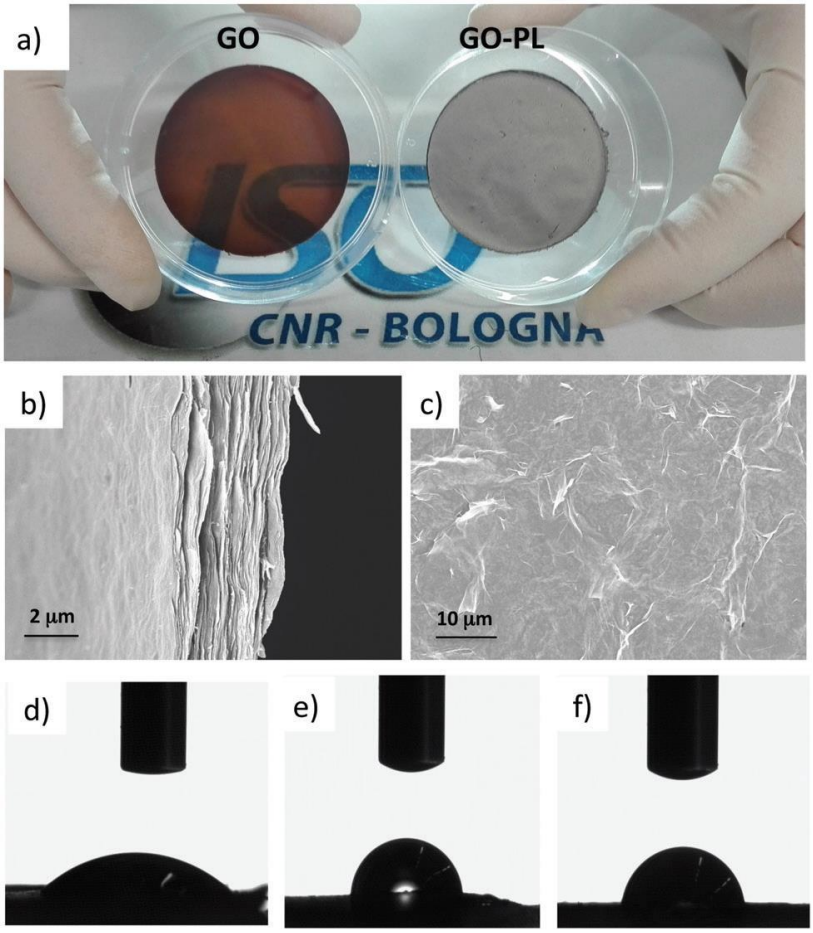

Figure 30. A) GO and GO-PL membranes. B) SEM image of a cross section. C) SEM image of a top view of GO-PL. (D-F) Shape of water droplet (1µL) on the surface of GO (D), rGO (E) and GO-PL (F). Reproduced from [333] published by The Royal Society of Chemistry.

2. GO–PL promotes cell adhesion without inducing gliosis

We next sought to verify the biocompatibility of GO-PL membranes with primary rat astroglial cells. We also plated on the state-of-the-art glass coverslip treated with Poly-D-lysine (PDL), pristine GO and rGO. We performed fluorescein diacetate (FDA) assay to mark viable cells after 2 days *in vitro* (DIV). Micrographs reported in Figure 31 A-D shows the viable cells stained with FDA (green) in the four different conditions. We observed that at this timepoint, the number of viable cells was higher on GO-PL samples. In order to get a quantitative result of cell viability we performed Alamar blue cell viability assay at 1, 2, 4 and 7 DIV (Figure 31 E). The histogram plot in Figure 31 E shows the normalized fluorescence represented by the F_t/F_{t0} ratio per area, that is

directly proportional to the number of cells that are viable per substrate[420]. The number of viable cells on GO and rGO samples were comparable with those on Glass + PDL, while the number of viable cells on GO-PL samples was more than doubled when the experiment was performed at DIV 1. The number of viable cells on GO-PL was also significantly higher at 2, 4 and 7 DIV. However, the proliferation rate was comparable in all the conditions (Figure 31 F) suggesting that a gliotic response is not the responsible for the higher number of viable cells observed. Altogether, these data suggest that the higher number of cells in GO-PL could be explained by a higher adhesion of astroglial cells to this substrate. The observed lower cell proliferation (in percentage) observed on GO-PL for higher DIVs could be explain by contact inhibition of proliferation as the available area for cell adhesion and proliferation was the same for all the samples and therefore astrocytes plated on GO-PL reached confluency earlier (Figure 31F). Moreover, the significantly higher number of cells that adhere to GO-PL when compared with rGO showed that astrocytes higher adhesion was not increased by a difference in hydrophobicity or roughness as both samples present comparable values for both properties. Thus, the higher adhesion observed on GO-PL suggest that surface chemistry is crucial in this process. Indeed, contact angle values of GO-PL samples indicate that the hydrophobic tails of PLs are exposed to the outer surface suggesting a possible direct interaction between GO-PL and astroglial cell membrane through the aliphatic apolar tails.

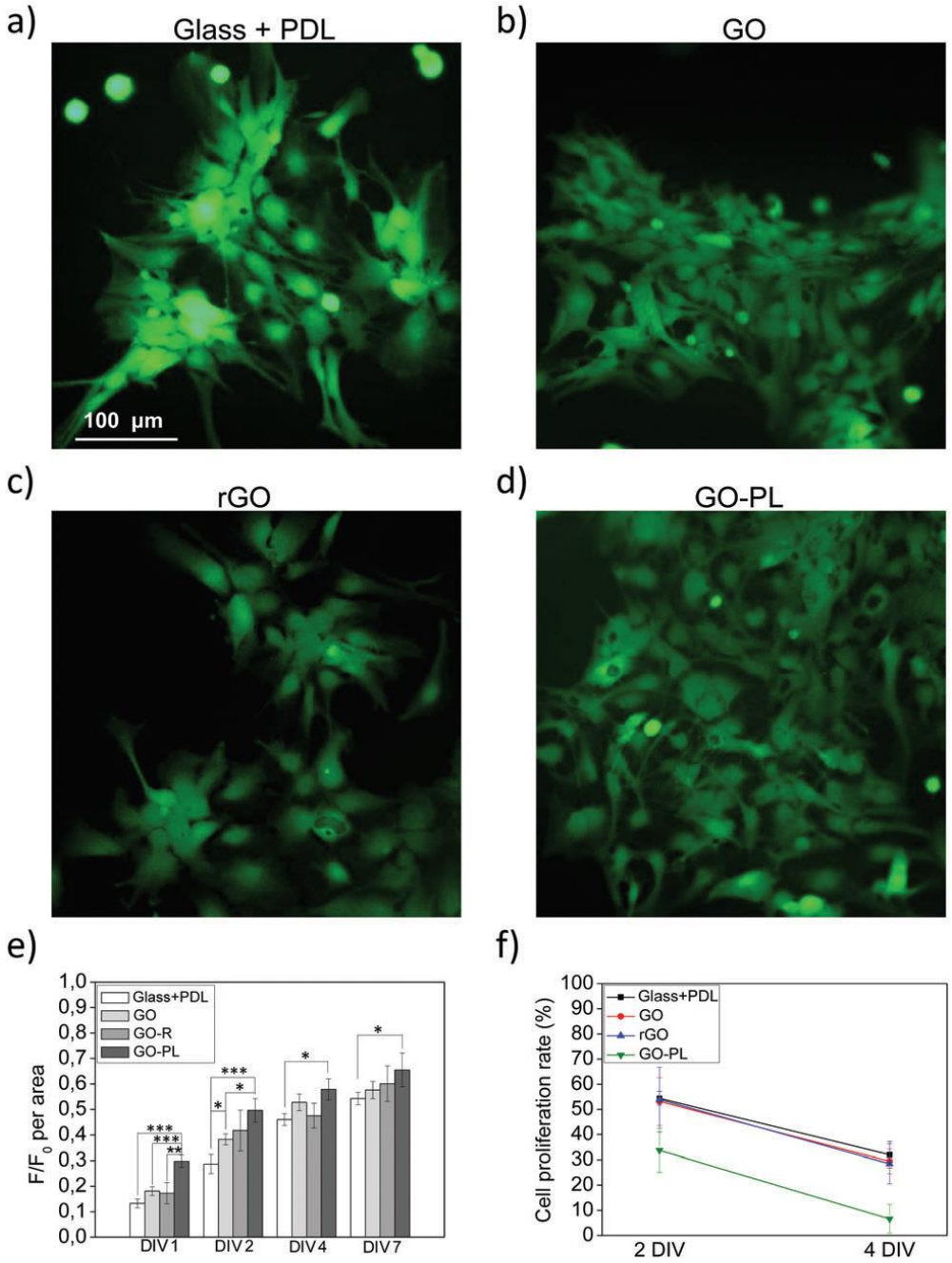

Figure 31. Biocompatibility study of GO, rGO and GO–PL. (a–d) Representative micrographs of FDA stained astrocytes plated on glass + PDL as reference, GO, rGO and GO–PL taken at 2 DIV. (e) Histogram plot shows averaged F_t/F_{t0} per area plated on GLASS + PDL (n = 18), GO (n = 17), rGO (n = 9) and GO–PL (n = 18), after 1, 2, 4 and 7 DIV. (*p o 0.05; **p o 0.01; ***p o 0.001, One-way ANOVA). Results represent at least three independent experiments. (f) Cell proliferation on the 4 substrates at DIV2 and DIV 4, calculated as indicated in materials and methods. The slope of the curve is identical, indicating that the proliferation rate was comparable for all substrates. Reproduced from [333] published by The Royal Society of Chemistry.

Lastly, we performed GFAP immunostaining to investigate a possible gliotic reaction triggered by GO, rGO or GO-PL. GFAP is a well-known marker of astrogliosis *in vitro* and *in vivo*[446]. Micrographs in Figure 32 A-D shows confocal images of GFAP immunostained astrocytes grown

on glass + PDL, GO, rGO and GO-PL respectively. Imaging and quantitative analysis of fluorescent signal (Figure 32 E) showed that the levels of GFAP expressed were comparative on the four different substrates. Collectively, proliferation study (Figure 32 E) and GFAP immunostaining suggests that GO, rGO and GO-PL did not promote reactive gliosis *in vitro*.

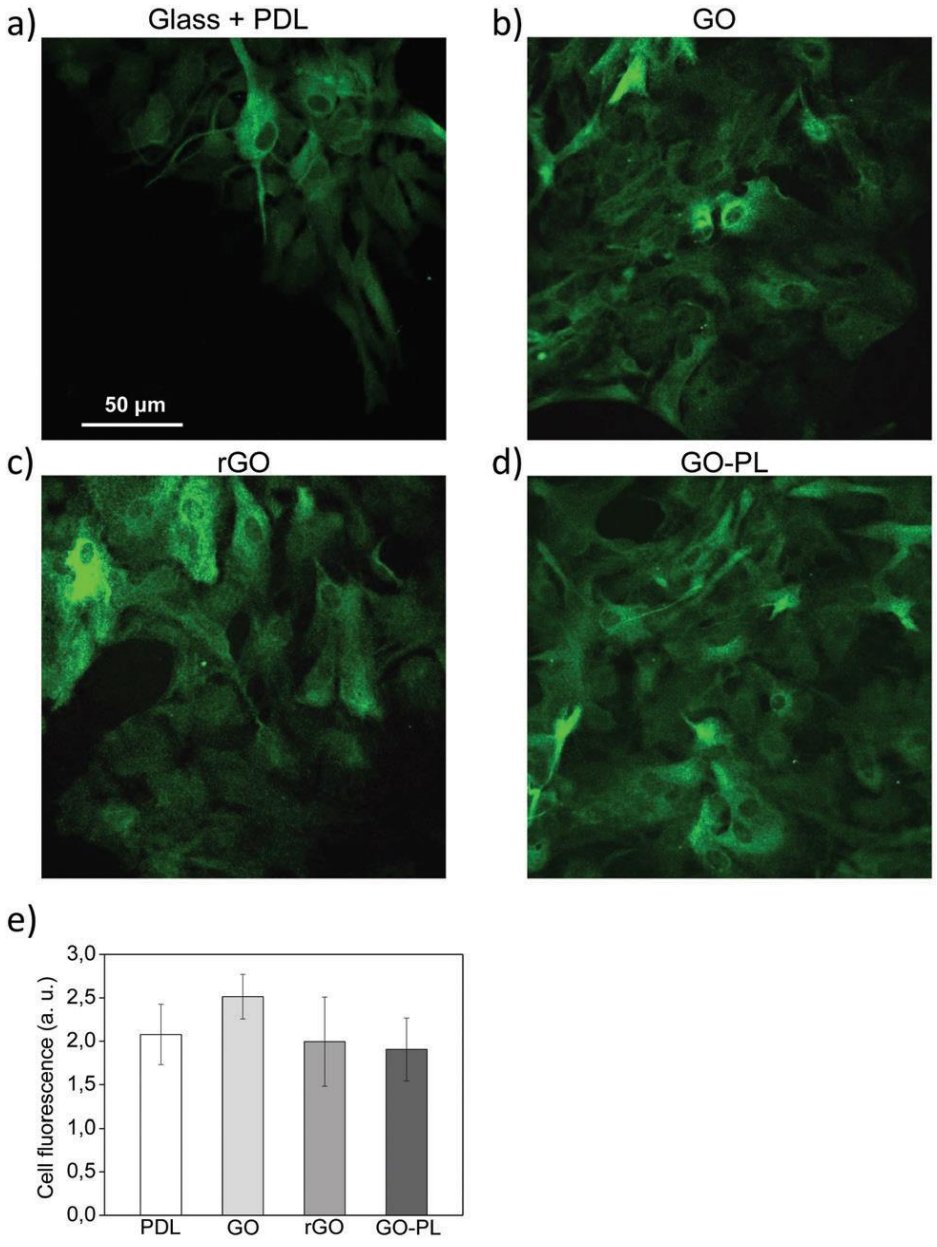

Figure 32. GFAP protein expression in astrocytes plated on PDL, GO, rGO and GO–PL. (A–D) Confocal imaging of astrocytes stained with GFAP. (E) Quantification of GFAP immunofluorescent signal. The analyses revealed that the immunofluorescent signal was comparable among different samples. Reproduced from [333] published by The Royal Society of Chemistry.

Chapter 5- Astrocyte modulation of intracellular calcium signaling by label-free pulsed infrared irradiation.

1. General overview

Label free tools enabling to investigate/modulate astrocytes protein channels and Ca^{2+} signaling are demanded to unravel biophysical mechanisms underpinning astrocytes physiology. Infrared neural stimulation (INS) has been shown to be an efficient label-free optical method to photostimulate/modulate neuronal firing. Nevertheless, the effect of INS on astrocytes have not been deeply investigated. Here, we explore the effect of INS on intracellular Ca^{2+} dynamics of astrocytes. In particular, we study the effect of INS in primary cortical astrocytes when a single pulse stimulation of 8 ms is applied *in vitro*. By performing microfluorimetric calcium imaging, we study the effect of INS in intracellular Ca^{2+} signaling. Furthermore, to dissect molecular clues underpinning the observed response we performed pharmacological study, we used TRPV4 knock down as well as AQP4 knock out astroglial cells. Lastly, we also study the influence of morphology and ion channel expression by using a nanostructured material capable of inducing astrocyte differentiation *in vitro*[420].

2. INS evoke intracellular Ca^{2+} signaling in primary astrocytes *in vitro*

To assess the effect of INS in primary cortical rat astrocytes we performed Fluo 4-AM calcium imaging in astroglial cells plated on glass + PDL substrates. Cells were stimulated with an optical fiber connected to an IR diode laser (Figure 33 A).

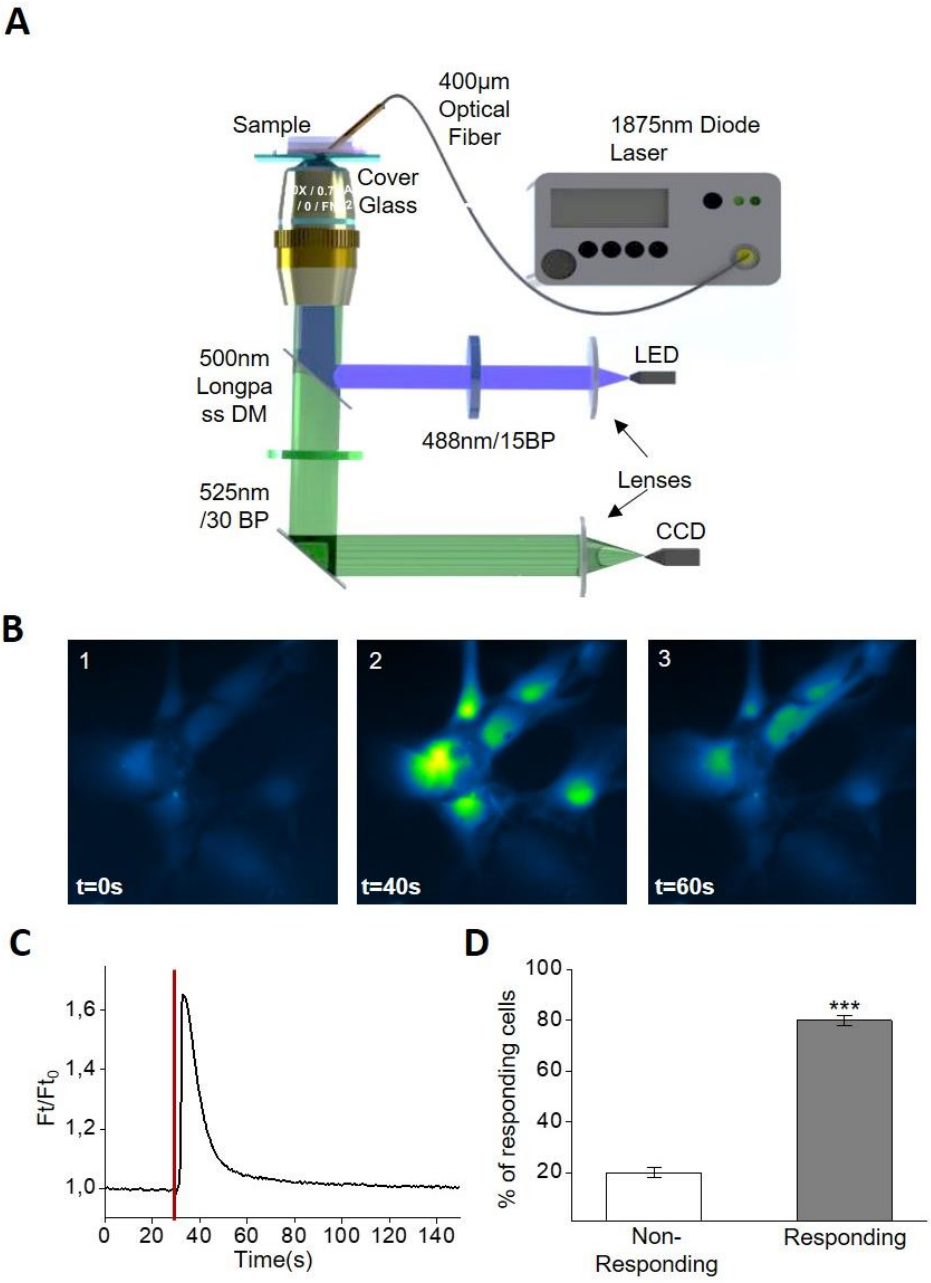

Figure 33. INS stimulate calcium imaging in cultured astrocytes. A) Schematic representation of the calcium imaging experiment of astrocyte INS stimulation (1875 nm). B) Sequential images obtained from Fluo-4-AM loaded rat cortical astrocytes plated on glass + PDL. Images depicts astrocytes fluorescence before the stimulation (t=0s), at the peak of fluorescence after stimulation (t=40s) and 20s after stimulation (t=60) C) Representative trace of astrocytes plated on glass + PDL depicting variation in cell fluorescence over time that reflects variation in $[Ca^{2+}]_i$. Red line marks INS stimulation. D) Histogram plot shows the percentage of cells responding. (N=589 (***: P<0.001)

Astroglial intracellular Ca^{2+} signaling was continuously monitored and after 30s from the beginning of the experiment a single pulse of 1875 nm and a duration of 8ms was applied. Figure 33 B shows time-lapse images of fluorescent astrocytes loaded with Fluo4-AM collected at t=0s, which

corresponds to the fluorescence collected at the beginning of the experiment, t=40s that corresponded to the timepoint at which we observed a maximal increase in fluorescence intensity after INS application, and t=60s where we can observe that the fluorescence of the cell returns to basal levels. The dynamics of F_t/F_{t0}, that reflected variation in $[Ca^{2+}]_i$ typically observed during experiments are reported in Figure 33 C. We observed that right after the photostimulation (Figure 33 C red line) a rapid increase in $[Ca^{2+}]_i$ occurred followed by a slower recovery of the value to the baseline (Figure 33 C). Here we prove for the first time that astrocytes calcium signaling can be evoked by using INS. Previous studies used infrared lasers to asses thermal damage on astrocytes without reporting the effect on calcium dynamics[447]. Others showed how to evoke astrocytic calcium response using near infrared light, only in the presence of conjugated nanoparticles[448]. Our method represents an easy, label-free and cost-effective approach to stimulate calcium signaling sacrificing the genetic specificity offered by optogenetics. Given the importance of astrocytes on brain physiology, the physiological modulation of astrocytes behavior by pulsed IR has an enormous potential to impact on brain function not only at a basic research level but also in neurological practice.

To explore the contribution of extracellular Ca^{2+} influx as well as of calcium release from intracellular stores, in the observed response, we performed experiments with a $0[Ca^{2+}]_{out}$ solution or containing intracellular store Ca^{2+} chelator named N,N,N',N'-tetrakis (2-pyridylmethyl)ethylene diamine (TPEN, 2mM)[449]. By removing extracellular Ca^{2+} we observed a significant reduction in fluorescence (Figure 34 A, trace green, B, green bar). However, we observed that the response did not disappear, suggesting the implication of intracellular Ca^{2+} stores in the response. We also observed a significant decrease in the number of cells responding to INS (Figure 34 C, green bar). Moreover, by using TPEN, we observed an even higher decrease in fluorescence (Figure 34 A and B, yellow, 34 A, yellow trace). The percentage of cells responding was also reduced (Figure 34 C, yellow bar). However, experiments to determine the mechanisms of intracellular calcium release are

needed. Despite direct evidence of involvement in the initiation of the observed response, we cannot fully rule out the involvement of secondary messengers capable of inducing calcium release from intracellular stores and hinder intercellular calcium wave propagation, affecting in this way the percentage of cells responding.

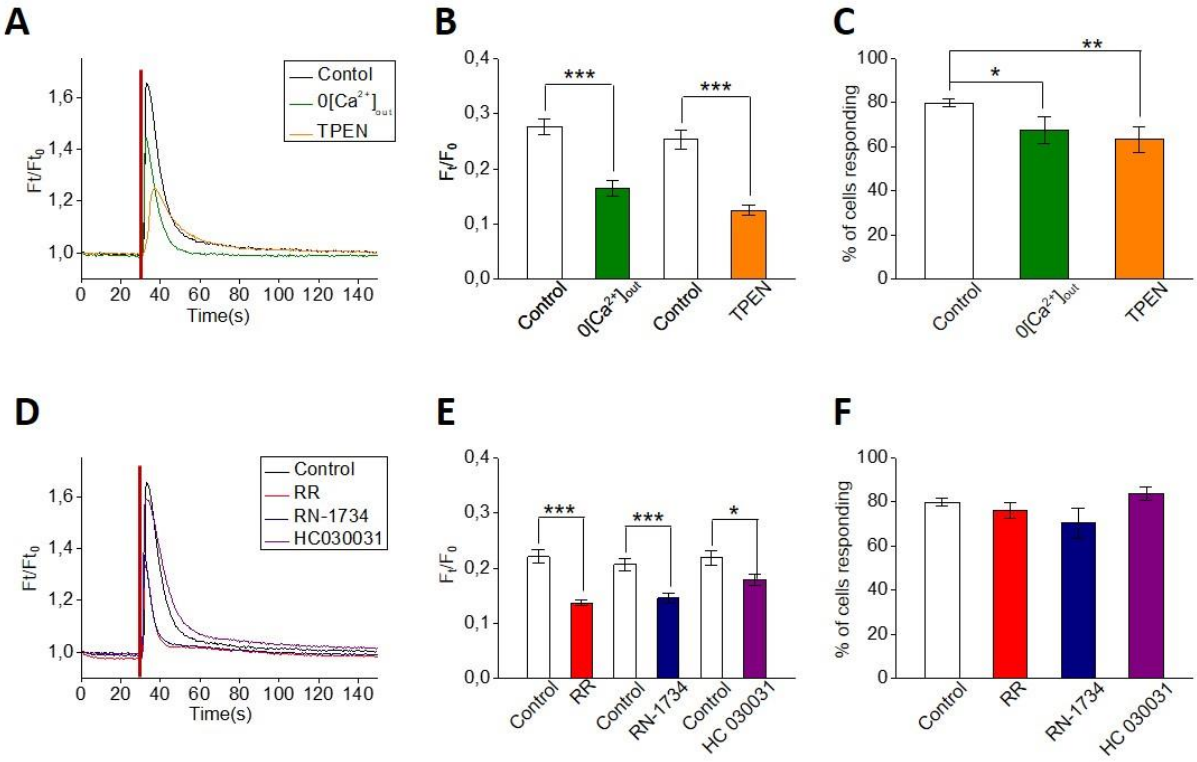

Figure 34. **Pharmacological study of the response of astrocytes on Glass + PDL to INS.** A) Representative trace of experiment performed with extracellular standard solution (black), using extracellular solution non-containing Ca^{2+} ($0[Ca^{2+}]_{out}$, green trace) and by adding intracellular store chelator, TPEN (2mM, yellow trace). B) Histogram plot depicting the maximal F_t/F_0 value calculated for each condition: white bars represent control experiments performed in external standard solution, green bar $0[Ca^{2+}]_{out}$ solution and yellow bar is TPEN C) Percentage of cells responding in experiments using $0[Ca^{2+}]_{out}$ solution (green bar) and TPEN (yellow bar). D) Representative trace of control condition in extracellular standard solution (black), and external solution added with Ruthenium Red (RR, 10 µM, red trace), RN1734 (10 µM, blue trace) and HC 030031 (40 µM, purple trace). Histogram plot depicting the averaged maximal F_t/F_0 value using a RR (10 µM, red bar), RN1734 (10 µM, blue bar) and HC 030031 (40 µM, purple bar). F) Percentage of cells responding after using RR (red bar), RN1734 (blue bar) and HC 030031 (purple bar). N=90 for $(0Ca^{2+})_{out}$ and N= 145 for control for $(0Ca^{2+})_{out}$; N=72 for TPEN and N=59 for control for TPEN; N=210 for RR and N=129 for control for RR; N=100 for RN-1734 and N= 140 for control for RN-1734; N=142 for HC-030031 and N=126 for control for HC 030031 (ANOVA one-way *: P<0,05; **: P<0,01; ***: P<0,001).

Previous works identified the role of TRPV4 channels in response to pulsed IR in sensory neurons[411]. As TRPV4 is abundantly expressed in cortical astrocytes, we also performed a pharmacological study to assess if this channel is the players implicated in the entry of Ca^{2+} from the extracellular space. We first used RR (10 µM, Figure 34 D, red trace), a general inhibitor of most of the members of TRP family. We observed a statistically significant decrease in the maximal recorded fluorescence intensity (Figure 34 E, red bar), while the number of cells responding was comparable to control experiments performed in external standard solution (Figure 34 F, red bar). We next applied a selective blocker of TRPV4, RN-1734 (10 µM). We observed that the response observed in presence of RN-1734 was characterized by a dynamic and a maximal fluorescence intensity resembling the one observed applying RR (Figure 34 D, blue trace). The number of cells responding was comparable to control experiments (Figure 34 F, blue bar).

We also explore a possible implication of TRPA1, another member of the TRP family, express in astrocytes *in vitro* and *in vivo*. To this end we used the selective inhibitor HC030031 (40 µM). While the dynamic of the response was similar to the one observed in control cells (Figure 29D, purple trace) the variation of F_t/F_{t0} was smaller compared to the one observed in control cells. Moreover, the percentage of cells responding was not significantly different when compared with control conditions (Figure 34F, purple bar).

Previous works demonstrated the role of TRPV4 in the Ca^{2+} response elicited by INS in neurons. Pharmacological characterization that we performed in cultured astrocytes is in agreement with a major role of TRPV4 in the observed effect. However, we also observed a major influence of intracellular Ca^{2+} stores. In this context, a recent study of the effect of INS in glioma U-87 cell line also showed the influence of intracellular PLC mediated Ca^{2+} release[450]. However, experiments to conclude if both extracellular, TRP mediated, and intracellular mechanisms are related or initiate independently are needed.

3. TRPV4 and AQP4 expression are essential for the intensity and for the dynamic of the INS evoked response in astrocytes

To confirm the involvement of TRPV4 in the INS evoked response, we performed experiments on astrocytes treated with specific TRPV4-siRNA, that we have previously shown to knock down TRPV4 [151]. Western blot analyses confirmed the ability of TRPV4 to specifically Knock down TRPV4 protein expression (not shown). Figure 35A shows representative traces of the calcium imaging performed on TRPV4 siRNA (Green) and scrambled siRNA, used as control (Black). It can be observed that the magnitude of the response was decreased when we knock-down TRPV4, Moreover, we observed a decrease in the number of cells responding (Figure 35 C). Collectively, these data confirmed that TRPV4 is a key player in the INS evoked response. However, they underline that the INS evoked Ca^{2+} response is still persistent when the TRPV4 protein was KD. In this context, TRPV4 might be relevant for the amplification of the response but not for the initiation, where instead the release from the intracellular stores might play a more important role.

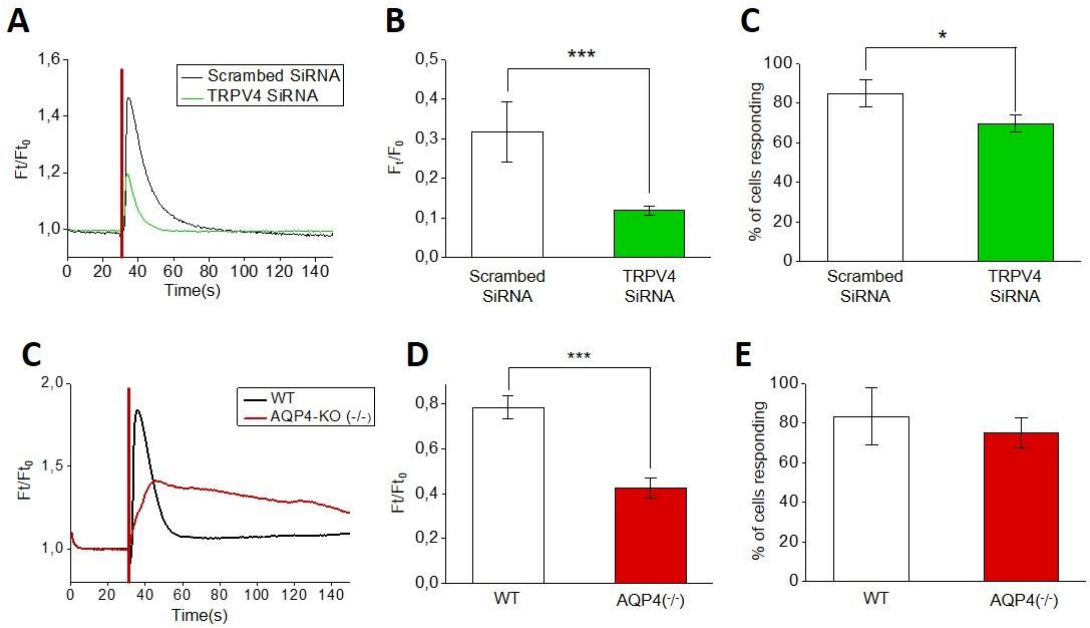

Figure 35. **Study of the role of TRPV4 and AQP4 in the $[Ca^{2+}]_i$ increase evoked by INS.** A) Representative traces of calcium fluorescence recorded in astrocytes transfected with scrambled siRNA (black trace) and TRPV4 siRNA (green trace) after INS. Red line represents the stimulation. B) Histogram plot showing the maximal fluorescence

amplitude F_t/F_0 for astrocytes transfected with scrambled siRNA (white bar) and TRPV4 siRNA (green bar). C) Percentage of cells responding to INS for astrocytes transfected with scrambled siRNA (white bar) and TRPV4 siRNA (green bar). D) Representative traces of calcium fluorescence recorded in WT mouse astrocytes (black trace) and mouse AQP4-KO ($^{-/-}$) (red trace). Red vertical line represents the stimulation. B) Histogram plot showing the F_t/F_0 maximal value recorded for mouse WT (white bar) AQP4-KO ($^{-/-}$) astrocytes (red bar). C) Percentage of cells responding to INS for WT mouse astrocytes (white bar) mouse AQP4-KO ($^{-/-}$) (red bar). N= 81 for Scrambed siRNA, N=156 for TRPV4 siRNA, N=59 for WT and N=57 for AQP4-KO ($^{-/-}$). (ANOVA one-way *: P<0,05; **: P<0,01; ***: P<0,001).

A previous study indicated that INS evoke a thermal increase in cell capacitance[410]. As the increase in cell capacitance might reflect an increase in cell volume, we sought to explore the role of a key molecular player in astrocytes water flux, namely AQP4. The latter hypothesis was also prompted by the molecular and functional interplay we have previously demonstrated between TRPV4 and AQP4 [151]. Thus, to investigate the involvement of AQP4 in the molecular and cellular mechanism underlying INS, we performed experiments on AQP4 KO ($^{-/-}$) mice to assess if there was any difference in the observe effect. We observed that in AQP4 KO ($^{-/-}$) the magnitude of the response was (Red) decreased (Figure 35D). Moreover, the dynamic of the response of AQP4 KO ($^{-/-}$) was characterized by a strongly delayed time to peak and by a longer duration of the response. Interestingly, the number of cells responding was comparable with the number of cells responding in the wild type (WT) (Figure 35F).

Collectively, results show the important role of TRPV4 and AQP4 in the increase in $[Ca^{2+}]_i$ mediated by pulse IR. Both AQP4 and TRPV4 play a pivotal role in the molecular mechanism underlying astrocyte swelling, thus their proper expression and function is crucial for optimal brain function[451]. Indeed, the loss of AQP4 from astrocytic endfeet is found in several pathological conditions such as traumatic brain injury[452] and epilepsy[453]. On the other hand, overexpression of AQP4 has been found in brain tumors[454] and hydrocephalus[455]. Furthermore, both AQP4 and TRPV4 were shown to play a role in brain edema[148]. However, experiments to elucidate a possible modulation of water permeability through AQP4 by means of pulsed IR are still needed. Indeed, tools for the modulation of astrocyte cell volume could represent a valuable instrument to fully understand the role of astrocytes in the control of brain extracellular space and the correlation with

proper brain functioning. Moreover, TRPV4 dysregulation was hypothesized to contribute to neurovascular dysfunction by mediating calcium entry that in turn trigger pro-inflammatory signals[456]. In this context, INS open a path for new tools to address the cross-talk between the vasculature and other glial cells.

4. INS response in differentiated astrocytes

Our group previously demonstrated that a nanostructured interface based on hydrotalcite (HTlc) nanoparticle films that allow to differentiate astrocytes, inducing a star-like shape morphology and accompanied by a localized and polarized expression of AQP4 in the endfeet of the elongations of the differentiated astrocytes[420]. Considering the effect of AQP4 deletion in the evoked $[Ca^{2+}]_i$ by INS, we decided to perform calcium imaging experiments on differentiated astrocytes where AQP4 is over-expressed with respect to the control. Figure 36 A shows sequential images of a calcium imaging experiment performed on rat cortical astrocytes plated on HTlc. A completely different morphology can be observed when compared with polygonal astrocytes plated on Glass + PDL (Figure 33 B). Indeed, we can observe long ramifications departing from the cell body, similarly to what it is seen in *in vivo* astrocytes. It is evident that the response to INS induce a $[Ca^{2+}]_i$ increase that spread from cell body to elongation to other cells. Calcium imaging analysis showed that differentiated astrocytes presented higher increases in fluorescence intensity but also a faster response with respect to the control. Given the higher expression of AQP4 of astrocytes in differentiated astrocytes on HTlc [420], these data supports the role of AQP4 in $[Ca^{2+}]_i$ rises mediated by INS. However, we cannot rule out that other differences of astrocytes plated on HTlc, such as, Kir 4.1 expression, morphological differentiation and ion channel polarization might also play an important role in the evoked response by INS.

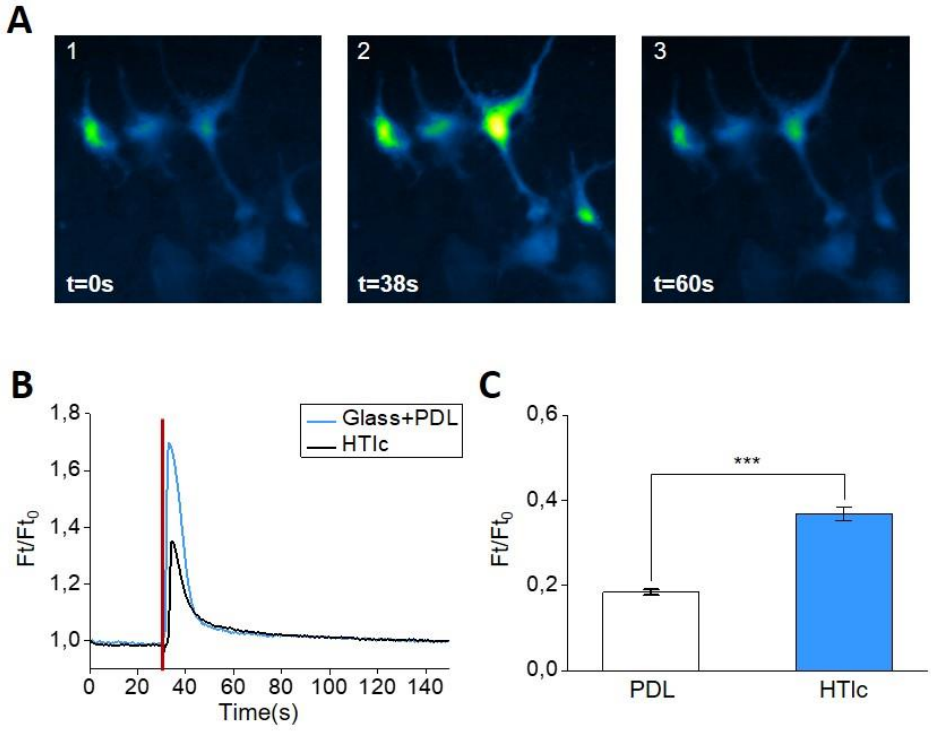

Figure 36. **INS response is different in differentiated astrocytes**. A) Sequential fluorescent images obtained from Fluo-4-AM loaded rat cortical astrocytes plated on HTlc. Images show cells at time 0 (t=0), at the peak of fluorescence after stimulation (t=38) and few seconds after stimulation (t=60). B) Representative traces of calcium imaging experiments performed on Glass + PDL (black trace) and HTlc (Blue trace). Red line represents the INS. C) Histogram plot showing F_t/F_0 in the peak of fluorescence for glass + PDL (white bar) and HTlc (Blue bar). N=356 for Glass + PDL and N= 99 for HTlc. ANOVA one-way (***: P<0,001).

Moreover, HTlc-cultured astrocytes serve as a unique *in vitro* model to study the effect of pulsed IR on astrocytes offering a unique perspective into what we might expect to observe *in vivo*. In this view, as we did on astrocytes plated on glass+PDL, we performed pharmacological studies to elucidate the cellular and molecular mechanism underlying the response of INS in differentiated astrocytes. Removal of extracellular Ca^{2+} from the bath reduced the magnitude of the response as previously observed. The use of TPEN (2mM) (Figure 37 A and B, yellow) also reduced fluorescence intensity. However, no significant difference was observed in the percentage of cells responding in both $0(Ca^{2+})_{out}$ and TPEN. Experiments performed with the TRP family inhibitor RR (10µM, red) induced a decrease in the fluorescence intensity (Figure 37 D and 37 E, red) and a reduction in the percentage of cells responding to INS (Figure 37 F, red). Interestingly, the addition of RN-1734 (10 µM) (Figure 37 D and E, dark blue) to selectively block TRPV4, produced a

significant inhibition of fluorescence amplitude in response to INS (Figure 37 E, dark blue) while the reduction in the number of cells responding to the stimulus was not significant. Lastly, by using HC-030031 (40 µM) (Figure 37 D and E, purple) to block TRPA1 we observed a significant decrease in the magnitude of the response to INS accompanied by a slower dynamic compared with control differentiated cells.

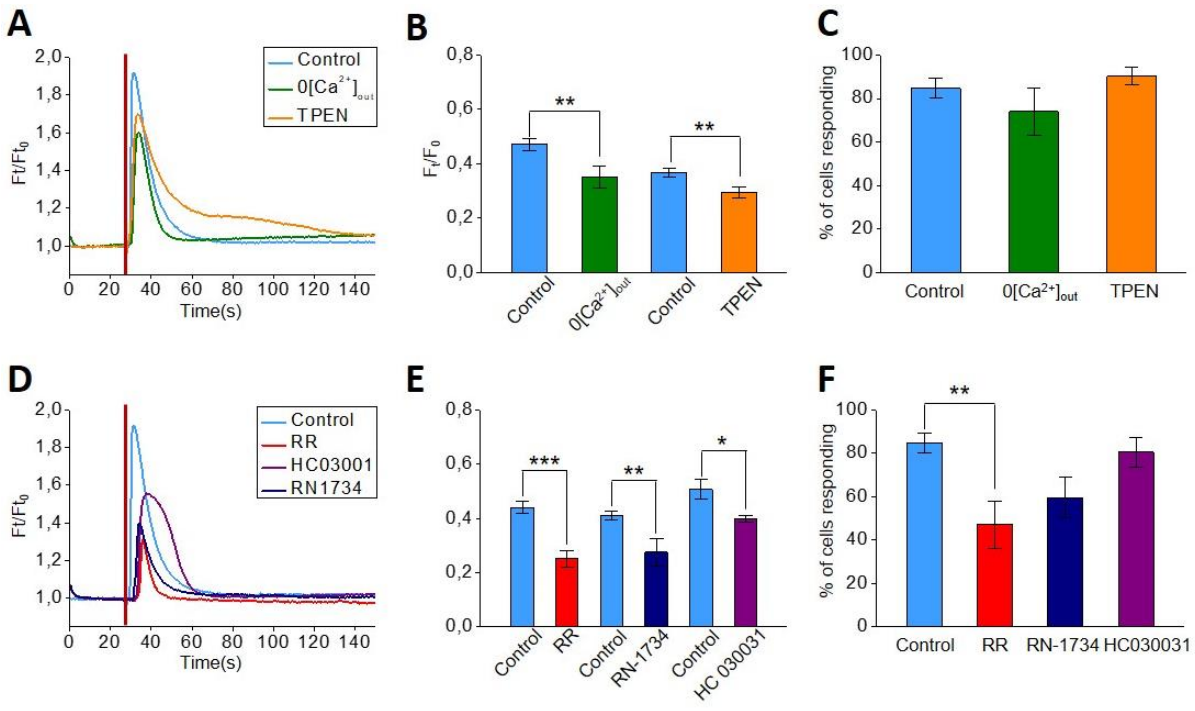

Figure 37. **Pharmacological study in differentiated astrocytes.** A) Representative traces of the response recorded in astrocytes exposed to extracellular solution non-containing Ca^{2+} ($0[Ca^{2+}]_{out}$, green trace) and TPEN (2mM, yellow trace) on HTlc. Representative trace of control condition in extracellular standard solution in light blue. B) Histogram plot depicting the F_t/F_0 in the peak of fluorescence when using a $0[Ca^{2+}]_{out}$ solution (green bar) and TPEN (2mM, yellow bar) on HTlc. Light blue bars represent control experiments performed in external standard solution. C) Percentage of cells responding after using $0[Ca^{2+}]_{out}$ solution (green bar) and TPEN (yellow bar). D) Representative traces of the response recorded in astrocytes exposed to ruthenium red (RR, 10 µM, red trace), RN1734 (10 µM, dark blue trace) and HC 030031 (40 µM, purple trace). Representative trace of control condition in extracellular standard solution light blue. Histogram plot depicting the F_t/F_0 in the peak when using a RR (10 µM, red bar), RN1734 (10 µM, dark blue bar) and HC 030031 (40 µM, purple bar). F) Percentage of cells responding after using RR (red bar), RN1734 (dark blue bar) and HC 030031 (purple bar). N=48 for $0Ca^{2+}$ and N=29 for control for $0Ca^{2+}$; N=73 for TPEN and N=78 for control for TPEN; N=53 for RR and N=67 for control for RR; N=59 for HC-030031 and N=41 for control HC 030031; N=54 for RN-1734 and N=28 for control for RN1734. (*: P<0,05; **: P<0,01; ***: P<0,001). (ANOVA one-way *: P<0,05; **: P<0,01; ***: P<0,001).

Although in general we can observe similar results when comparing the behavior of astrocytes plated on Glass+PDL and HTlc, results suggest that there might be some differences in the

mechanism prompting the response to INS, such as a lower implication in the response of Ca^{2+} form the intracellular stores observed by the use of TPEN as well as a more important role of TRPV4 as suggested by the reduction in the number of cells responding using RR. Nevertheless, detailed experiments to study these differences are needed. Indeed, differentiated astrocytes on HTlc give also the possibility to study in depth the initiation in the response comparing soma versus endfeet thanks to the ion channel polarization of astrocytes on these films. In this context, these experiments open the path for the combination of nanostructured materials and biophotonic tools to modulate astrocyte behavior to allow us to have a much better understanding of ion channel roles in astrocytes in physiological conditions by using a reliable in-vivo-like-in-vitro model.

Chapter 6- Conclusion

Neural engineering and biotechnologies for neuroscience investigation and neurology applications has been essentially targeted to the study of neurons. However, studies over the past four decades have revealed that astrocytes, which are non-excitable glial cells of the CNS, have a molecular, functional and cellular role in the brain physiology. Nonetheless the dysfunction of astrocytes ion channels, water channels and Ca^{2+} signaling is implicated, as cause and or effect, in acute and chronic neuropathologies. On these bases, it becomes evident that, to unravel molecular and cellular mechanisms underpinning brain function, there is a need of new tools targeting specific molecular, functional players selectively expressed by brain astrocytes. In this context the main purpose of my PhD research work was the study and the validation of advanced biomaterials and devices capable to alter and modulate ion channels, Ca^{2+} signaling and aquaporins functionality in astrocytes.

In particular we focused on devices based on carbon-based materials, such as organic semiconductors and graphene, that combine materials properties such as improved biocompatibility over a long term, softness and flexibility, with ion-electron conduction capability, optical transparency and light adsorption and emission properties. These properties make them very attractive for neuroscience applications targeted to stimulation of astrocytes functionality. Moreover, we sought to use Infrared photo stimulation that was demonstrated to be effective label free tool for excitation of neurons, but it has never been reported for stimulating astrocytes Ca^{2+} signaling.

A summary of the main result achieve is following:

- We demonstrate the use of transparent Organic Cell Stimulating and Sensing Transistor (O-CST) architecture, fabricated with N, N'-ditridecylperylene-3,4,9,10-tetracarboxylic diimide (P13), to elicit and monitor intracellular calcium concentration ($[Ca^{2+}]_i$) in primary rat

neocortical astrocytes. The transparency of O-CST allowed performing calcium imaging experiments showing that extracellular electrical stimulation of astrocytes induces a drastic increase in $[Ca^{2+}]_i$. Pharmacological studies indicate that Transient Receptor Potential (TRP) superfamily, are critical mediators of the $[Ca^{2+}]_i$ increase. Experimental and computational analyses shows that $[Ca^{2+}]_i$ response is enabled by the O-CST device architecture. Noteworthy, the extracellular field application induces a slight but significant increase in the cell volume. Collectively, we show that the O-CST is capable to selectively evoke astrocytes $[Ca^{2+}]_i$, paving the way to the development of organic bioelectronic devices as glial interfaces to excite and control physiology of non-neuronal brain cells.

- To fully exploit the functionality of another carbon-based materials, graphene, we demonstrated the effectiveness of a biomimetic approach to enhance the adhesion of astrocytes on graphene-oxide GO nanosheets, functionalizing the GO with a phospholipid moiety highly affine to the main building block of the cellular membrane. The successful grafting of the phospholipid to GO sheets was achieved we demonstrated a significant enhancement in the adhesion of astrocytes on GO-PL with respect to GO or glass substrates coated with PDL. The enhancement could not be ascribed to a change in roughness or hydrophobicity of the substrates. Comparative tests also confirmed that the favorable interaction of GO-PL with astrocytes did not cause an inflammatory response, which would be associated to gliosis change in cell morphology, increased GFAP expression high proliferation rate and hypertrophy.
- Finally we evaluated and reported, for the first time, the effect of INS on astroglial cells $[Ca^{2+}]_i$. We found that INS induce Ca^{2+} signaling in astrocytes mediated by intra- and extracellular Ca^{2+}. TRP channels, specially TRPV4, account for extracellular Ca^{2+}entry. Results also suggest an implication of AQP4 in the observe effect, leading to intriguing hypothesis that TRPV4 and AQP4 microdomains can be modulated by INS. Notably by

using a polarized cell culture model of differentiated astrocytes *in vitro* [420]we showed that INS evoked Ca^{2+} rise occurs locally at astrocytes endfeet, where AQP4 microdomains is enriched or spread as a wave from one astrocytes to another.

Taken together, we demonstrated that by using organic semiconductor based bioelectronic device as well as with graphene-based materials, we developed glial interfaces that are capable to control and to manipulate the cellular, molecular and functional properties of protein channel essential for astrocytes physiology *in vivo*, such as TRPV4 and AQP4. Moreover, we firstly reported the ability of photonic stimulation to excite Ca^{2+} oscillations in astrocytes. Interestingly, the same proteins observed for the response to electric field are also determinant in the mechanism of the response to photostimulation. In this view, we provided insight on cellular and molecular clues underpinning astrocyte response to bioelectronic and biphotonic approach, seed for further investigation on extremely sensitive biosensing and transduction capability of astrocytes. The latter, if deeply understood and tightly controlled, might be useful as a new pathway to dialogue with the brain and to uncover its function. Nonetheless, considering the role of astrocytes in brain pathology, future *in vivo* studies in pathophysiological mice model are foreseen.

Chapter 7- References

[1] R. B. Banati, *Br. Med. Bull.* **2003**, *65*, 121.

[2] R. Fu, Q. Shen, P. Xu, J. J. Luo, Y. Tang, *Mol. Neurobiol.* **2014**, *49*, 1422.

[3] A. Miyamoto, H. Wake, A. J. Moorhouse, J. Nabekura, *Front. Cell. Neurosci.* **2013**, *7*, 1.

[4] D. J. Loane, K. R. Byrnes, *Neurotherapeutics* **2010**, *7*, 366.

[5] M. M. Mariani, T. Kielian, *J. Neuroimmune Pharmacol.* **2009**, *4*, 448.

[6] K. Ohsawa, S. Kohsaka, *Glia* **2011**, *59*, 1793.

[7] S. G. Torres-Platas, S. Comeau, A. Rachalski, G. D. Bo, C. Cruceanu, G. Turecki, B. Giros, N. Mechawar, *J. Neuroinflammation* **2014**, *11*, 1.

[8] S. A. Ward, P. A. Ransom, P. L. Booth, W. E. Thomas, *J. Neurosci. Res.* **1991**, *29*, 13.

[9] Y. Wu, L. Dissing-Olesen, B. A. MacVicar, B. Stevens, *Trends Immunol.* **2015**, *36*, 605.

[10] B. R. Ransom, H. Sontheimer, **1992**, *9*, 224.

[11] J. M. Edgar, J. Garbern, *J. Neurosci. Res.* **2004**, *76*, 593.

[12] X. Dai, L. D. Lercher, P. M. Clinton, Y. Du, D. L. Livingston, C. Vieira, L. Yang, M. M. Shen, C. F. Dreyfus, *J. Neurosci.* **2003**, *23*, 5846.

[13] Y. Lee, B. M. Morrison, Y. Li, S. Lengacher, M. H. Farah, P. N. Hoffman, Y. Liu, A. Tsingalia, L. Jin, P. W. Zhang, et al., *Nature* **2012**, *487*, 443.

[14] E. R. Kandel, J. H. Schwartz, T. M. Jessell, *Principles of Neural Science*, New York McGraw-Hill, **2000**.

[15] E. M. Ullian, S. K. Sapperstein, K. S. Christopherson, B. A. Barres, *Science (80-.).* **2001**, *291*, 657.

[16] N. J. Allen, B. A. Barres, *Nature* **2009**, *457*, 675.

[17] S. Herculano-Houzel, *Front. Hum. Neurosci.* **2009**, *3*, 1.

[18] J. A. Filosa, A. D. Bonev, S. V. Straub, A. L. Meredith, M. K. Wilkerson, R. W. Aldrich, M. T. Nelson, *Nat. Neurosci.* **2006**, *9*, 1397.

[19] J. A. Filosa, *Circ. Res.* **2004**, *95*, e73.

[20] A. Verkhratsky, M. Nedergaard, *Physiol. Rev.* **2018**, *98*, 239.

[21] L. K. Kaczmarek, *Encycl. Cogn. Sci.* **2003**, 325.

[22] S. Barberis, **2018**, DOI 10.3390/philosophies3020011.

[23] R. W. Guillery, *Brain Res. Rev.* **2007**, *55*, 411.

[24] R. W. Guillery, *Philos. Trans. R. Soc. B Biol. Sci.* **2005**, *360*, 1281.

[25] J. A. Hubbard, D. K. Binder, *History of Astrocytes*, **2016**.

[26] H. Kettenmann, A. Verkhratsky, *Glial Cells: Neuroglia*, **2016**.

[27] E. Vecino, F. D. Rodriguez, N. Ruzafa, X. Pereiro, S. C. Sharma, *Prog. Retin. Eye Res.* **2016**, *51*, 1.

[28] V. Parpura, A. Verkhratsky, *Croat. Med. J.* **2012**, *53*, 518.

[29] A. Verkhratsky, *Pflugers Arch. Eur. J. Physiol.* **2006**, *453*, 411.

[30] C. Golgi, *Gazz. Med. Ital.* **1873**, *33*, 244.

[31] V. García-Marín, P. García-López, M. Freire, *Trends Neurosci.* **2007**, *30*, 479.

[32] P. del Río-Hortega, W. G. Penfield, *Bull Johns Hopkins Hosp* **1927**, *41*, 278.

[33] A. Sierra, F. de Castro, J. del Río-Hortega, J. Rafael Iglesias-Rozas, M. Garrosa, H. Kettenmann, *Glia* **2016**, *64*, 1801.

[34] W. Hild, I. Tasaki, *J. Neurophysiol* **1962**, *25*, 277304.

[35] S. W. Kuffler, D. D. Potter, *J Neurophysiol* **1964**, *27*, 290.

[36] L. Hertz, *Nature* **1965**, *206*, 1091.

[37] R. K. Orkand, J. G. Nicholls, S. W. Kuffler, *J. Neurophysiol.* **1966**, *29*, 788.

[38] B. M. W., T. S. Reese, *J Cell Biol* **1969**, *40*, 648.

[39] O. P. Hamill, A. Marty, E. Neher, B. Sakmann, F. J. Sigworth, *Pflügers Arch. Eur. J. Physiol.* **1981**, *391*, 85.

[40] R. Y. Tsien, *Biochemistry* **1980**, *19*, 2396.

[41] R. Y. Tsien, *Nature* **1981**, *290*, 527.

[42] K. Mccarthy, J. Vellis, *J. Cell Biol.* **1980**, *85*, 890.

[43] K. D. McCarthy, L. M. Partlow, *Brain Res.* **1976**, *114*, 391.

[44] C. L. Bowman, H. K. Kimelberg, *Nature* **1984**, *311*, 656.

[45] P. Gilbert, H. Kettenmann, M. Schachner, *J. Neurosci.* **1984**, *4*, 561.

[46] H. Kettenmann, P. Gilbert, M. Schachner, *Neurosci Lett* **1984**, *52*, 25.

[47] H. Kettenmann, P. Gilbert, *Neurosci. Lett.* **1984**, *47*, 271.

[48] A. H. Cornell-bell, S. M. Finkbeiner, M. S. Cooper, S. J. Smith, *Science (80-.).* **1990**, *247*, 2.

[49] V. Parpura, T. A. Basarsky, F. Liu, K. Jeftinija, S. Jeftinija, P. G. Haydon, *Nature* **1994**, *369*,

744.

[50] M. Nedergaard, A. Verkhratsky, *Glia* **2012**, *60*, 1013.

[51] M. Nedergaard, *Science (80-.).* **1994**.

[52] M. Simard, M. Nedergaard, *Neuroscience* **2004**, *129*, 877.

[53] S. R. Chebabo, M. A. Hester, J. Jing, P. G. Aitken, G. G. Somjen, *J. Physiol.* **1995**, *487*, 685.

[54] S. Hrabêtová, K. C. Chen, D. Masri, C. Nicholson, *J. Cereb. Blood Flow Metab.* **2002**, *22*, 80.

[55] C. M. Anderson, R. A. Swanson, *Glia* **2000**, *32*, 1.

[56] P. Kofuji, E. A. Newman, *Neuroscience* **2004**, *129*, 1045.

[57] V. Benfenati, S. Ferroni, in *Homeost. Control Brain Funct.*, **2016**.

[58] N. J. Abbott, L. Rönnbäck, E. Hansson, *Nat. Rev. Neurosci.* **2006**, *7*, 41.

[59] J. I. Alvarez, T. Katayama, A. Prat, *Glia* **2013**, *61*, 1939.

[60] R. Cabezas, M. Ávila, J. Gonzalez, R. Santos El-Bachá, E. Báez, L. M. Garcí-a-Segura, J. C. Jurado Coronel, F. Capani, G. P. Cardona-Gomez, G. E. Barreto, *Front. Cell. Neurosci.* **2014**, *8*, 1.

[61] M. Nedergaard, B. Ransom, S. A. Goldman, *Trends Neurosci.* **2003**, *26*, 523.

[62] V. Benfenati, S. Ferroni, *Neuroscience* **2010**, *168*, 926.

[63] M. Amiry-Moghaddam, O. P. Ottersen, *Nat. Rev. Neurosci.* **2003**, *4*, 991.

[64] E. Scemes, C. Giaume, *Glia* **2006**, *54*, 716.

[65] C. Steinhäuser, G. Seifert, P. Bedner, *Glia* **2012**, *60*, 1192.

[66] L. Hertz, Y. Chen, *Neurosci. Biobehav. Rev.* **2016**, *71*, 484.

[67] A. Bellot-Saez, O. Kékesi, J. W. Morley, Y. Buskila, *Neurosci. Biobehav. Rev.* **2017**, *77*, 87.

[68] L. L. Odette, E. A. Newman, *Glia* **1988**, *1*, 198.

[69] P. Kofuji, E. A. Newman, *Neuroscience* **2004**, *129*, 1045.

[70] W. Walz, E. C. Hinks, *Brain Res.* **1985**, *343*, 44.

[71] W. Walz, L. Hertz, *J. Neurochem.* **1982**, *39*, 70.

[72] R. K. ORKAND, *Ann. N. Y. Acad. Sci.* **1986**, *481*, 354.

[73] H. Kettenmann, K. H. Backus, M. Schachner, *Brain Res.* **1987**, *404*, 1.

[74] K. Egawa, J. Yamada, T. Furukawa, Y. Yanagawa, A. Fukuda, *J. Physiol.* **2013**, *591*, 3901.

[75] J. W. Deitmer, C. R. Rose, *Brain Res. Rev.* **2010**, *63*, 113.

[76] C. R. Rose, B. R. Ransom, *J. Neurosci.* **1996**, *16*, 5393.

[77] D. B. Hansen, N. Garrido-Comas, M. Salter, R. Fern, *J. Biol. Chem.* **2015**, *290*, 8039.

[78] J. E. Olson, D. Fleischhacker, W. B. Murray, D. Holtzman, *Glia* **1990**, *3*, 405.

[79] K. A. Parkerson, H. Sontheimer, *Glia* **2004**, *46*, 419.

[80] V. Benfenati, G. P. Nicchia, M. Svelto, C. Rapisarda, A. Frigeri, S. Ferroni, *J. Neurochem.* **2007**, *100*, 87.

[81] A. Araque, V. Parpura, R. P. Sanzgiri, P. G. Haydon, *TINS* **1999**, *22*, 208.

[82] M. L. Mayer, *Curr. Opin. Neurobiol.* **2011**, *21*, 283.

[83] M. D. Norenberg, A. Martinez-Hernandez, *Brain Res.* **1979**, *161*, 303.

[84] N. M. Uwechue, M. C. Marx, Q. Chevy, B. Billups, *J. Physiol.* **2012**, *590*, 2317.

[85] L. Hertz, *Front. Endocrinol. (Lausanne).* **2013**, *4*, 1.

[86] A. Gadea, A. M. López-Colomé, *J. Neurosci. Res.* **2001**, *63*, 461.

[87] J. Y. Chatton, L. Pellerin, P. J. Magistretti, *Proc Natl Acad Sci U S A* **2003**, *100*, 12456.

[88] G. Perea, M. Navarrete, A. Araque, *Trends Neurosci.* **2009**, *32*, 421.

[89] A. Araque, G. Carmignoto, P. G. Haydon, S. H. R. Oliet, R. Robitaille, A. Volterra, *Neuron* **2014**, *81*, 728.

[90] F. Petrelli, P. Bezzi, *Curr. Opin. Pharmacol.* **2016**, *26*, 138.

[91] W. Walz, S. Mukerji, *Glia* **1988**, *1*, 366.

[92] G. J. Guillemin, S. J. Kerr, G. A. Smythe, D. G. Smith, V. Kapoor, P. J. Armati, J. Croitoru, B. J. Brew, *J. Neurochem.* **2001**, *78*, 842.

[93] D. A. Sahlender, I. Savtchouk, A. Volterra, *Philos. Trans. R. Soc. B Biol. Sci.* **2014**, *369*, DOI 10.1098/rstb.2013.0592.

[94] S. Ochi, J. Y. Lim, M. N. Rand, M. J. During, K. Sakatani, J. D. Kocsis, *Glia* **1993**, *9*, 188.

[95] V. Benagiano, D. Virgintino, A. Rizzi, P. Flace, V. Troccoli, J. Bormann, P. Monaghan, D. Robertson, L. Roncali, G. Ambrosi, *Histochem. J.* **2000**, *32*, 557.

[96] K. Le Meur, J. Mendizabal-Zubiaga, P. Grandes, E. Audinat, *Front. Comput. Neurosci.* **2012**, *6*, 1.

[97] E. B. Malarkey, V. Parpura, *Neurochem. Int.* **2008**, *52*, 142.

[98] J. T. Ehmsen, Y. Liu, Y. Wang, N. Paladugu, A. E. Johnson, J. D. Rothstein, S. Du Lac, M. P. Mattson, A. Höke, *Sci. Rep.* **2016**, *6*, 1.

[99] C. Hilmas, E. F. R. Pereira, M. Alkondon, A. Rassoulpour, R. Schwarcz, E. X. Albuquerque,

J. Neurosci. **2001**, *21*, 7463.

[100] A. Pocivavsek, H. Q. Wu, M. C. Potter, G. I. Elmer, R. Pellicciari, R. Schwarcz, *Neuropsychopharmacology* **2011**, *36*, 2357.

[101] S. Beggiato, T. Antonelli, M. C. Tomasini, S. Tanganelli, K. Fuxe, R. Schwarcz, L. Ferraro, *Eur. J. Neurosci.* **2013**, *37*, 1470.

[102] A. Zmarowski, H. Q. Wu, J. M. Brooks, M. C. Potter, R. Pellicciari, R. Schwarcz, J. P. Bruno, *Eur. J. Neurosci.* **2009**, *29*, 529.

[103] A. Rassoulpour, H. Q. Wu, S. Ferre, R. Schwarcz, *J. Neurochem.* **2005**, *93*, 762.

[104] L. H. Bergersen, *J. Cereb. Blood Flow Metab.* **2015**, *35*, 176.

[105] F. Wang, T. Yuan, A. Pereira, A. Verkhratsky, J. H. Huang, *Neural Plast.* **2016**, *2016*, 15.

[106] S. Liao, T. P. Padera, *Lymphat. Res. Biol.* **2013**, *11*, 136.

[107] A. Aspelund, S. Antila, S. T. Proulx, T. V. Karlsen, S. Karaman, M. Detmar, H. Wiig, K. Alitalo, *J. Exp. Med.* **2015**, *212*, 991.

[108] A. Louveau, I. Smirnov, T. J. Keyes, J. D. Eccles, S. J. Rouhani, J. D. Peske, N. C. Derecki, D. Castle, J. W. Mandell, K. S. Lee, et al., *Nature* **2015**, *523*, 337.

[109] T. M. Mathiisen, K. P. Lehre, N. C. Danbolt, O. P. Ottersen, *Glia* **2010**, *58*, 1094.

[110] J. J. Iliff, H. Lee, M. Yu, T. Feng, J. Logan, M. Nedergaard, H. Benveniste, M. Wang, D. M. Zeppenfeld, A. Venkataraman, et al., *Sci Transl Med.* **2012**, *4*, 1.

[111] T. Gaberel, C. Gakuba, R. Goulay, S. M. De Lizarrondo, J. L. Hanouz, E. Emery, E. Touze, D. Vivien, M. Gauberti, *Stroke* **2014**, *45*, 3092.

[112] Q. Jiang, L. Zhang, G. Ding, E. Davoodi-Bojd, Q. Li, L. Li, N. Sadry, M. Nedergaard, M.

Chopp, Z. Zhang, *J. Cereb. Blood Flow Metab.* **2017**, *37*, 1326.

[113] B. T. Kress, J. J. Iliff, M. Xia, M. Wang, H. Wei, D. Zeppenfeld, L. Xie, H. Kang, Q. Xu, J. Liew, et al., *Ann. Neurol.* **2014**, *76*, 845.

[114] W. Peng, T. M. Achariyar, B. Li, Y. Liao, H. Mestre, E. Hitomi, S. Regan, T. Kasper, S. Peng, F. Ding, et al., *Neurobiol. Dis.* **2016**, *93*, 215.

[115] I. Lundgaard, B. Li, L. Xie, H. Kang, S. Sanggaard, J. D. R. Haswell, W. Sun, S. Goldman, S. Blekot, M. Nielsen, et al., *Nat. Commun.* **2015**, *6*, 1.

[116] I. Lundgaard, M. L. Lu, E. Yang, W. Peng, H. Mestre, E. Hitomi, R. Deane, M. Nedergaard, *J. Cereb. Blood Flow Metab.* **2017**, *37*, 2112.

[117] V. R. Thrane, A. S. Thrane, B. A. Plog, M. Thiyagarajan, J. J. Iliff, R. Deane, E. A. Nagelhus, M. Nedergaard, *Sci. Rep.* **2013**, *3*, 4.

[118] L. M. Prolo, *J. Neurosci.* **2005**, *25*, 404.

[119] L. Marpegan, A. E. Swanstrom, K. Chung, T. Simon, P. G. Haydon, S. K. Khan, A. C. Liu, E. D. Herzog, C. Beaule, *J. Neurosci.* **2011**, *31*, 8342.

[120] J. F. Burkeen, A. D. Womac, D. J. Earnest, M. J. Zoran, *J. Neurosci.* **2011**, *31*, 8432.

[121] F. R. Jackson, *Glia* **2011**, *59*, 1341.

[122] H. Hibino, A. Inanobe, K. Furutani, S. Murakami, I. Findlay, Y. Kurachi, *Physiol. Rev.* **2010**, *90*, 291.

[123] M. L. Olsen, H. Sontheimer, **2008**, *107*, 589.

[124] C. B. Ransom, H. Sontheimer, *J Neurophysiol* **1995**, *73*, 333.

[125] K. Higashi, A. Fujita, A. Inanobe, M. Tanemoto, K. Doi, T. Kubo, Y. Kurachi, *Am. J.*

Physiol. Physiol. **2001**, *281*, C922.

[126] Q. Kuang, P. Purhonen, H. Hebert, *Cell. Mol. Life Sci.* **2015**, *72*, 3677.

[127] H. Sontheimer, S. G. Waxman, *J. Neurophysiol.* **1993**, *70*, 1863.

[128] A. Bordey, H. Sontheimer, *Glia* **2000**, *30*, 27.

[129] M. L. Roy, D. Saal, T. Perney, H. Sontheimer, S. G. Waxman, L. K. Kaczmarek, *Glia* **1996**, *18*, 177.

[130] L. Edwards, R. Nashmi, O. Jones, P. Backx, C. Ackerley, L. Becker, M. G. Fehlings, *J. Comp. Neurol.* **2002**, *443*, 154.

[131] L. K. Bekar, *J. Neurophysiol.* **2004**, *93*, 1699.

[132] A. D. Wei, G. A. Gutman, R. Aldrich, K. G. Chandy, S. Grissmer, H. Wulff, *Pharmacol. Rev.* **2005**, *57*, 463.

[133] T. A. Longden, K. M. Dunn, H. J. Draheim, M. T. Nelson, A. H. Weston, G. Edwards, *Br. J. Pharmacol.* **2011**, *164*, 922.

[134] L. W. Pappalardo, J. A. Black, S. G. Waxman, N. Haven, W. Haven, **2016**, *64*, 1628.

[135] H. Sontheimer, E. Fernandez-Marques, N. Ullrich, C. a Pappas, S. G. Waxman, *J. Neurosci.* **1994**, *14*, 2464.

[136] W. a Catterall, E. Perez-Reyes, T. P. Snutch, J. Striessnig, *Pharmacol. Rev.* **2005**, *57*, 411.

[137] R. W. Tsien, D. Lipscombe, K. Bley, A. Fox, *Trends Neurosci* **1995**, *18*, 52.

[138] B. MacVicar, *Science (80-.).* **1984**, *226*, 1345.

[139] J. D. Cahoy, B. Emery, A. Kaushal, L. C. Foo, J. L. Zamanian, K. S. Christopherson, Y. Xing, J. L. Lubischer, P. A. Krieg, S. A. Krupenko, et al., *J. Neurosci.* **2008**, *28*, 264.

[140] I. Latour, J. Hamid, A. M. Beedle, G. W. Zamponi, B. A. Macvicar, *Glia* **2003**, *41*, 347.

[141] V. T. Cheli, D. A. Santiago Gonzalez, J. Smith, V. Spreuer, G. G. Murphy, P. M. Paez, *Glia* **2016**, *64*, 1396.

[142] B. Nilius, G. Appendino, G. Owsianik, *Pflugers Arch. Eur. J. Physiol.* **2012**, *464*, 425.

[143] B. Nilius, G. Appendino, *Rev. Physiol. Biochem. Pharmacol.* **2013**, DOI 10.1007/112.

[144] B. Nilius, G. Owsianik, *Genome Biol* **2011**, *12*, 218.

[145] G. Owsianik, K. Talavera, T. Voets, B. Nilius, *Annu. Rev. Physiol.* **2005**, *68*, 685.

[146] A. Verkhratsky, R. C. Reyes, V. Parpura, *Rev. Physiol. Biochem. Pharmacol.* **2013**, DOI 10.1007/112.

[147] N. Takahashi, D. Kozai, Y. Mori, *Front. Physiol.* **2012**, *3 AUG*, 1.

[148] O. Butenko, D. Dzamba, J. Benesova, P. Honsa, V. Benfenati, V. Rusnakova, S. Ferroni, M. Anderova, *PLoS One* **2012**, *7*, DOI 10.1371/journal.pone.0039959.

[149] V. Benfenati, M. Amiry-Moghaddam, M. Caprini, M. N. Mylonakou, C. Rapisarda, O. P. Ottersen, S. Ferroni, *Neuroscience* **2007**, *148*, 876.

[150] K. M. Dunn, D. C. Hill-Eubanks, W. B. Liedtke, M. T. Nelson, *Proc. Natl. Acad. Sci.* **2013**, *110*, 6157.

[151] V. Benfenati, M. Caprini, M. Dovizio, M. N. Mylonakou, S. Ferroni, O. P. Ottersen, M. Amiry-Moghaddam, *Proc. Natl. Acad. Sci.* **2011**, *108*, 2563.

[152] M. Auer-Grumbach, A. Olschewski, L. Papi, H. Kremer, M. E. McEntagart, S. Uhrig, C. Fischer, E. Fröhlich, Z. Bálint, B. Tang, et al., *Nat. Genet.* **2010**, *42*, 160.

[153] E. Shigetomi, X. Tong, K. Y. Kwan, D. P. Corey, S. Baljit, **2012**, *15*, 70.

[154] E. Shigetomi, O. Jackson-Weaver, R. T. Huckstepp, T. J. O'Dell, B. S. Khakh, *J. Neurosci.* **2013**, *33*, 10143.

[155] J. Chen, D. H. Hackos, *IJCAI Int. Jt. Conf. Artif. Intell.* **2016**, *2016–Janua*, 1519.

[156] E. Shigetomi, X. Tong, K. Y. Kwan, D. P. Corey, B. S. Khakh, *Nat. Neurosci.* **2012**, *15*, 70.

[157] E. B. Malarkey, Y. Ni, V. Parpura, *Glia* **2008**, *56*, 821.

[158] M. G. Matias, K. M. Gomolplitinant, D. G. Tamang, M. H. Saier, *BMC Res. Notes* **2010**, *3*, DOI 10.1186/1756-0500-3-158.

[159] M. Prakriya, R. S. Lewis, *Physiol. Rev.* **2015**, *95*, 1383.

[160] R. Kraft, *Channels* **2015**, *9*, 244.

[161] V. Ronco, A. A. Grolla, T. N. Glasnov, P. L. Canonico, A. Verkhratsky, A. A. Genazzani, D. Lim, *Cell Calcium* **2014**, *55*, 219.

[162] D. N. Hertle, M. F. Yeckel, *Neuroscience* **2007**, *150*, 625.

[163] L. A. Holtzclaw, S. Pandhit, D. J. Bare, G. A. Mignery, J. T. Russell, *Glia* **2002**, *39*, 69.

[164] A. Verkhratsky, J. J. Rodríguez, V. Parpura, *Mol. Cell. Endocrinol.* **2012**, *353*, 45.

[165] J. Petravicz, K. M. Boyt, K. D. McCarthy, *Front. Behav. Neurosci.* **2014**, *8*, 1.

[166] S. L. Hamilton, I. I. Serysheva, *J. Biol. Chem.* **2009**, *284*, 4047.

[167] H. R. Parri, V. Crunelli, *Neuroscience* **2003**, *120*, 979.

[168] A. Beck, R. N. Zur, H.-P. Schneider, J. W. Deitmer, *Cell Calcium* **2004**, *35*, 47.

[169] M. Matyash, V. Matyash, C. Nolte, V. Sorrentino, H. Kattenmann, *FASEB* **2002**, *16*.

[170] T. J. Jentsch, T. Friedrich, A. Schriever, H. Yamada, *Eur. J. Physiol.* **1999**, *437*, 738.

[171] A. Sík, R. L. Smith, T. F. Freund, *Neuroscience* **2000**, *101*, 51.

[172] R. M. Roman, R. L. Smith, a P. Feranchak, G. H. Clayton, R. B. Doctor, J. G. Fitz, *Am. J. Physiol. Gastrointest. Liver Physiol.* **2001**, *280*, G344.

[173] D. Daneka, M. Sawicka, A. K. M. Lam, C. Paulino, R. Dutzler, *Nature* **2018**, *448*, 254.

[174] H. K. Kimelberg, B. A. MacVicar, H. Sontheimer, *Glia* **2006**, *54*, 747.

[175] V. Benfenati, M. Caprini, G. P. Nicchia, A. Rossi, M. Dovizio, C. Cervetto, M. Nobile, S. Ferroni, *Channels* **2009**, *3*, DOI 10.4161/chan.3.5.9568.

[176] H. K. Kimelberg, S. K. Goderie, S. Higman, S. Pang, R. A. Waniewski, *J. Neurosci.* **1990**, *10*, 1583.

[177] Y. Fujii, S. Maekawa, M. Morita, *Sci. Rep.* **2017**, *7*, 1.

[178] J. Satoh, H. Tabunoki, T. Yamamura, K. Arima, H. Konno, *Neuropathology* **2007**, *27*, 245.

[179] J. Badaut, L. Hirt, C. Granziera, J. Bogousslavsky, P. J. Magistretti, L. Regli, *J. Cereb. Blood Flow Metab.* **2001**, *21*, 477.

[180] M. C. Papadopoulos, A. S. Verkman, *Nat. Rev. Neurosci.* **2013**, *14*, 265.

[181] J. E. Rash, T. Yasumura, C. S. Hudson, P. Agre, S. Nielsen, *Proc. Natl. Acad. Sci.* **1998**, *95*, 11981.

[182] E. A. Nagelhus, O. P. Ottersen, *Physiol. Rev.* **2013**, *93*, 1543.

[183] H. Wolburg, K. Wolburg-Buchholz, P. Fallier-Becker, S. Noell, A. F. Mack, *Structure and Functions of Aquaporin-4-Based Orthogonal Arrays of Particles*, Elsevier Inc., **2011**.

[184] E. Solenov, *AJP Cell Physiol.* **2004**, *286*, 426C.

[185] D. K. Binder, X. Yao, Z. Zador, T. J. Sick, A. S. Verkman, G. T. Manley, *Glia* **2006**, *53*,

631.

[186] D. Borja-Cacho, J. Matthews, *Nano* **2008**, *6*, 2166.

[187] V. A. Skucas, I. B. Mathews, J. Yang, Q. Cheng, A. Treister, A. M. Duffy, A. S. Verkman, B. L. Hempstead, M. A. Wood, D. K. Binder, et al., *J. Neurosci.* **2011**, *31*, 6392.

[188] M. G. Mola, A. Sparaneo, C. D. Gargano, D. C. Spray, M. Svelto, A. Frigeri, E. Scemes, G. P. Nicchia, *Glia* **2016**, *64*, 139.

[189] A. L. Harris, *Prog. Biophys. Mol. Biol.* **2007**, *94*, 120.

[190] E. Decrock, M. De Bock, N. Wang, G. Bultynck, C. Giaume, C. C. Naus, C. R. Green, L. Leybaert, *Cell. Mol. Life Sci.* **2015**, *72*, 2823.

[191] J. R. Wolff, K. Stuke, M. Missler, H. Tytko, P. Schwarz, A. Rohlmann, T. I. Chao, *Glia* **1998**, *24*, 121.

[192] R. Gajardo-Gómez, V. C. Labra, J. A. Orellana, *Front. Mol. Neurosci.* **2016**, *9*, 1.

[193] C. Giaume, C. Fromaget, A. El Aoumari, J. Cordier, J. Glowinski, D. Grost, *Neuron* **1991**, *6*.

[194] B. M. Altevogt, *J. Neurosci.* **2004**, *24*, 4313.

[195] C. Giaume, L. Leybaert, C. C. Naus, J. C. Sáez, *Front. Pharmacol.* **2013**, *4 JUL*, 1.

[196] J. L. Esseltine, D. W. Laird, *Trends Cell Biol.* **2016**, *26*, 944.

[197] R. Iglesias, G. Dahl, F. Qiu, D. C. Spray, E. Scemes, *J. Neurosci.* **2009**, *29*, 7092.

[198] H.-C. Pan, Y.-C. Chou, S. H. Sun, *Glia* **2015**, *63*, 877.

[199] S. O. Suadicani, R. Iglesias, J. Wang, G. Dahl, D. C. Spray, E. Scemes, *Glia* **2012**, *60*, 1106.

[200] W. R. Silverman, J. P. de Rivero Vaccari, S. Locovei, F. Qiu, S. K. Carlsson, E. Scemes, R. W. Keane, G. Dahl, *J. Biol. Chem.* **2009**, *284*, 18143.

[201] M. P. Abbracchio, G. Burnstock, A. Verkhratsky, H. Zimmermann, *Trends Neurosci.* **2009**, *32*, 19.

[202] R. North, *Physiol. Rev.* **2002**, *82*, 1013.

[203] R. A. North, A. Verkhratsky, *Eur. J. Physiol.* **2006**, *452*, 479.

[204] S. O. Suadicani, C. F. Brosnan, E. Scemes, *J Neurosci* **2006**, *26*, 1378.

[205] S. Duan, C. M. Anderson, E. C. Keung, Y. Chen, Y. Chen, R. A. Swanson, *J. Neurosci.* **2003**, *23*, 1320.

[206] H. Franke, A. Verkhratsky, G. Burnstock, P. Illes, *Purinergic Signal.* **2012**, *8*, 629.

[207] F. Di Virgilio, D. Ferrari, E. Adinolfi, *Purinergic Signal.* **2009**, *5*, 251.

[208] M. P. ABBRACCHIO, G. BURNSTOCK, J.-M. BOEYNAEMS, E. A. BARNARD, A. BOYER, JOSÉ L.CHARLES KENNEDY, GILLIAN E. KNIGHT, MARTA FUMAGALLI, CHRISTIAN GACHET, KENNETH A. JACOBSON, G. A. WEISMAN, *Pharmacol. Rev.* **2006**, *58*, 281.

[209] A. Verkhrasky, O. A. Krishtal, G. Burnstock, *Mol. Neurobiol.* **2009**, *39*, 190.

[210] B. Pearce, S. Murphy, J. Jeremy, C. Morrow, P. Dandona, *J. Neurochem.* **1989**, *52*, 971.

[211] B. Pearce, D. Langley, *Brain Res.* **1994**, *660*, 329.

[212] J. Espallergues, O. Solovieva, V. Técher, K. Bauer, G. Alonso, A. Vincent, N. Hussy, *Neuroscience* **2007**, *148*, 712.

[213] M. Fumagalli, R. Brambilla, N. D'Ambrosi, C. Volonté, M. Matteoli, C. Verderio, M. P. Abbracchio, *Glia* **2003**, *43*, 218.

[214] J. T. Neary, Y. Kang, Y. R. Bu, E. Yu, K. Akong, C. M. Peters, *J. Neurosci.* **1999**, *19*, 4211.

[215] J. T. Neary, Y. Kang, *J. Neurosci. Res.* **2006**, *84*, 515.

[216] G. A. Weisman, M. Wang, Q. Kong, N. E. Chorna, J. T. Neary, G. Y. Sun, F. A. González, C. I. Seye, L. Erb, *Mol. Neurobiol.* **2005**, *31*, 169.

[217] T. S. Peterson, J. M. Camden, Y. Wang, C. I. Seye, W. G. Wood, G. Y. Sun, L. Erb, M. J. Petris, G. A. Weisman, *Mol Neurobiol.* **2010**, *41*, 356.

[218] G. Seifert, C. Steinhäuser, *Prog. Brain Res.* **2001**, *132*.

[219] G. Seifert, C. Steinhäuser, *Eur. J. Neurosci.* **1995**, *7*, 1872.

[220] U. Lalo, *J. Neurosci.* **2006**, *26*, 2673.

[221] Y. Ota, A. T. Zanetti, R. M. Hallock, *Neural Plast.* **2013**, *2013*, 185463.

[222] J. M. Garcia-Barcina, C. Matute, *Eur. J. Neurosci.* **1996**, *8*, 2379.

[223] F. Conti, P. Barbaresi, M. Melone, A. Ducati, *Cereb. Cortex* **1999**, *9*.

[224] M.-C. Lee, K. K. Ting, S. Adams, B. J. Brew, R. Chung, G. J. Guillemin, *PLoS One* **2010**, *5*, e14123.

[225] U. Lalo, O. Palygin, R. A. North, A. Verkhratsky, Y. Pankratov, *Aging Cell* **2011**, *10*, 392.

[226] M. M. Maneshi, B. Maki, R. Gnanasambandam, S. Belin, G. K. Popescu, F. Sachs, S. Z. Hua, *Sci. Rep.* **2017**, *7*, 1.

[227] C. M. Niswender, P. J. Conn, *Annu Rev Pharmacol Toxicol* **2010**, *50*, 295.

[228] W. Sun, E. McConnell, J.-F. Pare, Q. Xu, M. Chen, W. Peng, D. Lovatt, X. Han, Y. Smith, M. Nedergaard, *Science (80-.).* **2013**, *339*, 197.

[229] A. Panatier, J. Vallée, M. Haber, K. K. Murai, J. C. Lacaille, R. Robitaille, *Cell* **2011**, *146*, 785.

[230] A. Pastor, A. Chvátal, E. Syková, H. Kattenmann, *Eur. J. Neurosci.* **1995**, *7*, 1188.

[231] M. Vélez-Fort, E. Audinat, M. C. Angulo, *Neurosci.* **2011**, DOI 10.1177/1073858411403317.

[232] B. A. MacVicar, F. W. Tse, S. A. Crichton, H. Kettenmann, *J. Neurosci.* **1989**, *9*, 3577.

[233] M. Nilsson, P. S. Eriksson, L. Rönnbäck, E. Hansson, *Neuroscience* **1993**, *54*, 605.

[234] G. Losi, L. Mariotti, G. Carmignoto, *Philos. Trans. R. Soc. B Biol. Sci.* **2014**, *369*, DOI 10.1098/rstb.2013.0609.

[235] L. Leybaert, M. J. Sanderson, *Physiol. Rev.* **2012**, *92*, 1359.

[236] K. Kanemaru, H. Sekiya, M. Xu, K. Satoh, N. Kitajima, K. Yoshida, Y. Okubo, T. Sasaki, S. Moritoh, H. Hasuwa, et al., *Cell Rep.* **2014**, *8*, 311.

[237] M. A. Di Castro, J. Chuquet, N. Liaudet, K. Bhaukaurally, M. Santello, D. Bouvier, P. Tiret, A. Volterra, *Nat. Neurosci.* **2011**, *14*, 1276.

[238] A. Volterra, N. Liaudet, I. Savtchouk, *Nat. Rev. Neurosci.* **2014**, *15*, 327.

[239] W. J. Nett, S. H. Oloff, K. D. Mccarthy, A. Nimmerjahn, *J. Neurophysiol.* **2002**, *87*, 528.

[240] E. Shigetomi, S. Kracun, M. V. Sofroniew, B. S. Khakh, *Nat. Neurosci.* **2010**, *13*, 759.

[241] E. Scemes, *Mol. Neurobiol.* **2000**, *22*, 167.

[242] O. Palygin, U. Lalo, A. Verkhratsky, Y. Pankratov, *Cell Calcium* **2010**, *48*, 225.

[243] R. Maroto, A. Raso, T. G. Wood, A. Kurosky, B. Martinac, O. P. Hamill, *Nat. Cell Biol.* **2005**, *7*, 179.

[244] W. Kresse, I. Sekler, A. Hoffmann, O. Peters, C. Nolte, A. Moran, H. Kettenmann, *Eur. J. Neurosci.* **2005**, *21*, 1626.

[245] A. Araque, V. Parpura, R. P. Sanzgiri, P. G. Haydon, *Eur. J. Neurosci.* **1998**, *10*, 2129.

[246] T. Fellin, G. Carmignoto, *J. Physiol.* **2004**, *559*, 3.

[247] A. Volterra, J. Meldolesi, *Nat. Neurosci.* **2005**, *6*, 626.

[248] Y. Bernardinelli, P. J. Magistretti, J.-Y. Chatton, *Proc. Natl. Acad. Sci.* **2004**, *101*, 14937.

[249] S. J. Mulligan, B. A. MacVicar, *Nature* **2004**, *431*, 195.

[250] M. Zonta, M. C. Angulo, S. Gobbo, B. Rosengarten, K.-A. Hossmann, T. Pozzan, G. Carmignoto, *Nat. Neurosci.* **2003**, *6*, 43.

[251] T. Takano, G.-F. Tian, W. Peng, N. Lou, W. Libionka, X. Han, M. Nedergaard, *Nat. Neurosci.* **2006**, *9*, 260.

[252] D. Rossi, A. Volterra, *Brain Res. Bull.* **2009**, *80*, 224.

[253] U. Wilhelmsson, E. A. Bushong, D. L. Price, B. L. Smarr, V. Phung, M. Terada, M. H. Ellisman, M. Pekny, *Proc. Natl. Acad. Sci.* **2006**, *103*, 17513.

[254] Y. Chen, R. A. Swanson, *J. Cereb. Blood Flow Metab.* **2003**, *23*, 137.

[255] M. V. Sofroniew, H. V. Vinters, *Acta Neuropathol.* **2010**, *119*, 7.

[256] E. Dossi, F. Vasile, N. Rouach, *Brain Res. Bull.* **2018**, *136*, 139.

[257] M. V. Sofroniew, *Trends Neurosci.* **2009**, *32*, 638.

[258] A. Becerra-Calixto, G. P. Cardona-Gómez, *Front. Mol. Neurosci.* **2017**, *10*, 1.

[259] A. Chvátal, M. Anděrová, H. Neprašová, I. Prajerová, J. Benešová, O. Butenko, A. Verkhratsky, *Physiol. Res.* **2008**, *57*.

[260] J. A. Stokum, D. B. Kurland, V. Gerzanich, J. M. Simard, *Neurochem. Res.* **2014**, *40*, 317.

[261] K. Mori, M. Miyazaki, H. Iwase, M. Maeda, *J. Neurotrauma* **2002**, *19*, 1261.

[262] G. T. Manley, M. Fujimura, T. Ma, N. Noshita, F. Filiz, A. W. Bollen, P. Chan, A. S. Verkman, *Nat. Med.* **2000**, *6*, 159.

[263] N. N. Haj-Yasein, G. F. Vindedal, M. Eilert-Olsen, G. A. Gundersen, O. Skare, P. Laake, A. Klungland, A. E. Thoren, J. M. Burkhardt, O. P. Ottersen, et al., *Proc. Natl. Acad. Sci.* **2011**, *108*, 17815.

[264] T. Da, A. S. Verkman, *Investig. Ophthalmol. Vis. Sci.* **2004**, *45*, 4477.

[265] M. C. Papadopoulos, *FASEB J.* **2004**, *18*, 1.

[266] E. Steiner, G. U. Enzmann, S. Lin, S. Ghavampour, M.-J. Hannocks, B. Zuber, M. A. Rüegg, L. Sorokin, B. Engelhardt, *Glia* **2012**, *60*, 1646.

[267] Y. Katayama, D. P. Becker, T. Tamura, D. A. Hovda, *J. Neurosurg.* **1990**, *73*, 889.

[268] A. I. Faden, P. Demediuk, S. S. Panter, R. Vink, *Science (80-.).* **1989**, *244*, 798.

[269] G.-F. Tian, H. Azmi, T. Takano, Q. Xu, W. Peng, J. Lin, N. Oberheim, N. Lou, X. Wang, H. R. Zielke, et al., *Nat. Med.* **2005**, *11*, 973.

[270] M. Thom, *Neuropathol. Appl. Neurobiol.* **2014**, *40*, 520.

[271] S. Hinterkeuser, W. Schröder, G. Hager, G. Seifert, I. Blümcke, C. E. Elger, J. Schramm, C. Steinhäuser, *Eur. J. Neurosci.* **2000**, *12*, 2087.

[272] A. Bordey, D. D. Spencer, *Epilpsy Res.* **2004**, *59*, 107.

[273] A. Das, G. C. Wallace IV, C. Holmes, M. L. McDowell, J. A. Smith, J. D. Marshall, L. Bonilha, J. C. Edwards, S. S. Clazier, S. K. Ray, et al., *Neuroscience* **2012**, *220*, 237.

[274] T. S. Lee, T. Eid, S. Mane, J. H. Kim, D. D. Spencer, O. P. Ottersen, N. C. de Lanerolle, *Acta*

Neuropathol. **2004**, *108*, 493.

[275] I. Cavus, J. W. Pan, H. P. Hetherington, W. Abi-Saab, H. P. Zaveri, K. P. Vives, J. H. Krystal, S. S. Spencer, D. D. Spencer, *Epilepsia* **2008**, *49*, 1358.

[276] E. A. Proper, G. Hoogland, S. M. Kappen, G. H. Jansen, M. G. A. Rensen, L. H. Schrama, C. W. M. Van Veelen, P. C. Van Rijen, O. Van Nieuwenhuizen, W. H. Gispen, et al., *Brain* **2002**, *125*, 32.

[277] M. J. During, D. D. Spencer, *Lancet* **1993**, *341*, 1607.

[278] E. R. O'Connor, H. Sontheimer, D. D. Spencer, N. C. De Lanerolle, *Epilepsia* **1998**, *39*, 347.

[279] J. Lee, A. K. Borboa, A. Baird, B. P. Eliceiri, *BMC Neurosci.* **2011**, *12*, DOI 10.1186/1471-2202-12-9.

[280] M. Roslin, R. Henriksson, P. Bergström, U. Ungerstedt, A. T. Bergenheim, *J. Neurooncol.* **2003**, *61*, 151.

[281] J. Kurzwelly, U. Herrlinger, M. Simon, in *Low-Grade Gliomas. Adv. Tech. Stand. Neurosurg.*, **2010**.

[282] P. Pu, Z. Xia, S. Yu, Q. Huang, *Clin. Neurol. Neurosurg.* **2004**, *107*, 49.

[283] A. Bordey, H. Sontheimer, *J. Neurophysiol.* **1998**, *79*, 2782.

[284] M. Wortmann, *Alzheimer's Res. Ther.* **2012**, *4*, 4.

[285] H. W. Querfurth, F. M. LaFerla, *N Engl J Med* **2010**, *362*, 329.

[286] J. E. Simpson, P. G. Ince, G. Lace, G. Foster, P. J. Shaw, F. Matthews, G. Savva, C. Brayne, S. B. Wharton, *Neurobiol. Aging* **2010**, *31*, 578.

[287] J. E. Simpson, P. G. Ince, P. J. Shaw, P. R. Heath, R. Raman, C. J. Garwood, C. Gelsthorpe,

L. Baxter, G. Forster, F. E. Matthews, et al., *Neurobiol. Aging* **2011**, *32*, 17951807.

[288] D. A. DeWitt, G. Perry, M. Cohen, C. Doller, J. Silver, *Exp. Neurol.* **1998**, *149*, 329.

[289] R. G. Nagele, M. R. D'Andrea, H. Lee, V. Venkataraman, H.-Y. Wang, *Brain Res.* **2003**, *971*, 197.

[290] S. Li, M. Mallory, M. Alford, S. Tanaka, E. Masliah, *J. Neuropathol. Exp. Neurol.* **1997**, *56*, 901.

[291] S. Mitew, M. T. K. Kirkcaldie, T. C. Dickson, J. C. Vickers, *Neurobiol. Aging* **2013**, *34*, 2341.

[292] J. I. Nagy, W. Li, E. L. Hertzberg, C. A. Marotta, *Brain Res.* **1996**, *717*, 173.

[293] D. M. Wilcock, M. P. Vitek, C. A. Colton, *Neuroscience* **2009**, *159*, 1055.

[294] K. V. Kuchibhotla, C. R. Lattarulo, B. T. Hyman, B. J. Bacskai, *Science (80-.).* **2009**, *323*, 1211.

[295] D. Lim, A. Iyer, V. Ronco, A. A. Grolla, P. L. Canonico, E. Aronica, A. A. Genazzani, *Glia* **2013**, *61*, 1134.

[296] G. Rajkowska, J. J. Miguel-Hidalgo, J. Wei, G. Dilley, S. D. Pittman, H. Y. Meltzer, J. C. Overholser, B. L. Roth, C. A. Stockmeier, *Biol. Psychiatry* **1999**, *45*, 1085.

[297] A. Medina, S. J. Watson, W. B. Jr., R. M. Myers, A. Schatzberg, J. Barchas, H. Akil, R. C. Thompson, *J. Psychiatr. Res.* **2016**, *72*, 15.

[298] G. Rajkowska, J. Hughes, C. A. Stockmeier, J. J. Miguel-Hidalgo, D. Maciag, *A J. Psychiatr. Neurosci. Ther.* **2013**, *73*, 613.

[299] R. M. Paredes, J. C. Etzler, L. T. Watts, W. Zheng, J. D. Lechleiter, *Methods* **2008**, *46*, 143.

[300] A. M. B. Reeves, E. Shigetomi, B. S. Khakh, *J. Neurosci.* **2011**, *31*, 9353.

[301] O. Garaschuk, R. I. Milos, A. Konnerth, *Nat. Protoc.* **2006**, *1*, 380.

[302] C. Nolte, M. Matyash, T. Pivneva, C. G. Schipke, C. Ohlemeyer, U. K. Hanisch, F. Kirchhoff, H. Kettenmann, *Glia* **2001**, *33*, 72.

[303] T. Knöpfel, *Nat. Rev. Neurosci.* **2012**, *13*, 687.

[304] E. Shigetomi, E. A. Bushong, M. D. Haustein, X. Tong, O. Jackson-Weaver, S. Kracun, J. Xu, M. V. Sofroniew, M. H. Ellisman, B. S. Khakh, *J. Gen. Physiol.* **2013**, *141*, 633.

[305] E. Chaigneau, A. J. Wright, S. P. Poland, J. M. Girkin, R. A. Silver, *Opt. Express* **2011**, *19*, 6540.

[306] D. Li, C. Agulhon, E. Schmidt, M. Oheim, N. Ropert, *Front. Cell. Neurosci.* **2013**, *7*, 1.

[307] S. Berning, K. I. Willig, H. Steffens, P. Dibaj, S. W. Hell, *Science (80-.).* **2012**, *335*, 551.

[308] G. Nagel, T. Szellas, W. Huhn, S. Kateriya, N. Adeishvili, P. Berthold, D. Ollig, P. Hegemann, E. Bamberg, *Proc. Natl. Acad. Sci.* **2003**, *100*, 13940.

[309] E. S. Boyden, F. Zhang, E. Bamberg, G. Nagel, K. Deisseroth, *Nat. Neurosci.* **2005**, *8*, 1263.

[310] G. Nagel, M. Brauner, J. F. Liewald, N. Adeishvili, E. Bamberg, A. Gottschalk, *Curr. Biol.* **2005**, *15*, 2279.

[311] X. Li, D. V. Gutierrez, M. G. Hanson, J. Han, M. D. Mark, H. Chiel, P. Hegemann, L. T. Landmesser, S. Herlitze, *Proc. Natl. Acad. Sci.* **2005**, *102*, 17816.

[312] T. Ishizuka, M. Kakuda, R. Araki, H. Yawo, *Neurosci. Res.* **2006**, *54*, 85.

[313] A. Bi, J. Cui, Y. P. Ma, E. Olshevskaya, M. Pu, A. M. Dizhoor, Z. H. Pan, *Neuron* **2006**, *50*, 23.

[314] T. Sasaki, K. Beppu, K. F. Tanaka, Y. Fukazawa, R. Shigemoto, K. Matsui, *PNAS* **2012**, *109*, 20720.

[315] D. Li, K. Hérault, E. Y. Isacoff, M. Oheim, N. Ropert, *J. Physiol.* **2012**, *590*, 855.

[316] J. W. Salatino, B. M. Winter, M. H. Drazin, E. K. Purcell, *J. Neurophysiol.* **2017**, *118*, 194.

[317] J. W. Salatino, K. A. Ludwig, T. D. Y. Kozai, E. K. Purcell, *Nat. Biomed. Eng.* **2017**, *1*, DOI 10.1038/s41551-017-0154-1.

[318] T. Kim, J. G. McCall, Y. H. Jung, X. Huang, E. R. Siuda, Y. Li, J. Song, Y. M. Song, H. A. Pao, R.-H. Kim, et al., **2013**, *340*, 211.

[319] P. Fattahi, G. Yang, G. Kim, M. R. Abidian, *Adv. Mater.* **2014**, *26*, 1846.

[320] S. Bonetti, A. Pistone, M. Brucale, S. Karges, L. Favaretto, M. Zambianchi, T. Posati, A. Sagnella, M. Caprini, S. Toffanin, et al., *Adv. Healthc. Mater.* **2015**, *4*, 1190.

[321] S. Bonetti, M. Prosa, A. Pistone, L. Favaretto, A. Sagnella, I. Grisin, M. Zambianchi, S. Karges, A. Lorenzoni, T. Posati, et al., *J. Mater. Chem. B* **2016**, *4*, 2921.

[322] M. C. Dodla, R. V. Bellamkonda, *Biomaterials* **2008**, *29*, 33.

[323] Y. Zhong, R. V. Bellamkonda, *Brain Res.* **2007**, *1148*, 15.

[324] P. Moshayedi, G. Ng, J. C. F. Kwok, G. S. H. Yeo, C. E. Bryant, J. W. Fawcett, K. Franze, J. Guck, *Biomaterials* **2014**, *35*, 3919.

[325] J. K. Nguyen, D. J. Park, J. L. Skousen, A. E. Hess-Dunning, D. J. Tyler, S. J. Rowan, C. Weder, J. R. Capadona, *J. Neural Eng.* **2014**, *11*, DOI 10.1088/1741-2560/11/5/056014.

[326] T. Ware, D. Simon, C. Liu, T. Musa, S. Vasudevan, A. Sloan, E. W. Keefer, R. L. R. Ii, W. Voit, **2013**, 1.

[327] T. Ware, D. Simon, D. E. Arreaga-Salas, J. Reeder, R. Rennaker, E. W. Keefer, W. Voit, *Adv. Funct. Mater.* **2012**, *22*, 3470.

[328] J. L. Skousen, S. M. E. Merriam, O. Srivannavit, G. Perlin, K. D. Wise, P. A. Tresco, *Reducing Surface Area While Maintaining Implant Penetrating Profile Lowers the Brain Foreign Body Response to Chronically Implanted Planar Silicon Microelectrode Arrays*, Elsevier B.V., **2011**.

[329] S. Suner, M. R. Fellows, C. Vargas-Irwin, G. K. Nakata, J. P. Donoghue, *IEEE Trans. Neural Syst. Rehabil. Eng.* **2005**, *13*, 524.

[330] M. Velliste, S. Perel, M. C. Spalding, A. S. Whitford, A. B. Schwartz, *Nature* **2008**, *453*, 1098.

[331] J. L. Collinger, B. Wodlinger, J. E. Downey, W. Wang, E. C. Tyler-Kabara, D. J. Weber, A. J. C. McMorland, M. Velliste, M. L. Boninger, A. B. Schwartz, *Lancet* **2013**, *381*, 557.

[332] A. Prasad, J. C. Sanchez, *J. Neural Eng.* **2012**, *9*, DOI 10.1088/1741-2560/9/2/026028.

[333] M. Durso, A. I. Borrachero-Conejo, C. Bettini, E. Treossi, A. Scidà, E. Saracino, M. Gazzano, M. Christian, V. Morandi, G. Tuci, et al., *J. Mater. Chem. B* **2018**, *6*, 5335.

[334] T. Kuila, S. Bose, A. K. Mishra, P. Khanra, N. H. Kim, J. H. Lee, *Prog. Mater. Sci.* **2012**, *57*, 1061.

[335] Y. Yang, A. M. Asiri, Z. Tang, D. Du, Y. Lin, *Mater. Today* **2013**, *16*, 365.

[336] Y. Zhang, S. F. Ali, E. Dervishi, Y. Xu, Z. Li, D. Casciano, A. S. Biris, *ACS Nano* **2010**, *4*, 3181.

[337] M. Lv, Y. Zhang, L. Liang, M. Wei, W. Hu, X. Li, Q. Huang, *Nanoscale* **2012**, *4*, 3861.

[338] R. Rauti, N. Lozano, V. León, D. Scaini, M. Musto, I. Rago, F. P. Ulloa Severino, A. Fabbro,

L. Casalis, E. Vázquez, et al., *ACS Nano* **2016**, *10*, 4459.

[339] M. Bramini, S. Sacchetti, A. Armirotti, A. Rocchi, E. Vázquez, V. León Castellanos, T. Bandiera, F. Cesca, F. Benfenati, *ACS Nano* **2016**, *10*, 7154.

[340] M. C. P. Mendonça, E. S. Soares, M. B. de Jesus, H. J. Ceragioli, S. P. Irazusta, Â. G. Batista, M. A. R. Vinolo, M. R. Maróstica Júnior, M. A. Cruz-Höfling, *J. Nanobiotechnology* **2016**, *14*, 1.

[341] M. Bramini, G. Alberini, E. Colombo, M. Chiacchiaretta, M. L. DiFrancesco, J. F. Maya-Vetencourt, L. Maragliano, F. Benfenati, F. Cesca, *Front. Syst. Neurosci.* **2018**, *12*, 1.

[342] P. Garg, P. Gupta, D. Kumar, O. Parkash, **2016**, *7*, 1461.

[343] M. Nasrollahzadeh, F. Babaei, P. Fakhri, B. Jaleh, *RSC Adv.* **2015**, *5*, 10782.

[344] C. Chen, Q. H. Yang, Y. Yang, W. Lv, Y. Wen, P. X. Hou, M. Wang, H. M. Cheng, *Adv. Mater.* **2009**, *21*, 3007.

[345] V. Georgakilas, J. N. Tiwari, K. C. Kemp, J. A. Perman, A. B. Bourlinos, K. S. Kim, R. Zboril, *Chem. Rev.* **2016**, *116*, 5464.

[346] A. A. John, A. P. Subramanian, M. V. Vellayappan, A. Balaji, H. Mohandas, S. K. Jaganathan, *Int. J. Nanomedicine* **2015**, *10*, 4267.

[347] M. Chiacchiaretta, M. Bramini, A. Rocchi, A. Armirotti, E. Giordano, E. Vázquez, T. Bandiera, S. Ferroni, F. Cesca, F. Benfenati, *Nano Lett.* **2018**, acs. nanolett.8b02487.

[348] K. Zhou, S. Motamed, G. A. Thouas, C. C. Bernard, D. Li, H. C. Parkington, H. A. Coleman, D. I. Finkelstein, J. S. Forsythe, *PLoS One* **2016**, *11*, 1.

[349] S. Toffanin, V. Benfenati, A. Pistone, S. Bonetti, W. Koopman, T. Posati, A. Sagnella, M. Natali, R. Zamboni, G. Ruani, et al., *J. Mater. Chem. B* **2013**, *1*, 3850.

[350] V. Benfenati, K. Stahl, C. Gomis-Perez, S. Toffanin, A. Sagnella, R. Torp, D. L. Kaplan, G. Ruani, F. G. Omenetto, R. Zamboni, et al., *Adv. Funct. Mater.* **2012**, *22*, 1871.

[351] V. Guarino, V. Benfenati, I. Cruz-Maya, A. I. Borrachero-Conejo, R. Zamboni, L. Ambrosio, *Bioinspired Scaffolds for Bone and Neural Tissue and Interface Engineering*, Elsevier Ltd, **2017**.

[352] N. Lago, A. Cester, *Appl. Sci.* **2017**, *7*, 1292.

[353] J. E. Anthony, A. Facchetti, M. Heeney, S. R. Marder, X. Zhan, *Adv. Mater.* **2010**, *22*, 3876.

[354] H. S. Mandal, J. S. Kastee, D. G. McHail, J. F. Rubinson, J. J. Pancrazio, T. C. Dumas, *Neuromodulation* **2015**, *18*, 657.

[355] R. Wadhwa, C. F. Lagenaur, X. T. Cui, *J. Control. Release* **2006**, *110*, 531.

[356] P. M. George, D. A. Lavan, J. A. Burdick, C. Y. Chen, E. Liang, R. Langer, *Adv. Mater.* **2006**, *18*, 577.

[357] S. Löffler, B. Libberton, A. Richter-Dahlfors, *Electronics* **2015**, *4*, 879.

[358] R. Balint, N. J. Cassidy, S. H. Cartmell, *Acta Biomater.* **2014**, *10*, 2341.

[359] T. Nezakati, A. Seifalian, A. Tan, A. M. Seifalian, *Chem. Rev.* **2018**, *118*, 6766.

[360] M. H. Bolin, K. Svennersten, X. Wang, I. S. Chronakis, A. Richter-Dahlfors, E. W. H. Jager, M. Berggren, *Sensors Actuators, B Chem.* **2009**, *142*, 451.

[361] G. Cellot, P. Lagonegro, G. Tarabella, D. Scaini, F. Fabbri, S. Iannotta, M. Prato, G. Salviati, L. Ballerini, *Front. Neurosci.* **2016**, *9*, 1.

[362] A. F. Quigley, J. M. Razal, B. C. Thompson, S. E. Moulton, M. Kita, E. L. Kennedy, G. M. Clark, G. G. Wallace, R. M. I. Kapsa, *Adv. Mater.* **2009**, *21*, 4393.

[363] N. Kasoju, U. Bora, *Adv. Healthc. Mater.* **2012**, *1*, 393.

[364] Y. Wang, H. J. Kim, G. Vunjak-Novakovic, D. L. Kaplan, *Biomaterials* **2006**, *27*, 6064.

[365] L. Fernández-García, N. Marí-Buyé, J. A. Barios, R. Madurga, M. Elices, J. Pérez-Rigueiro, M. Ramos, G. V. Guinea, D. González-Nieto, *Acta Biomater.* **2016**, *45*, 262.

[366] L. Uebersax, M. Mattotti, M. Papaloïzos, H. P. Merkle, B. Gander, L. Meinel, *Biomaterials* **2007**, *28*, 4449.

[367] A. Sagnella, A. Pistone, S. Bonetti, A. Donnadio, E. Saracino, M. Nocchetti, C. Dionigi, G. Ruani, M. Muccini, T. Posati, et al., *RSC Adv.* **2016**, *6*, 9304.

[368] A. Pistone, A. Sagnella, C. Chieco, G. Bertazza, G. Varchi, F. Formaggio, T. Posati, E. Saracino, M. Caprini, S. Bonetti, et al., *Biopolymers* **2016**, *105*, 287.

[369] S. Tang, X. Liao, B. Shi, Y. Qu, Z. Huang, Q. Lin, X. Guo, F. Pei, *PLoS One* **2014**, *9*, 1.

[370] V. Benfenati, S. Toffanin, R. Capelli, L. M. A. Camassa, S. Ferroni, D. L. Kaplan, F. G. Omenetto, M. Muccini, R. Zamboni, *Biomaterials* **2010**, *31*, 7883.

[371] M. Hutzler, A. Lambacher, B. Eversmann, M. Jenkner, R. Thewes, P. Fromherz, *J. Neurophysiol.* **2006**, *96*, 1638.

[372] L. Berdondini, K. Imfeld, A. MacCione, M. Tedesco, S. Neukom, M. Koudelka-Hep, S. Martinoia, *Lab Chip* **2009**, *9*, 2644.

[373] T. J. Blanche, M. A. Spacek, J. F. Hetke, N. V. Swindale, *J. Neurophysiol.* **2005**, *93*, 2987.

[374] X. Duan, R. Gao, P. Xie, T. Cohen-Karni, Q. Qing, H. S. Choe, B. Tian, X. Jiang, C. M. Lieber, *Nat. Nanotechnol.* **2012**, *7*, 174.

[375] J. T. Robinson, M. Jorgolli, A. K. Shalek, M. H. Yoon, R. S. Gertner, H. Park, *Nat. Nanotechnol.* **2012**, *7*, 180.

[376] A. Hai, J. Shappir, M. E. Spira, *J. Neurophysiol.* **2010**, *104*, 559.

[377] M. Berggren, A. Richter-Dahlfors, *Adv. Mater.* **2007**, *19*, 3201.

[378] V. Benfenati, S. Toffanin, S. Bonetti, G. Turatti, A. Pistone, M. Chiappalone, A. Sagnella, A. Stefani, G. Generali, G. Ruani, et al., *Nat. Mater.* **2013**, *12*, 672.

[379] D. Khodagholy, T. Doublet, P. Quilichini, M. Gurfinkel, P. Leleux, A. Ghestem, E. Ismailova, T. Hervé, S. Sanaur, C. Bernard, et al., *Nat. Commun.* **2013**, *4*, DOI 10.1038/ncomms2573.

[380] L. Kergoat, B. Piro, M. Berggren, G. Horowitz, M. C. Pham, *Anal. Bioanal. Chem.* **2012**, *402*, 1813.

[381] D. T. Simon, E. O. Gabrielsson, K. Tybrandt, M. Berggren, *Chem. Rev.* **2016**, *116*, 13009.

[382] J. H. Burroughes, C. A. Jones, R. H. Friend, *Nature* **1988**, *335*, 137.

[383] C. W. Tang, S. A. Vanslyke, *Appl. Phys. Lett.* **1987**, *51*, 913.

[384] J. Mattis, K. M. Tye, E. A. Ferenczi, C. Ramakrishnan, D. J. O'Shea, R. Prakash, L. A. Gunaydin, M. Hyun, L. E. Fenno, V. Gradinaru, et al., *Nat. Methods* **2012**, *9*, 159.

[385] A. Morton, C. Murawski, S. R. Pulver, M. C. Gather, *Sci. Rep.* **2016**, *6*, 1.

[386] A. Tsumura, H. Koezuka, T. Ando, *Appl. Phys. Lett.* **1986**, *49*, 1210.

[387] M. E. Roberts, S. C. B. Mannsfeld, N. Queraltó, C. Reese, J. Locklin, W. Knoll, Z. Bao, *Proc. Natl. Acad. Sci. U. S. A.* **2008**, *105*, 12134.

[388] P. Bergveld, *IEEE Trans. Biomed. Eng.* **1970**, *BME-17*, 70.

[389] C. Bartic, B. Palan, A. Campitelli, G. Borghs, *Sensors Actuators, B Chem.* **2002**, *83*, 115.

[390] C. Bartic, A. Campitelli, S. Borghs, *Appl. Phys. Lett.* **2003**, *82*, 475.

[391] K. Melzer, M. Brändlein, B. Popescu, D. Popescu, P. Lugli, G. Scarpa, *Faraday Discuss.* **2014**, *174*, 399.

[392] T. Cramer, B. Chelli, M. Murgia, M. Barbalinardo, E. Bystrenova, D. M. de Leeuw, F. Biscarini, *Phys. Chem. Chem. Phys.* **2013**, 3897.

[393] D. Wang, V. Noël, B. Piro, *Electronics* **2016**, *5*, 9.

[394] A. Williamson, M. Ferro, P. Leleux, E. Ismailova, A. Kaszas, T. Doublet, P. Quilichini, J. Rivnay, B. Rõzsa, G. Katona, et al., *Adv. Mater.* **2015**, *27*, 4405.

[395] I. Gualandi, D. Tonelli, F. Mariani, E. Scavetta, M. Marzocchi, B. Fraboni, *Sci. Rep.* **2016**, *6*, 1.

[396] A. E. Kirchan, K. T. Kim, M. K. Steward, S. Choi, *TRANSDUCERS 2017 - 19th Int. Conf. Solid-State Sensors, Actuators Microsystems* **2017**, 214.

[397] R. L. Fork, *Science (80-.).* **1971**, *3*, 18.

[398] J. Walker, *Neurosci. Lett.* **1983**, *43*, 330.

[399] K. Tsuchiya, M. Kawatani, C. Takeshige, T. Sato, I. Matsumoto, *Neurosci. Lett.* **1993**, *161*, 65.

[400] K. Tsuchiya, M. Kawatani, C. Takeshige, I. Matsumoto, *Brain Res. Bull.* **1994**, *34*, 369.

[401] E. M. Callaway, L. C. Katz, *Proc. Natl. Acad. Sci.* **1993**, *90*, 7661.

[402] K. R. Gee, R. Wieboldt, G. P. Hess, *J. Am. Chem. Soc.* **1994**, *116*, 8366.

[403] R. H. Kramer, D. L. Fortin, D. Trauner, *Curr. Opin. Neurobiol.* **2009**, *19*, 544.

[404] H. Hirase, V. Nikolenko, R. Yuste, *Cold Spring Harb. Protoc.* **2002**, *7*, 237.

[405] J. Wells, C. Kao, K. Mariappan, J. Albea, E. D. Jansen, P. Konrad, A. Mahadevan-Jansen,

Opt. Lett. **2005**, *30*, 504.

[406] W. J., K. C., J. E. D., K. P., M.-J. A., *J Biomed Opt* **2005**, *10*.

[407] J. Wells, C. Kao, P. Konrad, T. Milner, J. Kim, A. Mahadevan-Jansen, E. D. Jansen, *Biophys. J.* **2007**, *93*, 2567.

[408] J. M. Cayce, R. M. Friedman, G. Chen, E. D. Jansen, A. Mahadevan-Jansen, A. W. Roe, *Neuroimage* **2014**, *84*, 181.

[409] J. M. Cayce, M. B. Bouchard, M. M. Chernov, B. R. Chen, L. E. Grosberg, E. D. Jansen, E. M. C. Hillman, A. Mahadevan-Jansen, *Cell Calcium* **2014**, *55*, 183.

[410] M. G. Shapiro, K. Homma, S. Villarreal, C. P. Richter, F. Bezanilla, *Nat. Commun.* **2012**, *3*, 310.

[411] E. S. Albert, J. M. Bec, G. Desmadryl, K. Chekroud, C. Travo, S. Gaboyard, F. Bardin, I. Marc, M. Dumas, G. Lenaers, et al., *J. Neurophysiol.* **2012**, *107*, 3227.

[412] D. Ghezzi, M. R. Antognazza, M. Dal Maschio, E. Lanzarini, F. Benfenati, G. Lanzani, *Nat. Commun.* **2011**, *2*, 164.

[413] V. Benfenati, N. Martino, M. R. Antognazza, A. Pistone, S. Toffanin, S. Ferroni, G. Lanzani, M. Muccini, *Adv. Healthc. Mater.* **2014**, *3*, 392.

[414] J. Wells, C. Kao, E. D. Jansen, P. Konrad, A. Mahadevan-Jansen, *J. Biomed. Opt.* **2005**, *10*, 064003.

[415] H. Monai, M. Ohkura, M. Tanaka, Y. Oe, A. Konno, H. Hirai, K. Mikoshiba, S. Itohara, J. Nakai, Y. Iwai, et al., *Nat. Commun.* **2016**, *7*, 1.

[416] S. Ferroni, C. Marchini, P. Schubert, C. Rapisarda, *FEBS Lett.* **1995**, *367*, 319.

[417] G. P. Nicchia, A. Frigeri, G. M. Liuzzi, M. P. Santacroce, B. Nico, G. Procino, F.

Quondamatteo, R. Herken, L. Roncali, M. Svelto, *Glia* **2000**, *31*, 29.

[418] M. D. Bootman, K. Rietdorf, T. Collins, S. Walker, M. Sanderson, *Cold Spring Harb. Protoc.* **2013**, *8*, 83.

[419] V. Benfenati, M. Caprini, M. Nobile, C. Rapisarda, S. Ferroni, *J. Neurochem.* **2006**, *98*, 430.

[420] T. Posati, A. Pistone, E. Saracino, F. Formaggio, M. G. Mola, E. Troni, A. Sagnella, M. Nocchetti, M. Barbalinardo, F. Valle, et al., *Sci. Rep.* **2016**, *6*, 1.

[421] A. I. Borrachero-conejo, E. Saracino, M. Natali, F. Prescimone, S. Karges, S. Bonetti, G. P. Nicchia, F. Formaggio, M. Caprini, R. Zamboni, et al., *Adv. Healthc. Mater.* **2018**, *1801139*, 1.

[422] A. Bouron, K. Kiselyov, J. Oberwinkler, *Pflugers Arch. Eur. J. Physiol.* **2015**, *467*, 1143.

[423] F. Vincent, A. Acevedo, M. T. Nguyen, M. Dourado, J. DeFalco, A. Gustafson, P. Spiro, D. E. Emerling, M. G. Kelly, M. A. J. Duncton, *Biochem. Biophys. Res. Commun.* **2009**, *389*, 490.

[424] L. H. Jiang, a B. Mackenzie, R. a North, a Surprenant, *Mol. Pharmacol.* **2000**, *58*, 82.

[425] T. Voets, J. Prenen, J. Vriens, H. Watanabe, A. Janssens, U. Wissenbach, M. Bödding, G. Droogmans, B. Nilius, *J. Biol. Chem.* **2002**, *277*, 33704.

[426] B. Nilius, V. Flockerzi, in *Handb. Exp. Pharmacol.*, **2014**.

[427] E. HANSSON, *FASEB J.* **2003**, *17*, 341.

[428] R. E. Day, P. Kitchen, D. S. Owen, C. Bland, L. Marshall, A. C. Conner, R. M. Bill, M. T. Conner, *Biochim. Biophys. Acta - Gen. Subj.* **2014**, *1840*, 1492.

[429] H. Pasantes-Morales, S. Cruz-Rangel, *Neuroscience* **2010**, *168*, 871.

[430] A. Gordon-Shaag, W. N. Zagotta, S. E. Gordon, *Channels* **2008**, *2*, 125.

[431] X. Chen, F.-J. Sun, Y.-J. Wei, L.-K. Wang, Z.-L. Zang, B. Chen, S. Li, S.-Y. Liu, H. Yang, *Neurosci. Ther.* **2016**, *22*, 280.

[432] B. W. Connors, *Epilepsy Curr.* **2012**, *12*, 66.

[433] R. Strotmann, C. Harteneck, K. Nunnenmacher, G. Schultz, T. D. Plant, *Nat. Cell Biol.* **2000**, *2*, 695.

[434] W. Liedtke, Y. Choe, M. A. Martí-Renom, A. M. Bell, C. S. Denis, AndrejŠali, A. J. Hudspeth, J. M. Friedman, S. Heller, *Cell* **2000**, *103*, 525.

[435] S. K. W. Chang, *IEEE Trans. Biomed. Eng.* **1993**, *40*, 1054.

[436] O. M. Nesin, O. N. Pakhomova, S. Xiao, A. G. Pakhomov, *Biochim. Biophys. Acta - Biomembr.* **2011**, *1808*, 792.

[437] M. G. Mola, A. Sparaneo, C. D. Gargano, D. C. Spray, M. Svelto, A. Frigeri, E. Scemes, G. P. Nicchia, *Glia* **2016**, *64*, 139.

[438] A. Fry Davidson, A. Z. Higgins, *J. Fluoresc.* **2013**, *23*, 393.

[439] J. A. Garate, N. J. English, J. M. D. MacElroy, *J. Chem. Phys.* **2011**, *134*, DOI 10.1063/1.3529428.

[440] S. Marchesan, L. Ballerini, M. Prato, *Science* **2017**, *356*, 1010.

[441] Ç. Defterali, R. Verdejo, L. Peponi, E. D. Martín, R. Martínez-Murillo, M. Á. López-Manchado, C. Vicario-Abejón, *Biomaterials* **2016**, *82*, 84.

[442] A. Domínguez-Bajo, A. González-Mayorga, E. López-Dolado, M. C. Serrano, *Front. Syst. Neurosci.* **2017**, *11*, DOI 10.3389/fnsys.2017.00071.

[443] T. Cohen-Karni, Q. Qing, Q. Li, Y. Fang, C. M. Lieber, *Nano Lett.* **2010**, *10*, 1098.

[444] F. Veliev, Z. Han, D. Kalita, A. Briançon-Marjollet, V. Bouchiat, C. Delacour, *Front. Neurosci.* **2017**, *11*, 1.

[445] N. Liu, A. Chortos, T. Lei, L. Jin, T. R. Kim, W. G. Bae, C. Zhu, S. Wang, R. Pfattner, X. Chen, et al., *Sci. Adv.* **2017**, *3*, 1.

[446] L. F. Eng, R. S. Ghirnikar, *Brain Pathol.* **1994**, *4*, 229.

[447] A. N. Alle, **2013**, DOI 10.1007/s10439-013-0940-1.

[448] K. Eom, S. Hwang, S. Yun, K. M. Byun, S. B. Jun, S. J. Kim, **2017**, *8*, 1.

[449] A. M. Hofer, C. Fasolato, T. Pozzan, **1998**, *140*, 325.

[450] D. Moreau, C. Lefort, J. Pas, S. M. Bardet, P. Leveque, R. P. O'Connor, *J. Biophotonics* **2018**, *11*, 1.

[451] A. D. Lafrenaye, **2019**, DOI 10.3390/ijms20020330.

[452] G. Nase, P. J. Helm, R. Enger, O. P. Ottersen, *Glia* **2008**, *56*, 895.

[453] T. Eid, T. W. Lee, M. J. Thomas, M. Amiry-moghaddam, L. P. Bjørnsen, D. D. Spencer, P. Agre, O. P. Ottersen, N. C. De Lanerolle, **2005**, *102*.

[454] S. Noell, K. Wolburg-Buchholz, A. F. Mack, R. Ritz, M. Tatagiba, R. Beschorner, H. Wolburg, *Cell Tissue Res.* **2012**, *347*, 429.

[455] X. Mao, T. L. Enno, M. R. Del Bigio, *Eur. J. Neurosci.* **2006**, *23*, 2929.

[456] D. Krizaj, D. A. Ryskamp, N. Tian, G. Tezel, C. H. Mitchell, V. Z. Slepack, V. I. Shestopalov, *Curr. Eye Res.* **2014**, *39*.